1-1-2016

Fatigue Behavior and Modeling of Polyether Ether Ketone (PEEK) under Constant and Variable Amplitude Loadings

Rakish Shrestha

Fatigue behavior and modeling of polyether ether ketone (PEEK) under constant and variable amplitude loadings

By

Rakish Shrestha

A Thesis
Submitted to the Faculty of
Mississippi State University
in Partial Fulfillment of the Requirements
for the Degree of Master of Science
in Mechanical Engineering
in the Department of Mechanical Engineering

Mississippi State, Mississippi

December 2016

Fatigue behavior and modeling of polyether ether ketone (PEEK)

under constant and variable amplitude loadings

By

Rakish Shrestha

Approved:

_____

Nima Shamsaei
(Major Professor)

_____

Steven R. Daniewicz
(Committee Member)

_____

Mark F. Horstemeyer
(Committee Member)

_____

Yucheng Liu
(Graduate Coordinator)

_____

Jason M. Keith
Dean
Bagley College of Engineering

Name: Rakish Shrestha

Date of Degree: December 9, 2016

Institution: Mississippi State University

Major Field: Mechanical Engineering

Major Professor: Nima Shamsaei

Title of Study: Fatigue behavior and modeling of polyether ether ketone (PEEK) under constant and variable amplitude loadings

Pages in Study: 161

Candidate for Degree of Master of Science

The fatigue behavior and cyclic deformation of polyether ether ketone (PEEK) subjected to various uniaxial cyclic loading conditions were experimentally investigated. These include constant amplitude and multi-block loading conditions at various frequencies with zero and non-zero mean strains. Under constant amplitude loading, increasing the test frequency generally resulted in longer fatigue lives for PEEK, while a minimal effect of tensile mean strain was observed. For all fatigue tests under fully-reversed multi-block loadings, pre-loading was found to have a significant beneficial effect on PEEK fatigue resistance irrespective to the load sequence. However, no obvious load history and sequence effect on fatigue behavior was observed for pulsating tension block loading tests. Additionally, three models; strain-based, strain-stress-based, and energy-based models, were correlated to the experimental data in this study. The energy approach was found to provide better fatigue life predictions for PEEK under constant and multi-block loadings with various strain ratios and frequencies.

ACKNOWLEDGEMENTS

I would like to thank my advisor Dr. Nima Shamsaei for giving me an opportunity to pursue my Master's degree in Mechanical Engineering in the first place. Secondly, I am very grateful for his support, guidance, and knowledge without which this research would not have been possible.

I am also very grateful to my mentor Dr. Jutima Simsiriwong, for providing me with her guidance and support in each and every step of this research. I would also like to thank her for her patience and introducing me to the world of graduate school.

I would also like to thank my committee members Dr. Steven Daniewicz and Dr. Mark Horstemeyer for providing me with their precious time and valuable suggestions to improve the quality of this thesis.

I would also like to thank the Engineering Research & Development Center under Cooperative Agreement number W912HZ-15-2-0004 for their financial supports.

I would also like to thank Center for Advance Vehicular Systems (CAVS) at Mississippi State University and all the people working there for providing me with the equipment and training needed to perform my experiments.

TABLE OF CONTENTS

LIST OF TABLES

LIST OF FIGURES

LIST OF NOMENCLATURE

A	Alternating stress ratio
B	Material constant in the temperature rise equation
b	Fatigue strength exponent
C	Material constant in the temperature rise equation
c	Fatigue ductility exponent
D	Cumulative damage
D_i	Damage induced by a specific stress/strain level of i
E	Modulus of elasticity
E'	Cyclic modulus of elasticity
f	Test frequency
i	Number of loading blocks
K'	Cyclic strength coefficient
N	Number of cycles
N_f	Cycles to failure
N_{f_i}	Cycles to failure for a specific stress/strain level of i
$N_{f,e}$	Experimentally obtained fatigue life
$N_{f,p}$	Predicted fatigue life
N_i	Number of cycles for a specific stress/strain level of i
N_t	Transition fatigue life
$2N_f$	Reversals to failure
n'	Cyclic strain hardening exponent
R_ε	Ratio of minimum to maximum strain
T_g	Glass transition temperature
ΔT	Temperature rise on the surface of specimen
W^E	Elastic strain energy density
W^P	Plastic strain energy density

W^T	Total strain energy density
W_0	Total strain energy at the fatigue limit endurance level
W_{avg}^E	Average elastic strain energy density
W_{HL}^E	Elastic strain energy density at half-life cycle
W_{HL}^P	Plastic strain energy density at the half-life cycle
W_{avg}^P	Average plastic strain energy density
W_{HL}^T	Total strain energy densities at half-life cycle
γ	Material constant in the total strain energy density equation
ε_0	Strain amplitude at the fatigue limit
ε_m	Mean strain
ε_f'	Fatigue ductility coefficient
$\frac{\Delta\varepsilon}{2}$, ε_a	Total strain amplitude
$\frac{\Delta\varepsilon_e}{2}$	Elastic strain amplitude
$\frac{\Delta\varepsilon_p}{2}$	Plastic strain amplitude
κ	Material constant in the total strain energy density equation
σ_0	Stress amplitude at the fatigue limit
σ_f'	Fatigue strength coefficient
σ_y'	Cyclic yield strength
σ_m	Mean stress
σ_{max}	Maximum stress
$\frac{\Delta\sigma}{2}$, σ_a	Stress amplitude
ψ	Equivalent damage parameter
ψ_0	Fatigue limit
ΣW^E	Cumulative elastic strain energy density
ΣW^P	Cumulative plastic strain energy density
ΣW^T	Cumulative total strain energy density
ΣW_i^T	Cumulative total strain energy density for a specific stress/strain level in i^{th} block

CHAPTER I

DEFORMATION AND FATIGUE BEHAVIOR OF POLYETHER ETHER KETONE (PEEK) UNDER UNIAXIAL CYCLIC LOADING

(International Journal of Fatigue, 2016, 82, 411-427)

1.1 Abstract

In this study, the fatigue behavior of a semi-crystalline thermoplastic polyether ether ketone (PEEK) is investigated. A series of tests at ambient temperature, including uniaxial monotonic (tension and compression) at different strain rates and uniaxial fully-reversed strain-controlled cyclic tests at strain amplitudes ranging from 0.02 mm/mm to 0.04 mm/mm at various frequencies, were conducted. The frequency influence on the strain-controlled fatigue lives of unfilled PEEK specimens was found to be highly dependent on the strain level. A minimal frequency effect was observed at a lower strain amplitude of 0.02 mm/mm, whereas increasing the test frequency at higher strain amplitudes resulted in longer fatigue lives. Additionally, load-controlled cyclic tests that utilized applied loads corresponding to stress responses obtained from the strain-controlled fatigue tests were performed. The cyclic behavior under the two control modes were compared and discussed. Three types of fatigue models including a strain-based (Coffin-Manson) model, a strain-stress-based (Smith-Watson-Topper) model, and an energy-based model were employed to correlate the data in this study.

Among the three fatigue models, the energy approach was found to better correlate the PEEK experimental data at various frequencies.

1.2 Introduction

Durable lightweight materials have gained increased interest over the past decades in different applications such as automotive and aerospace industries. This tendency has pushed the engineering community to further investigate the use of polymers as lightweight materials in different structural applications to enhance fuel efficiency while maintaining a high level of performance reliability. Other important advantages of polymers are low cost and their capability to be processed into a wide range of fabricated forms such as films, fibers, membranes, filters, moldings, and extrudates [1].

The material of interest in this study is a thermoplastic polyether ether ketone (PEEK). PEEK polymer exhibits excellent mechanical and electrical properties at elevated temperature as well as high toughness, low tendency to creep, and good dimensional stability over a wide range of temperatures. Due to these reasons, PEEK is an ideal candidate as a matrix in composite materials, which are widely used in various applications such as aerospace, automotive, oil and gas, and medical industries. Examples include brackets, clamps, thermal acoustic insulation and fasteners in aerospace applications, gears, bearings, brushings, shift fork wear pads in automotive applications, and as biomaterials to replace metal implant components in orthopedics and trauma [2-3]. Experimental studies have indicated that the cyclic damage process of polymer matrix composites is initiated from the cracks in polymer matrix [4]. Since most PEEK composite structures, systems, and components in these applications are typically

subjected to cyclic loadings, understanding the fatigue behavior of PEEK is of practical importance and is an inevitable part of the engineering design.

While there has been a large amount of research performed over the past decades to gain an understanding of fatigue failure in metals, considerably less work has been focused on polymers. Unlike metals, the fatigue behavior of polymeric materials is significantly affected by their inherent viscoelastic (time- and frequency-dependent) properties [5]. At high frequencies, the softening and melting of polymers can also occur in which the fatigue failure can be accelerated through thermal softening [6].

Nonetheless, various well-established fatigue prediction models for metals have been explored to obtain their applicability to polymeric materials. The fatigue model, which was originally proposed for metallic materials (steels, aluminum, and copper) by Kujawski and Ellyin [7], has been employed for the life prediction of an epoxy (thermoset polymer) under uniaxial strain-controlled tests [8] and a polyacetal (thermoplastic polymer) under uniaxial load controlled tests [9]. In [8-9], the relationship between the fatigue life and the damage parameter ψ, which can be based on either stress, strain, or strain energy density, was expressed as:

$$\psi = \kappa\left(N_f\right)^{\gamma} + \psi_0 \tag{1.1}$$

where, ψ is the equivalent damage parameter, κ and γ are the material constants, and N_f represents the total fatigue life. The nomenclature ψ_0 in Eq. (1.1) represents the stress, strain, or strain energy density associated with the material endurance limit, based on the approach chosen. For a uniaxial fully reversed cyclic loading, the stress, strain, and strain energy approaches can be expressed as Eqs. (1.2)-(1.4), respectively [8-9].

$$\sigma_a = \kappa\left(N_f\right)^{\gamma} + \sigma_0 \tag{1.2}$$

$$\varepsilon_a = \kappa\left(N_f\right)^{\gamma} + \varepsilon_0 \tag{1.3}$$

$$W^T = W^P_{avg} + W^E_{avg} = \kappa\left(N_f\right)^{\gamma} + W_0 \tag{1.4}$$

where $\sigma_a$is the stress amplitude, ε_a is the strain amplitude, and W^T is the total strain energy density. In Eq. (1.4), W^P_{avg} is the average value of dissipated strain energy density and W^E_{avg} is the average value of elastic strain energy density, which are obtained for all cycles [8]. While each of the three approaches provided a good correlation between the predictions and the experimental data in [8], using the strain energy density as the damage parameter was found to be more successful in predicting fatigue life of an epoxy polymer that was subjected to the strain-controlled cyclic loading. For a polycetel polymer under load-controlled tests, however, both stress and energy approaches provided a better correlation than the strain based approach [9].

Mellott and Fatemi [10] conducted a number of cyclic tests to evaluate fatigue behavior of two thermoplastics; a polypropylene copolymer (PP) and a compounded polymer referred to as PO. Uniaxial load controlled tests were performed under various test conditions to evaluate the effects of mold flow direction, specimen thickness, mean stress, test temperature, and test frequency on fatigue life. In their study [10], the Modified Goodman, Goodman-Boller, and Walker models that are commonly used for metallic materials were employed to correlate the experimental data of the PP and PO polymers. They reported that the Walker model with a correction factor predicted fatigue life of both thermoplastics under cyclic test with and without (ratio of minimum to maximum stress, R_ε = -1) mean stresses fairly well, while the Modified Goodman and Goodman-Boller equations were not able to provide an acceptable prediction.

Due to their unique microstructure and viscoelastic nature, the mechanical and fatigue behavior of polymers are sensitive to frequency and temperature. Therefore, fatigue models developed for metals may not be suitable for accurately predicting the fatigue life of polymers. In addition, the majority of polymer fatigue studies in the literature have been performed using a crack growth approach, assuming that the material is initially flawed [5]. Only a few researchers focused on obtaining the fatigue lifetime of polymeric materials by means of stress life (S-N) or strain life (ε-N) approaches. However, because of the limited literature available on the fatigue models of polymers, traditional strain/stress based fatigue models, which are extensively used in fatigue life modeling of metals, are employed here to analyze fatigue data for PEEK thermoplastic. The energy based method, which has been shown to be more successful in predicting fatigue life of polymers under different types of control (strain-controlled and load-controlled) [8-9], is also used to correlate fatigue data in this work.

The objective of this study is to investigate the fatigue behavior of PEEK polymer subjected to fully-reversed uniaxial cyclic loading. The experimental details and results obtained from monotonic tensile and compression tests as well as strain-controlled and load-controlled fatigue tests conducted at room temperature are presented. Additionally, the effect of test frequency on the cyclic deformation behavior and fatigue life is investigated. A comparison between the fatigue behavior obtained from strain-controlled and load-controlled cyclic tests is made. Three fatigue models, including a strain-based model, a strain-stress-based model, and an energy-based model, are utilized to correlate fatigue data at different frequencies. Finally, conclusions based on experimental observations and analyses performed are made.

1.3 Material and Experimental Procedure

1.3.1 Material and Specimen

The material selected in this study was an unfilled PEEK (TECAPEEK™ by Ensinger) with a melt temperature of 334ºC and a glass transition temperature (T_g) of 143ºC. PEEK rods were machined from bar stock parallel to the extrusion direction to create cylindrical specimens with uniform gage section for tensile and fatigue tests. The specimens had a gage length of 18 mm and a gage diameter of 6.35 mm in accordance with the ASTM E606-04 standard [11] as shown in Fig. 1.1. For the compression tests, cylindrical specimens with a diameter of 12.7 mm and a length of 6.35 mm following the geometric configuration in [12] were used to reduce the probability of buckling. An oil-soluble coolant agent was used during machining to minimize the generated heat. The specimens were carefully polished using sandpapers in the gage section to obtain a smooth surface finish with a minimum surface roughness of approximately 3.4 μm prior being stored in a climate controlled environment (cool dry) [13].

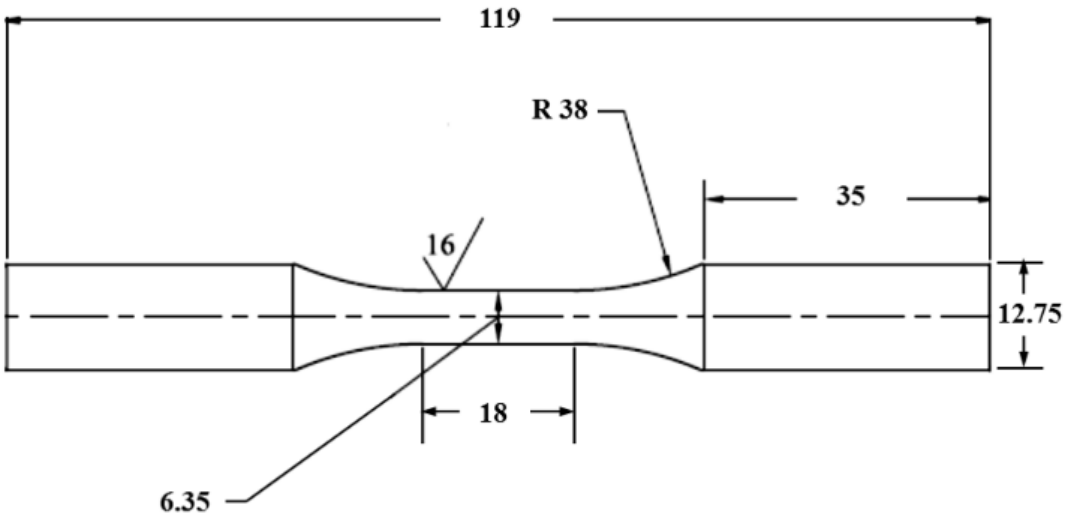

Figure 1.1 Specimen geometry and dimensions for uniaxial monotonic tensile and fatigue tests (dimensions in mm).

1.3.2 Monotonic Loading

Both monotonic tension and compression tests were performed at ambient temperature and at three strain rates of 0.001/s, 0.01/s, and 0.1/s. Two tests were conducted at each strain rate. Based on the quasi-static tension and compression tests, an average of the duplicate tests at each strain rate level was obtained and the corresponding engineering stress-strain curves were determined. For the compression tests, a moly-paste lubricant was used between the specimens and the compression plates to minimize friction as well as to prevent specimen barreling.

1.3.3 Cyclic Loading

Due to the fact that polymers have low thermal conductivity (i.e., good thermal insulator) and high damping, heat transfer through polymers generally occurs at a lower rate than those with high thermal conductivity [14]. Similar to some materials, some of

the input energy in polymers is dissipated as heat during fatigue testing. This results in an initial rise in the temperature, which eventually may be stabilized as the heat transfer between the specimen and its surrounding becomes equal to the heat dissipated through the mechanical loading. In certain cases where the applied stress/strain amplitude or test frequency is sufficiently high, the input energy is continuously dissipated and causes the temperature of the material to gradually increase without reaching stabilization, leading to a thermal softening failure as opposed to a conventional fatigue failure [15]. Therefore, to ensure that failure is due to the mechanical fatigue failure, the temperature of the specimens in this study was carefully monitored throughout testing.

Fully-reversed tension-compression fatigue tests were conducted according to ASTM Standard D7791 12 [16] at ambient laboratory temperature and humidity. For the strain-controlled fatigue tests, constant strain amplitudes ranging from 0.02 mm/mm to 0.04 mm/mm were applied. A sinusoidal waveform was used and the applied frequency ranged from 0.4 Hz to 3 Hz with the intent to maintain the same nominal temperature rise ($\Delta T \approx 50^{\circ}C$) on the specimen surface in all tests. The temperature on the specimen surface during fatigue test was maintained below the T_g of PEEK ($T_g = 143^{\circ}C$). The failure criterion was defined as a 50% load drop in all strain-controlled fatigue tests. Three fatigue tests were performed for each prescribed strain amplitude. Runout tests were stopped after a minimum of 10^6 cycles. For the load-controlled fatigue tests, the applied loads were calculated from the stress responses obtained from the strain-controlled fatigue tests at a prescribed strain level. The failure criterion in load-controlled tests was defined as a significant increase in strain amplitude and subsequent complete

separation of a specimen. The temperature of the specimen surface on the gage section in all tests was monitored using a laser thermometer (Optris laser thermometer LS LT) [13].

1.4 Experimental Results and Discussions

1.4.1 Monotonic Behavior

The average engineering stress-strain responses were obtained at each strain rate (0.001/s, 0.01/s, and 0.1/s) and at room temperature. The effect of strain rate on the mechanical behavior of the PEEK polymer in tension and compression is given in Figs. 1.2(a) and 1.2(b), respectively. The engineering tensile stress strain responses indicate a ductile behavior for PEEK. As can be seen from Fig. 1.2(a), the relationship between the stress and strain is initially linear up to the yield point, followed by a period of nonlinear behavior. The specimen then exhibits a significant elongation due to necking deformation and cold drawing that is indicated by the plateau region in the stress strain curves. The necking deformation is the process in which the specimen forms a constriction (i.e., neck) due to localized plastic deformation as the applied load increases [17]. The necking may stabilize, enabling the shoulders of the neck to travel along the specimen, which is called cold drawing [17]. The continuing increase in the plastic deformation beyond the plateau region ultimately led to the strain hardening and fracture of all specimens, except for the specimens subjected to 0.1/s strain rate in which the fracture occurred without prior strain hardening. It should be noted that the yielding point referred to this study is associated with the local maximum nominal stress and the corresponding strain in the engineering stress strain curves prior to the necking deformation. The micromechanical mechanisms underlying the deformation in a ductile fashion of semi-crystalline polymers include the changes of macromolecules in both the amorphous and crystalline regions, the

reorganization of the crystalline phase, and the orientation of macromolecules [18]. As the loading increases, there is an unfolding and breaking of molecular chains within the crystalline lamellae and, subsequently, the rearrangement of the lamellae in the crystalline regions to align in the direction of the applied load [19]. As a result, the lamellae is reorganized into a highly oriented fibrillar structure during yielding and the subsequent cold drawing stage [18].

In Fig. 1.2(a), the strain rate dependency can be observed especially in the nonlinear region. With an increasing testing speed (i.e., strain rate), the stress at the yield point increases and the material becomes less ductile with a corresponding decrease in the elongation to failure. As the strain rate increases from 0.001/s to 0.1/s, the tensile stress at the yield point increases by approximately 20% from 105 MPa to 125 MPa and the elongation to failure decreases from 0.27 mm/mm to 0.2 mm/mm. However, the initial tensile modulus of PEEK remains unaffected by strain rates and was measured to be 4.5 GPa, which is in good agreement with material specifications provided by the manufacturer (Ensinger). The increase of the stress at the yield point can be associated with the secondary molecular process (i.e., secondary relaxation) [20-21]. When a polymer is subjected to a load at a high strain rate and at a temperature below its T_g, its molecular mobility suddenly decreases due to the stiffening molecular chains [20]. Hence, the material behaves in a more brittle fashion as the strain rate increases.

Similar trends were observed for PEEK responses from compression tests, where the strength moderately increases with increasing strain rate as shown in Fig. 1.2(b). The compressive stress-strain responses show a linear behavior with subsequent yielding, strain softening, and strain hardening at all strain rates except for the compression tests at

0.001/s. The absence of strain hardening in the tests performed at the lowest strain rate of 0.001/s is possibly due to the insufficient strain induced crystallization at the slow strain rate [12].

As stated previously, the stiffness in the specimens increases with an increase in the strain rate. Therefore, the strain hardening was observed in compression tests at higher strain rates, whereas for low strain rate test at 0.001/s, strain hardening was absent. The compressive stress at the yield point increases about 26% due to the decrease in molecular mobility in polymer when the strain rate increases from 0.001/s to 0.1/s. The compressive stress at the yield point was found to be approximately 20% higher than that in tension for all strain rates, which is typically observed in polymers.

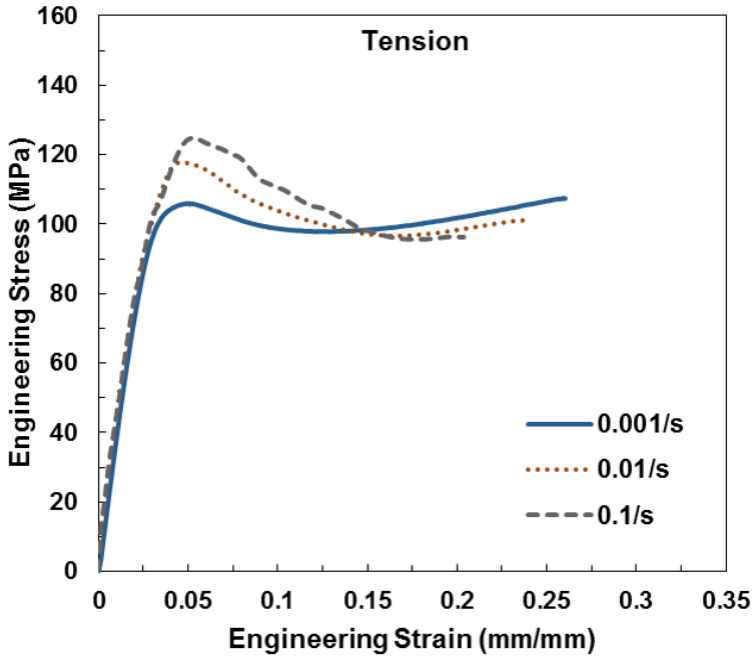

(a)

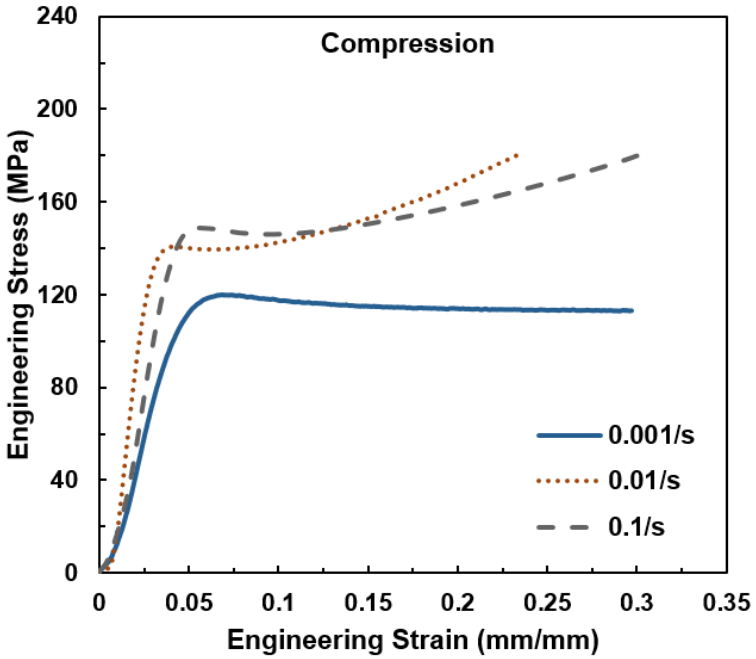

(b)

Figure 1.2 Monotonic stress-strain responses of PEEK in (a) tension and (b) compression with different strain rates and at room temperature.

1.4.2 Cyclic Behavior

As mentioned previously, a portion of the input energy in the polymeric specimen under cyclic loading is dissipated as heat, which results in the self-heating of the test specimen. Therefore, a set of fatigue tests was conducted at selected frequencies in order to maintain the same nominal temperature rise ($\Delta T \approx 50^0$C) on the specimen surface. These nominal temperature rise fatigue tests were conducted at 0.02, 0.025, 0.03, 0.035, and 0.04 mm/mm strain amplitudes and the corresponding data are presented in Table 1.1. The data include strain amplitude, $\frac{\Delta\varepsilon}{2}$, test frequency, stress amplitude, $\frac{\Delta\sigma}{2}$, mean stress, σ_m, reversals to failure, $2N_f$, and temperature rise on the surface of the specimen, ΔT. Although the experiments were conducted using uniaxial fully reversed strains (R_ε = -1) waveforms, there was a compressive mean stress in all tests due to the flow strength differential effect, commonly observed in ductile and semi ductile polymers [22]. However, the mean stress values in these tests were varied from test to test and did not significantly affect the fatigue life of PEEK in this study. It should also be noted that the stress amplitude, $\frac{\Delta\sigma}{2}$, and mean stress, σ_m, presented in Table 1.1 were obtained from the half life cycle.

The cyclic behavior from the fatigue testing at a constant strain amplitude of 0.035 mm/mm and at 0.5 Hz is illustrated in Fig. 1.3. Figures 1.3(a) and 1.3(b) display the constant strain amplitude versus cycle and the corresponding stress measurement, respectively. As reported for polycarbonate (PC) [22], four distinct regions of cyclic stress behavior were also observed in this study as shown in Fig. 1.3(b). These regions are initial, transition, cyclic stability, and crack propagation and fracture. In the initial

region, the stress/strain response is unchanged and the magnitude of the peak compressive stress is observed to be slightly larger than that for the tensile stress. The material then reaches the transition stage, where the peak stresses in both tension and compression decreases rapidly as cyclic softening occurs. The softening rate gradually decreases until the stress strain behavior remains constant in the cyclic stability region, which contains the majority of the fatigue cycles.

Table 1.1 Experimental results for strain-controlled fatigue tests of PEEK at nominal temperature rise.

Specimen ID	$\frac{\Delta\varepsilon^*}{2}$ (mm/mm)	Frequency (Hz)	$\frac{\Delta\sigma^*}{2}$ (MPa)	σ_m* (MPa)	$2N_f$ (Reversals)	ΔT (°C)	$W_{HL}^{P\ *}$ (MJ/m^3)	$W_{HL}^{E\ *}$ (MJ/m^3)	$\sum W^P$ (MJ/m^3)
S50	0.02	3	30.1	-3.7	1,449,114	64	0.58	0.11	412,597
S21			32.2	-4.5	948,248	62	0.62	0.17	286,025
S22			31.0	-1.2	946,032	58	0.61	0.18	285,125
S19	0.025	1	46.8	-12.1	475,810	51	1.19	0.22	282,923
S30			48.9	-11.6	231,964	52	1.17	0.24	134,898
S31			48.3	-16.6	179,018	52	1.29	0.22	114,677
S46	0.03	0.75	46.4	-4.8	208,896	55	1.84	0.32	192,289
S48			51.4	-17.7	125,856	48	1.92	0.23	120,954
S47			49.8	-1.6	124,030	51	1.84	0.34	113,841
S42	0.035	0.5	49.0	-5.0	92,078	52	2.51	0.36	115,738
S43			49.3	-5.5	48,090	53	2.41	0.36	57,887
S35			45.3	-16.6	46,772	56	2.16	0.21	50,463
S24	0.04	0.5	50.3	-5.4	18,454	44	3.07	0.38	28,292
S25			52.9	-7.1	14,172	48	3.01	0.39	21,149
S23			52.1	-4.1	7,766	57	3.02	0.42	11,500

* Measured at half-life cycle

This is followed by a region of crack propagation in which the magnitude of the peak compressive stress remains essentially unchanged, while the peak tensile stress decreases until the final fracture. The latter region was found to be small for PEEK specimens in this study. The temperature of the specimen surface was monitored as shown in these figures, where it remains constant during the initial region and increases rapidly until it reaches the cyclic stability region. As previously discussed, there are dissipative losses in polymers under cyclic loading conditions that contribute to heat generation, and subsequently, an increase in specimen temperature. The polymer chains undergo the stretching and reordering as the specimen temperature continues to increase during the transition region. When the specimen temperature is stabilized (i.e., the heat generated is equal to the heat dissipated per cycle), the molecular chains are further aligned and begin to inelastically stretch until reaching the ultimate failure [19]. Additionally, the hysteresis loops for the initial, transition, and cyclic stability regions of strain-controlled fatigue tests at a strain amplitude of 0.035 mm/mm are presented in Fig. 1.3(c). The contrast between the stress-strain responses in different regions at constant frequency is due to the cyclic softening effect, which is more pronounced at higher strain amplitudes. A considerable amount of plastic deformation and the softening effect for PEEK can be seen in Fig. 1.3(c).

A large variation in fatigue behavior under the same test conditions was also observed. For example, the fatigue life of specimens S19, S30, and S31 in Table 1.1, which were all subjected to the strain-controlled tests at a strain amplitude of 0.025 mm/mm and a frequency of 1 Hz, are 475,810, 231,964, and 179,018 reversals, respectively. As shown in Fig. 1.4 which presents the stress responses of specimens S19,

S30, and S31, the peak stress of these specimens during the initial region of cyclic softening was approximately 80 MPa in tension and 90 MPa in compression before reducing to approximately 35 MPa in tension and 50 MPa in compression in the cyclic stability region. The number of reversals spent in the initial region of cyclic softening is approximately 300, 700, and 800 for specimens S19, S30, and S31, respectively. Specimen S19, which undergoes the shortest number of cycles in the initial region, exhibits the longest fatigue life when compared to those of specimens S30 and S31. On the other hand, specimen S31, which experiences the longest number of cycles in the initial region, displays the shortest fatigue life. A similar trend was also observed in all fatigue tests conducted at each strain level. From these observations for the strain-controlled tests, one may conclude that the number of cycles spent in the initial region of cyclic behavior significantly affects the fatigue life of PEEK specimens

Additionally, it should be noted that some polymers, such as ultra-high molecular weight polyethylene, require more loading cycles to reach the cyclic steady state in compression than in tension [23]. Such observation was obtained from the experimental study of the fully-reversed (R_ε = -1) tension compression cyclic straining performed at room temperature. This may be due to the fact that the reorientation of crystalline lamellae and the stretching of non crystalline region of certain polymers can occur in a faster rate in tension than in compression [23]. However, a comparable number of softening cycles in both tensile and compressive stresses was observed for PEEK, suggesting the morphological rearrangement during uniaxial straining occurs at a similar rate in both tension and compression for this thermoplastic.

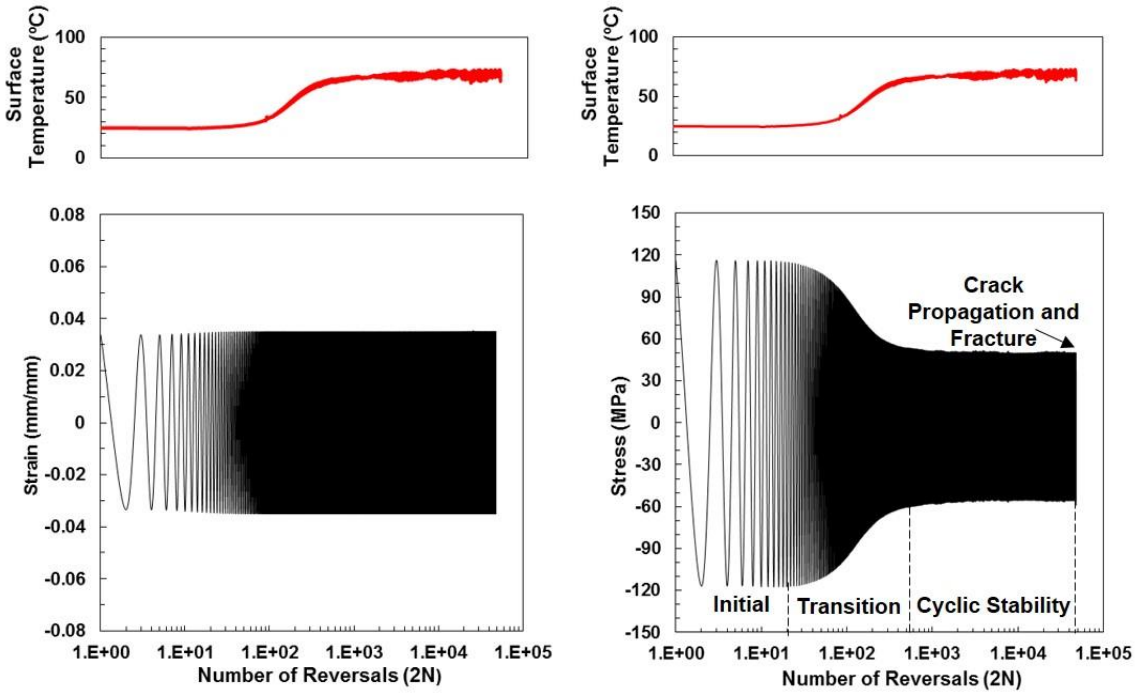

(a) (b)

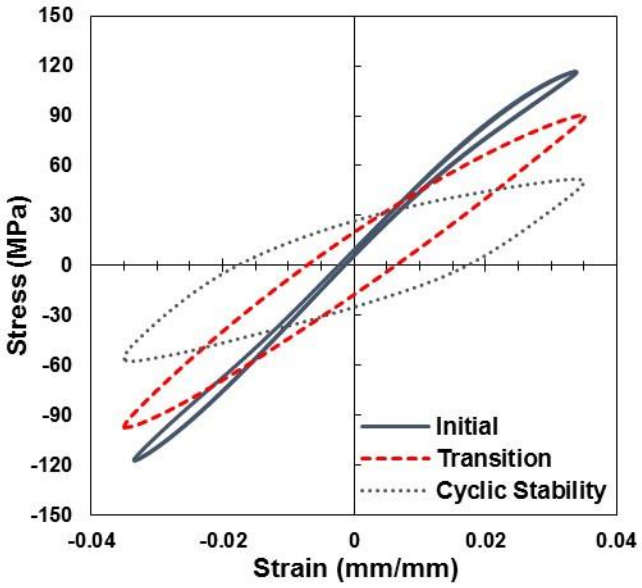

(c)

Figure 1.3 Loading history of strain-controlled fatigue tests of PEEK at ε_a = 0.035 mm/mm and 0.5 Hz showing the (a) strain and (b) stress response versus number of reversals (2*N*) and (c) hysteresis loops at different stages of cyclic behavior at room temperature.

The comparison between the stress amplitude versus the number of cycles at strain amplitudes of 0.02, 0.025, 0.03, 0.035, and 0.04 mm/mm is given in Fig. 1.5. As seen, the stress histories of all PEEK specimens exhibit the described initial, transition and cyclic stability regions. The specimens at higher strain amplitudes reach the transition region and the subsequent cyclic stability region faster than those at the lower strain amplitudes. The faster cyclic softening rate with the increasing strain amplitude was also observed for a thermoset epoxy polymer under fully-reversed uniaxial strain-controlled cyclic loading [24]. As reported in [24], the modulus of elasticity, which was calculated from the stress-strain response at the beginning of each loading cycle, dropped faster at higher strain amplitudes. The magnitude of applied strain in fatigue loading, therefore, affects the cyclic softening rate due to modulus degradation.

To obtain the cyclic stress-strain properties of PEEK, the total strain amplitude, $\frac{\Delta\varepsilon}{2}$, at the stabilized hysteresis loops (i.e., hysteresis loop at half-life) was first separated into elastic strain component, $\frac{\Delta\varepsilon_e}{2}$, and plastic strain component, $\frac{\Delta\varepsilon_p}{2}$. The elastic strain amplitude was calculated using the Hooke's law as:

$$\frac{\Delta\varepsilon_e}{2} = \frac{\Delta\sigma}{2E} \tag{1.5}$$

where $\frac{\Delta\,\sigma}{2}$ is the stress amplitude and E is modulus of elasticity obtained at half-life. Hence, the plastic strain amplitude was determined by subtracting the elastic strain amplitude from the total strain amplitude as [25]:

$$\frac{\Delta\varepsilon_p}{2} = \frac{\Delta\varepsilon}{2} - \frac{\Delta\sigma}{2E} \tag{1.6}$$

The calculated plastic strain amplitude, $\frac{\Delta\varepsilon_p}{2}$, and the stress amplitude, $\frac{\Delta\sigma}{2}$, at different strain amplitudes from the strain-controlled fatigue test were plotted in log log scale resulting in a linear relationship that can be represented by a power function as [25]:

$$\frac{\Delta\sigma}{2} = K'\left(\frac{\Delta\varepsilon_p}{2}\right)^{n'} \tag{1.7}$$

where K' is the cyclic strength coefficient (the intercept) and n' is the cyclic strain hardening exponent (the slope of the fit). Using Eqs. (1.5)-(1.7), the steady-state cyclic stress strain behavior of PEEK was obtained through the Ramberg-Osgood type relationship that represents the elastic and plastic strain components as [25]:

$$\frac{\Delta\varepsilon}{2} = \frac{\Delta\varepsilon_e}{2} + \frac{\Delta\varepsilon_p}{2} = \frac{\Delta\sigma}{2E} + \left(\frac{\Delta\sigma}{2K'}\right)^{\frac{1}{n'}} \tag{1.8}$$

The summary of the cyclic stress-strain properties of PEEK, which was obtained from the strain-controlled tests with nominal temperature rise at five strain amplitudes, is given in Table 1.2. Additionally, the strain rates performed in the strain-controlled fatigue test in Table 1.1 are within the same order of magnitude as 0.1/s strain rate of the monotonic tests. Hence, the comparison between the cyclic stress-strain curve and the monotonic tensile stress-strain curve at 0.1/s strain rate was generated as displayed in Fig. 1.6. As seen, when compared to the monotonic stress-strain responses, PEEK undergoes a significant cyclic softening.

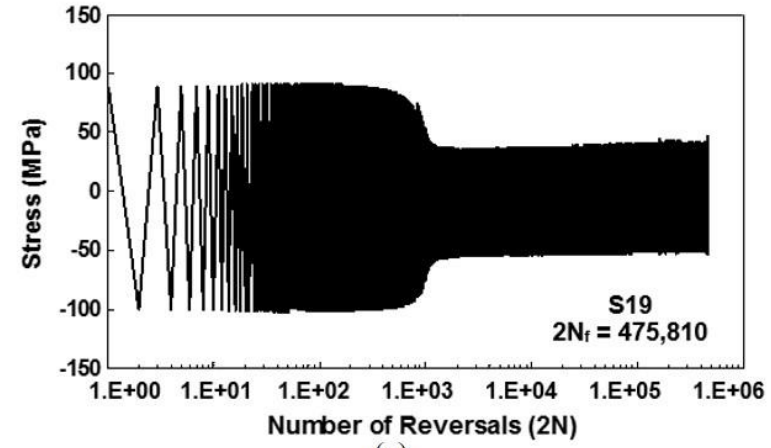

(a)

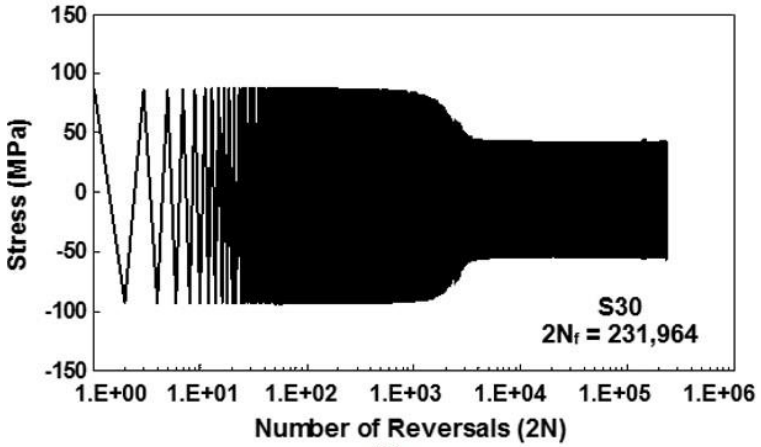

(b)

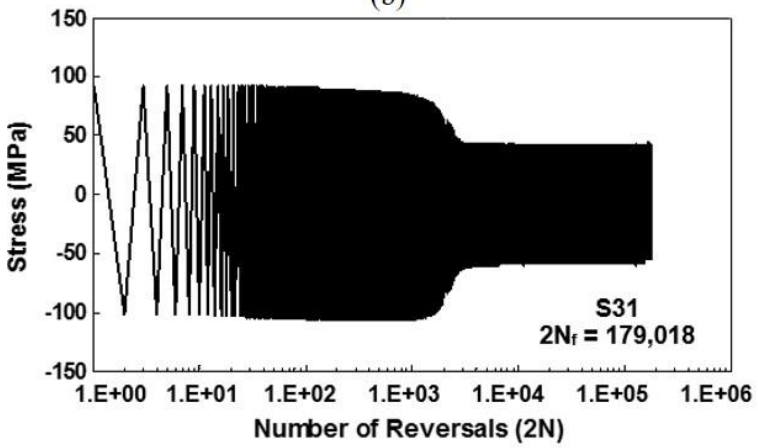

(c)

Figure 1.4 PEEK stress responses of strain-controlled fatigue tests at 0.025 mm/mm strain amplitude and frequency of 1 Hz of specimens (a) S19, (b) S30, and (c) S31 in Table 1.1.

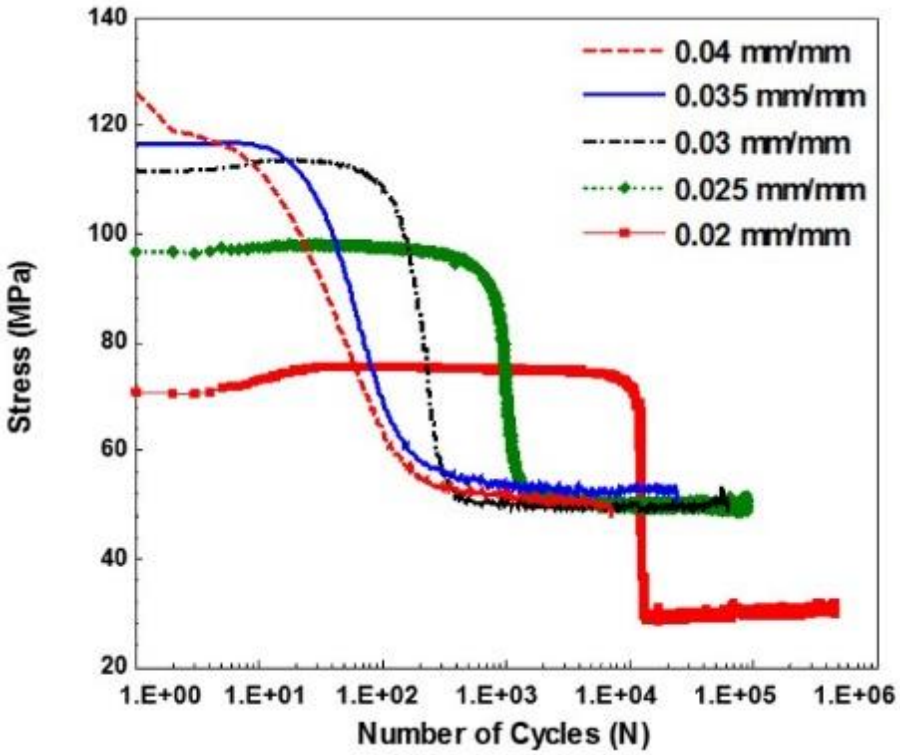

Figure 1.5 Stress amplitude versus number of cycles at different applied strain amplitudes for PEEK fatigue specimens from Table 1.1.

Table 1.2 Cyclic deformation and fatigue properties of PEEK obtained from the nominal temperature rise (Table 1.1) at room temperature.

Properties	**Value**
Cyclic modulus of elasticity, E' (GPa)	2.56
Cyclic yield strength, σ'_y (MPa)	16
Cyclic strength coefficient, K' (MPa)	275
Cyclic strain hardening exponent, n'	0.46
Fatigue strength coefficient, σ'_f (MPa)	246
Fatigue ductility coefficient, ε'_f	0.23
Fatigue strength exponent, b	-0.15
Fatigue ductility exponent, c	-0.21

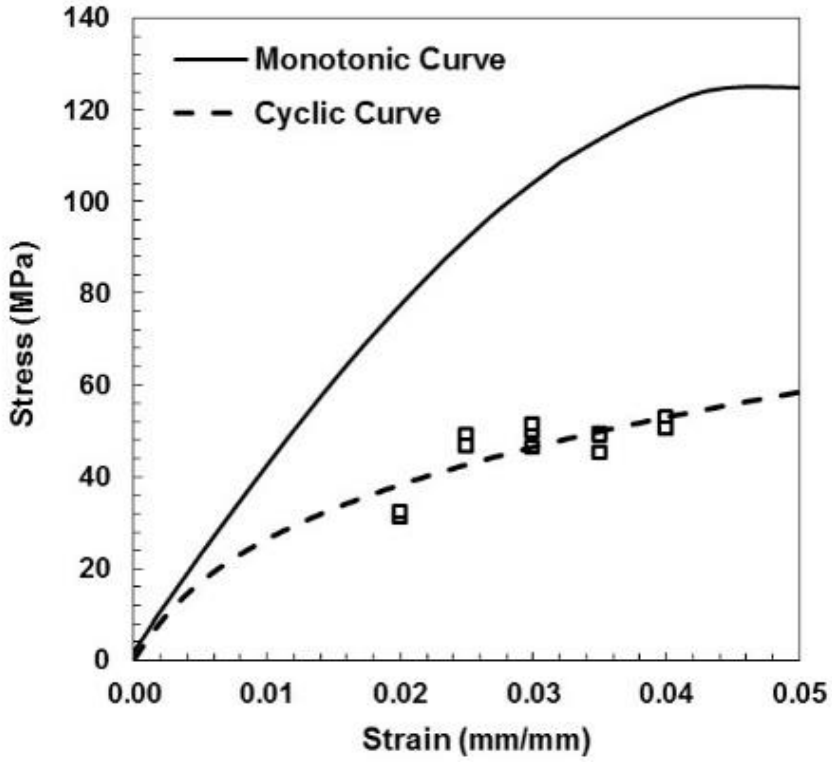

Figure 1.6 Cyclic and monotonic tension stress strain curves for PEEK. The monotonic tensile test data were obtained from the test conducted at 0.1/s strain rate.

1.4.2.1 Frequency Effect on Cyclic Behavior

As previously discussed, polymers may exhibit sensitivity to the frequency of cyclic loading due to their viscoelastic nature, which is highly material dependent. It has been reported that the fatigue crack propagation decreases with increasing test frequency in polystyrene, high impact polystyrene, and polymethyl methacrylate (PMMA), while the test frequency does not have any apparent effects on fatigue resistance of some other polymers such as PC, polysulfone, nylon 66, and polyvinylidene fluoride [5]. Therefore, the effect of loading frequency (i.e., strain rate) on the fatigue behavior of PEEK was also investigated in this study.

Fatigue lives at different frequencies for PEEK specimens are tabulated in Table 1.3 and the strain life diagram under various test frequencies is illustrated in Fig. 1.7, which includes data from Tables 1.1 and 1.3. Numbers in the figure indicate the number of data points on top of each other. At a lower stain amplitude of 0.02 mm/mm, there is a negligible effect of test frequency on the fatigue life of PEEK, as seen in Fig. 1.7. As the frequency increases from 1 Hz to 3 Hz at 0.02 mm/mm strain amplitude, the reversals to failure is observed to slightly decrease from 1,591,982, which is the average life of specimens S20 and S94 (Table 1.3), to 1,114,464, which is the average life of specimens S22, S21, and S50 (Table 1.1). It should be noted that these observations may not fully demonstrate frequency effects on PEEK fatigue behavior with a high level of confidence due to the limited number of experiments performed in this study. Nonetheless, similar effect of frequency on fatigue behavior was also evident in both PP and PO thermoplastics tested at different stress amplitudes and stress ratios [10].

First cycle and half-life hysteresis loops at 1 Hz (specimen S94 in Table 3) and 3 Hz (specimen S22 in Table 1) and the corresponding temperature increases due to self-heating are presented in Fig. 1.8. The temperature rise in specimens S94 and S22 was observed to be 17ºC and 58ºC, respectively, whereas the dissipated strain energy density calculated at half-life for specimens S94 and S22 were 0.69 MJ/m^3 and 0.61 MJ/m^3, respectively. Therefore, one may conclude that an increase in temperature of these specimens which were subjected to different test frequencies is mostly due to an increase in the rate of heat generation (i.e., the amount of strain energy density dissipation per second). In addition, a higher cyclic plasticity at a higher loading frequency is noticeable from the evolution of the hysteresis loop as displayed in Fig. 1.8(a). At this strain

amplitude, PEEK exhibits higher self-heating and a slightly shorter fatigue life when it is subjected to a faster cyclic loading rate, as seen in Fig. 1.8(b).

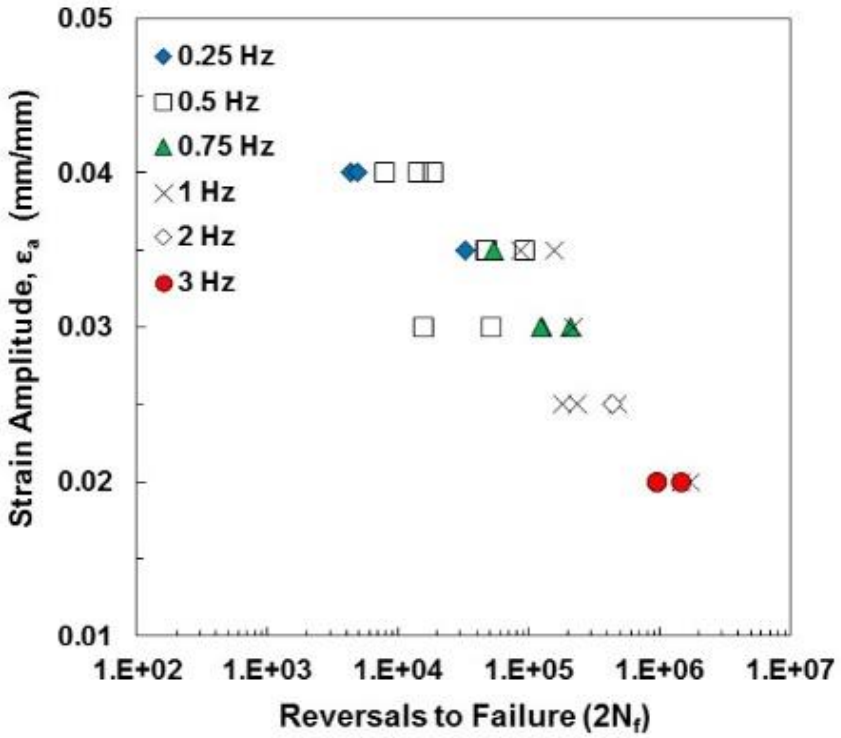

Figure 1.7 Strain-life fatigue behavior of PEEK specimens tested at room temperature and various test frequencies.

Numbers in the figure indicate the number of data points on top of each other.

Table 1.3 Experimental results for strain-controlled fatigue tests of PEEK to study the test frequency effects.

Specimen ID	$\frac{\Delta\varepsilon}{2}$ (mm/mm)	Frequency (Hz)	$\frac{\Delta\sigma^*}{2}$ (MPa)	σ_m* (MPa)	$2N_f$ (Reversals)	ΔT (°C)	$W_{HL}^{P\ *}$ (MJ/m^3)	$W_{HL}^{E\ *}$ (MJ/m^3)	$\sum W^P$ (MJ/m^3)
S20	0.02	1	57	-19	1,723,898	27	0.62	0.28	550,116
S94			55	-23	1,460,066	17	0.69	0.26	489,564
S55	0.025	2	31	-16	437,176	77	0.84	0.11	185,860
S26	0.03	0.5	60	-3.3	51,472	39	1.83	0.51	43,781
S28			57	-6.8	15,716	36	1.95	0.47	21,096
S53		1	41	-13.0	216,650	66	1.59	0.2	172,375
S59	0.035	0.25	46	-1.75	32,076	21	2.51	0.5	40,919
S34		0.75	61	-12.1	53,968	66	2.07	0.2	55,798
S4		1	37	-26	155,206	N/A	1.7	0.12	102,174
S8			38	-20	86,514	N/A	1.8	0.17	75,820
S56	0.04	0.25	59	-11.8	4,924	42	3.37	0.44	8,300
S95			58	-15	4,306	35	3.36	0.4	7,197

The frequency influence on the cyclic behavior of thermoplastics is also highly dependent on the stress/strain level [26]. Based on the experimental results, the opposite frequency effects on PEEK fatigue behavior were observed at other higher strain amplitudes (0.025, 0.03, 0.035, and 0.04 mm/mm), where an increase of test frequency leads to longer fatigue lives, as seen in Fig. 1.7. Again, more confidence in the conclusion regarding the frequency effects on PEEK fatigue behavior can be made by conducting more experiments at each test condition. An increase of the applied frequency in fatigue tests produces a subsequent increase in the strain rate during loading and unloading. Consequently, the stress response of the material tested at a higher test frequency is also expected to increase. Figure 1.9(a) presents the stress strain hysteresis loops for the first and half-life cycles obtained from the test data at a 0.03 mm/mm strain amplitude with frequencies of 0.5 Hz (specimen S28 in Table 1.3) and 1 Hz (specimen S53 in Table 1.3). Although the size of the hysteresis loop measured at half-life cycle of both specimens is not notably different, the stress amplitude of specimen S28 is larger than that of specimen S53. Again, the specimen tested at a higher test frequency generated a higher self-heating ($\Delta T \approx 66°C$) when compared to that ($\Delta T \approx 36°C$) at a lower test frequency.

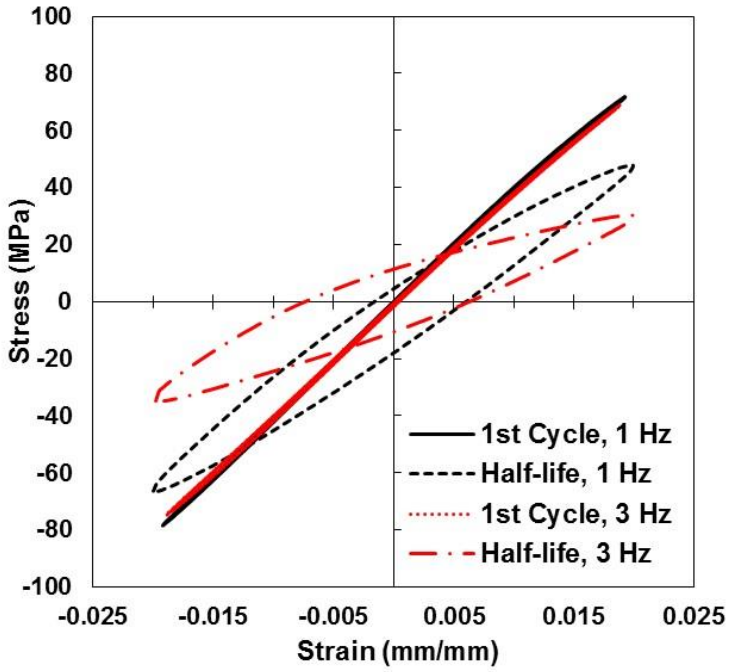

(a)

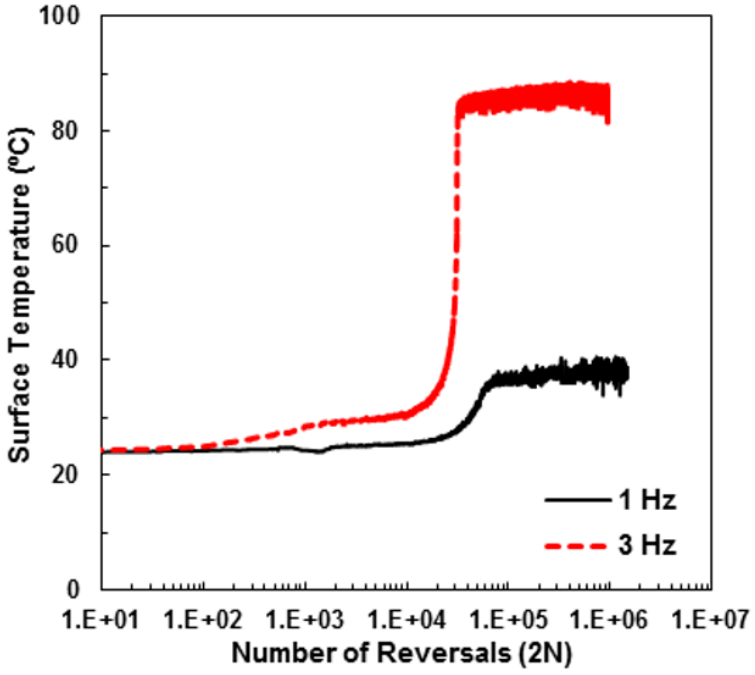

(b)

Figure 1.8 (a) First cycle and half-life cycle hysteresis loops for PEEK tested at 1 Hz (specimen S94) and 3 Hz (specimen S22) with applied strain amplitude of 0.02 mm/mm at room temperature and (b) corresponding temperature increases due to self-heating.

In a study of fatigue behavior of a conditioned short glass fiber reinforced polyamide 6, Bernasconi et al. [27] investigated the effects of test frequency, and dissipated strain energy on the rise in temperature at the surface of the specimen due to self-heating. Based on their experimental results, a linear relationship was obtained as [27]:

$$\Delta T = BW_{HL}^{P} f \tag{1.9}$$

where ΔT is the rise in temperature, f is the test frequency, and B is a material constant. The parameter W_{HL}^{P} is the area of the hysteresis loop at the half-life cycle, which also represents the plastic strain energy density dissipated by the specimen. The detailed description of the dissipated energy related to fatigue testing in this study will be discussed in a later section.

Using the linear relation given in Eq. (1.9), the ratio of the rise in temperature to test frequency, $\Delta T/f$, of all strain-controlled fatigue tests reported in both Tables 1.1 and 1.3 was plotted against the plastic strain energy density at the half-life cycle, W_{HL}^{P}, as displayed in Fig. 1.10. The correlation in Fig. 1.10 indicates the combined effects of both test frequency with subsequent temperature rise on the dissipated strain energy density. In general trend, for all strain amplitudes, the increase in test frequency resulted in a higher self-heating in the PEEK specimens. As frequency increases, the heat generated in the specimen due to dissipated strain energy cannot transfer to the surrounding because of shorter time period as well as low thermal conductivity of polymers, which results to the higher self-heating in the specimen [28]. As observed from Fig 1.10, a good correlation between frequency, temperature rise on the specimen, and strain energy density is obtained with some scatter in the test data at lower frequencies (0.25 Hz and 0.5 Hz).

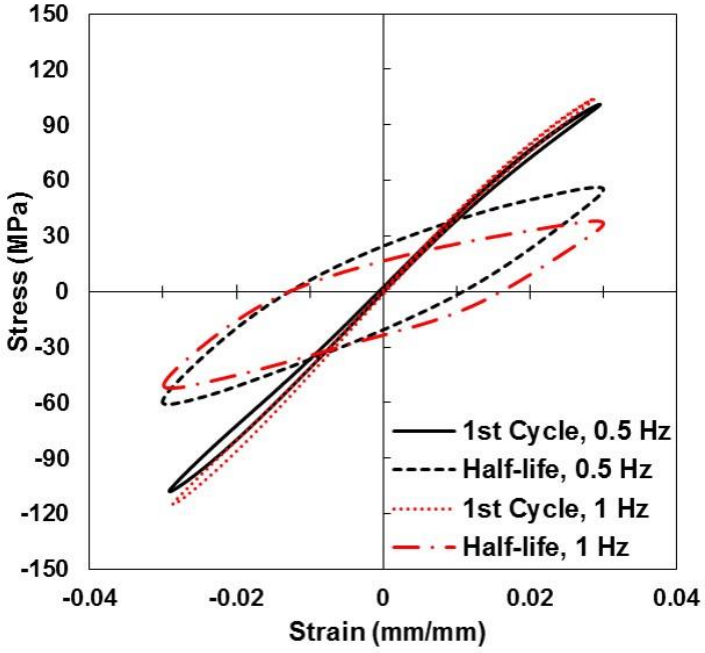

(a)

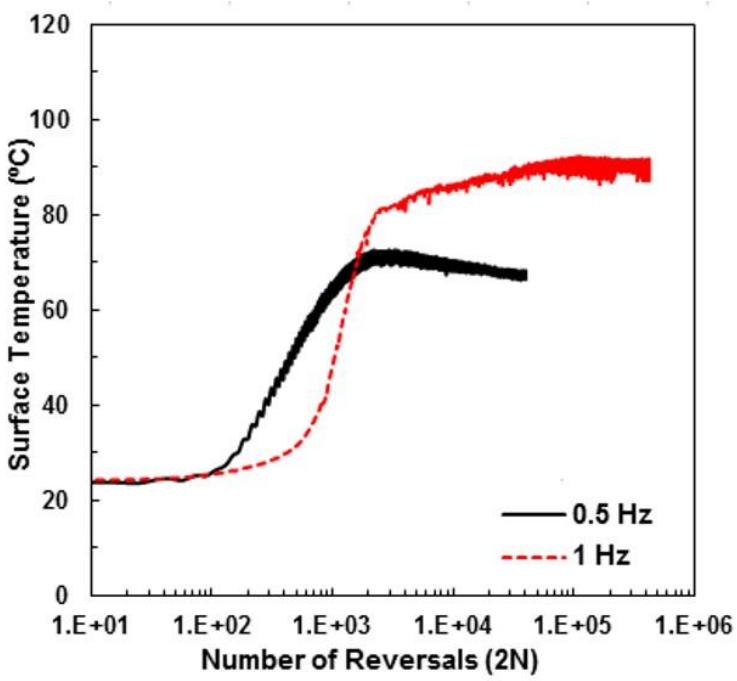

(b)

Figure 1.9 (a) First cycle and half-life cycle hysteresis loops for PEEK tested at 0.5 Hz (specimen S28) and 1 Hz (specimen S53) with applied strain amplitude of 0.03 mm/mm at room temperature and (b) corresponding temperature increases due to self-heating.

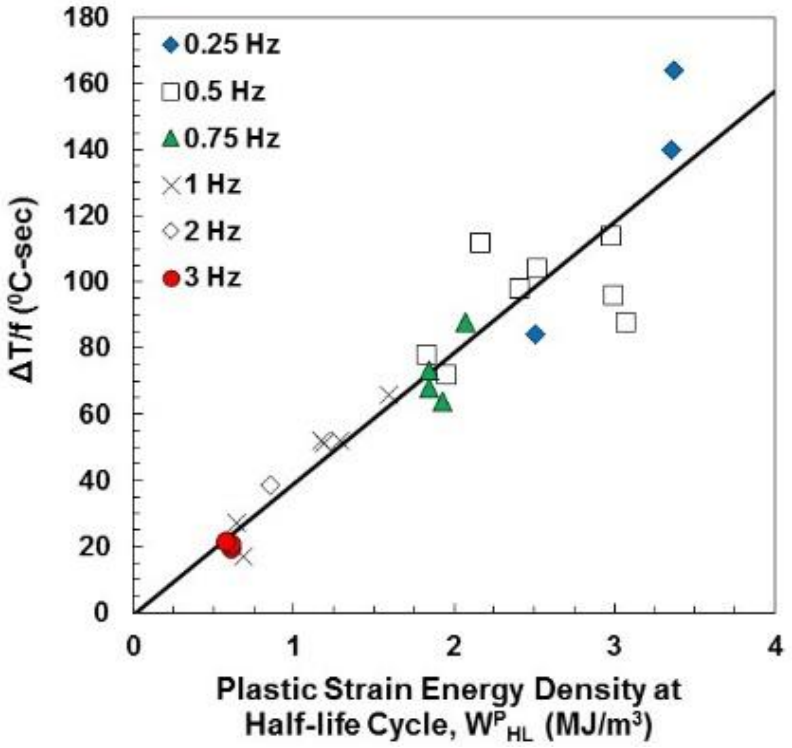

Figure 1.10 The ratio of the rise in temperature to test frequency, $\Delta T/f$, of all strain-controlled fatigue tests versus the plastic strain energy density at half-life (cyclic stability region), W^{HL}.

1.4.2.2 Test Control Effect on Cyclic Behavior

For most metals and some polymers, incremental step deformation tests are generally conducted to obtain the cyclic stress and strain behavior [10]. From these results, the stress life fatigue properties can be used to determine the strain life fatigue properties of a given material. In this study, a series of load-controlled tests were performed to investigate the cyclic deformation and fatigue life of PEEK, which were then compared to those obtained under strain-controlled loading. The applied loads corresponding to stress responses obtained from the strain-controlled tests were utilized to conduct the load-controlled cyclic tests.

The summary of the load-controlled test results with R_σ =-1 is given in Table 1.4. The applied loads for specimens S61, S63, S64, S65, and S66 in Table 1.4 were calculated based on the stress responses obtained from the uniaxial fully-reversed strain-controlled tests at the strain amplitude of 0.03 mm/mm and at a frequency of 0.75 Hz in Table 1.1. Under strain-controlled condition, the fatigue lives ranged from 124,030 to 208,896 reversals with temperature rise ranging from 48°C to 55°C, as presented in Table 1.1. The amplitudes of the stress response are approximately 100 MPa, 65 MPa (average value), and 45 MPa in the initial, transition, and cyclic stability regions of the corresponding strain-controlled tests, respectively. The load-controlled test on specimen S61 was first performed at 0.75 Hz using the applied load corresponding to the tensile stress response during the cyclic stability region (45 MPa). However, the measured strain amplitude was observed to be significantly lower than 0.03 mm/mm with only a 5°C temperature increase. As a result, specimen S61 was able to withstand the prescribed cyclic loading beyond 2,000,000 reversals before the test was terminated.

To account for the stress responses in the three regions of cyclic behavior under the strain-controlled mode, the incremental step fatigue tests under load-controlled condition were performed. Specimen S63 was tested at 0.75 Hz using the following loading profile; 100 MPa for 0 to 80 reversals, 65 MPa for 81 to 1,000 reversals, and 45 MPa for the remaining cycles. Figure 1.11 illustrates the applied stress, strain responses, and the hysteresis loops for specimen S63. The strain responses are also observed to be much lower than 0.03 mm/mm with a temperature rise of only 4°C. Additionally, the evolution of the stress-strain hysteresis loops of specimen S63 presented in Fig. 1.11(c)

displays negligible plastic deformation in all the initial, transition, and cyclic stability regions. The test was finally terminated after 2,000,000 reversals.

Table 1.4 Experimental results for load-controlled fatigue tests of PEEK.

Specimen ID	$\frac{\Delta\sigma}{2}$ (MPa)	Frequency (Hz)	$\frac{\Delta\varepsilon^*}{2}$ (mm/mm)	ε_m^* (mm/mm)	$2N_f$ (Reversals)	ΔT (°C)
S65	100-45**	0.4	0.031	0.0100	172***	6
S64	100-45**	0.4	0.029	0.0060	306***	6
S66	100-45**	0.6	0.011	0.0053	> 52,810	6
S63	100-45**	0.75	0.011	-0.00009	> 2,000,000	4
S61	45	0.75	0.011	-0.0004	> 2,000,000	5
S68	80	0.5	0.020	-0.0005	6,444***	21
S69	80	0.75	0.021	-0.0005	7,404***	24
S70	80	1.5	0.021	0.0002	9,716***	24
S71	70	1	0.020	-0.0010	95,830***	40
S72	70	2	0.020	0.0020	109,294***	44

* Measured at half-life cycle, ** Step test, *** Specimen failed due to necking

Additional load-controlled tests were performed using a similar loading profile at reduced test frequencies of 0.4 Hz (specimens S64 and S65) and 0.6 Hz (specimen S66). The rise in temperature, ΔT, of specimens S64-S66 was stabilized at approximately 6°C. However, at a test frequency of 0.4 Hz, both specimens S64 and S65 failed due to cyclic necking at 306 and 172 reversals, respectively. On the other hand, the evolution of the stress-strain hysteresis loops for specimen S66 did not reveal significant plastic deformation, and therefore, the fatigue test was terminated at 52,810 reversals. Unlike the thermal fatigue failure, which is attributed to the steady increase of self-heating in the material, the cyclic necking described in this study is referred to the failure due to a significant increase in both strain response and surface temperature in the last cycle.

Furthermore, tests were conducted at stress amplitudes ranging from 70 MPa to 80 MPa at various test frequencies. However, all of the specimens (S68-S72) cycled under these load-controlled test conditions did not exhibit a mechanical fatigue failure but rather a failure due to cyclic necking. Figure 1.12 presents the applied stress and strain responses of specimen S68 that was subjected to constant stress amplitude of 80 MPa at 0.5 Hz. Relatively steady strain responses of 0.02 mm/mm were observed throughout the life prior to cyclic necking, where the strain responses abruptly increased to 0.07 mm/mm. Additionally, the stress-strain hysteresis curve at half-life cycle in Fig. 1.12(c) does not display an apparent plastic deformation. An image of specimen S68 that failed due to cyclic necking is shown in Fig. 1.12(d).

It can be concluded from these uniaxial fully-reversed fatigue test results that fatigue behavior of PEEK, such as stress/strain responses, temperature, fatigue life, and failure mode, differs significantly depending on the test control mode (strain-controlled or load-controlled). With given applied stresses corresponding to those attained from the strain-controlled tests, the strain responses under the load-controlled tests are substantially smaller than expected as illustrated in Figs. 1.11 and 1.12. In Table 1.4, it can be seen that the differences between the fatigue lives of specimens S63 S65 with the identical applied load corresponding to the stress responses obtained from the strain-controlled tests at the strain amplitude of 0.03 mm/mm may be attributed to the test frequency. It is evident that, under load-controlled cyclic tests, an increase in frequency leads to somewhat smaller strain amplitude responses, which subsequently is reflected in a longer fatigue life. However, at a sufficiently high applied load and frequency, PEEK material can exhibit a cyclic necking failure under cyclic loading despite the small

increase in the specimen temperature due to the hysteresis heating (i.e., specimens S64 and S65). The similar effect of test frequency on fatigue behavior was also observed at higher stress amplitudes of 80 MPa in specimens S68 to S70 and 70 MPa in specimens S71 and S72. Furthermore, at these stress amplitudes, the temperature rise on the specimens' surfaces were comparatively higher than those of specimens S63-S65. The self-heating in these specimens under load-controlled mode were also observed to increase as test frequency increased.

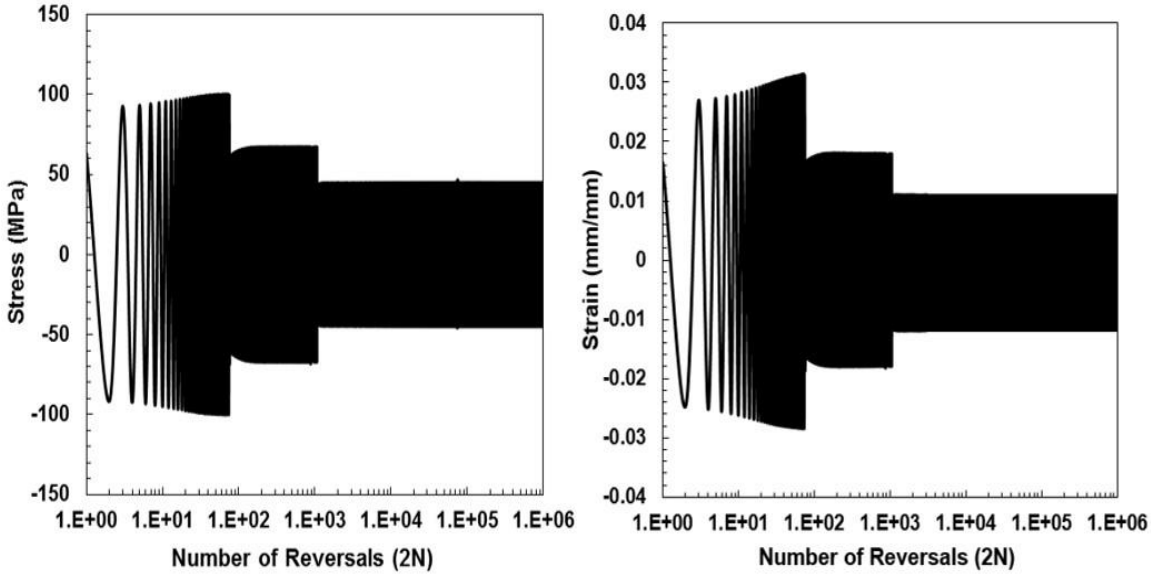

(a) (b)

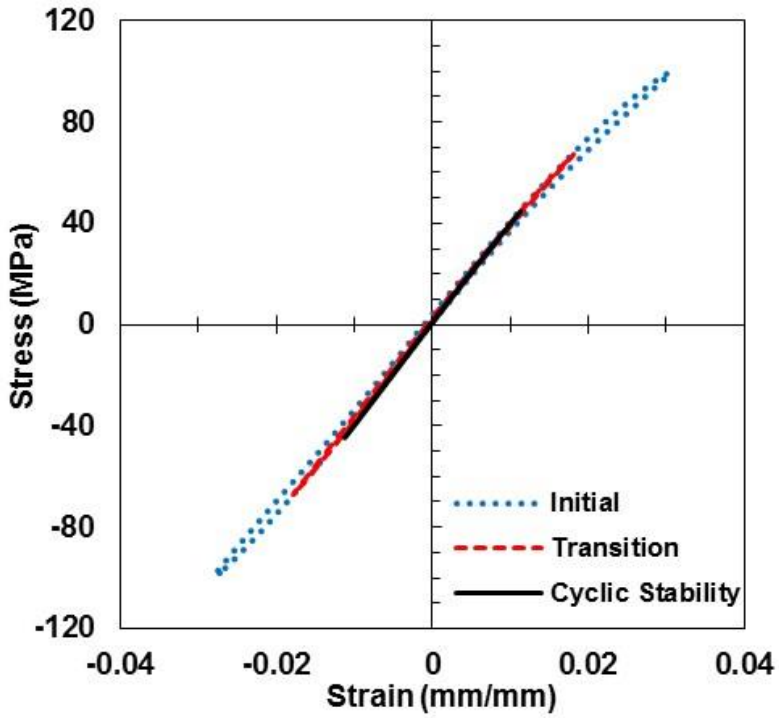

(c)

Figure 1.11 Loading history of load-controlled fatigue tests of PEEK (specimen S63 in Table 1.4) at 0.75 Hz showing the (a) stress and (b) strain amplitudes versus number of reversals and (c) hysteresis loops at different regions.

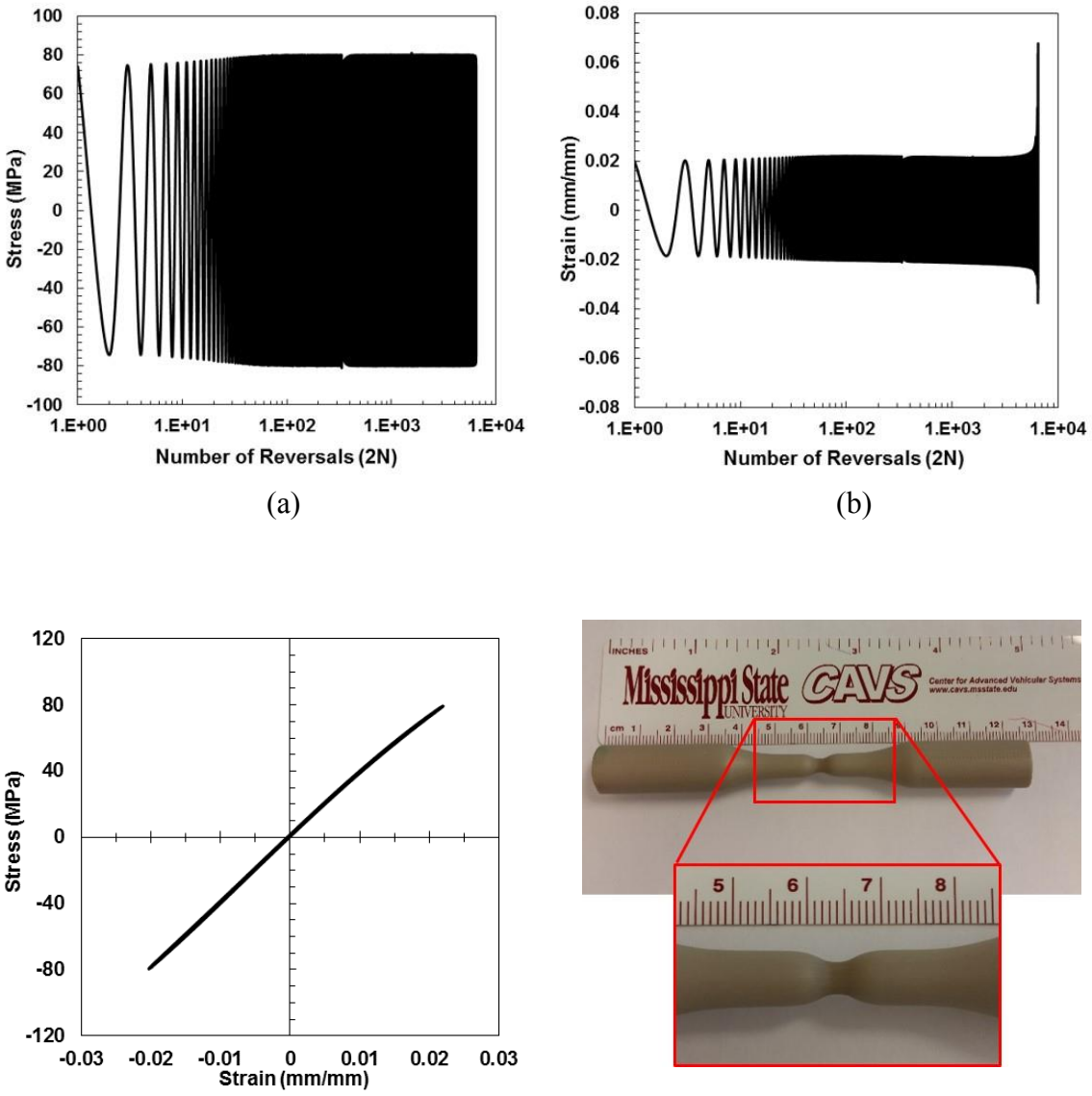

Figure 1.12 Loading history of load-controlled fatigue tests of PEEK (specimen S68 in Table 1.4) at 0.5 Hz showing the (a) stress and (b) strain amplitudes versus number of reversals, (c) hysteresis loop, and (d) cyclic necking image of specimen S68.

1.4.3 Fatigue Models

1.4.3.1 Strain-Based Approach

The fatigue test data in total strain amplitude, $\frac{\Delta\varepsilon}{2}$, versus reversals to failure, $2N_f$, were used to develop the strain-life fatigue curves. The total strain amplitude can be separated into elastic strain component, $\frac{\Delta\varepsilon_e}{2}$, and plastic strain component, $\frac{\Delta\varepsilon_p}{2}$, from the stabilized hysteresis loops (i.e., hysteresis loop at half-life). These components were plotted (log-log) against the reversals to failure, $2N_f$, in which the linear relationship between the elastic strain amplitude, $\frac{\Delta\varepsilon_e}{2}$, and fatigue life was obtained using the following equation [25]:

$$\frac{\Delta\varepsilon_e}{2} = \frac{\sigma_f'}{E}(2N_f)^b \tag{1.10}$$

where σ_f' and b are the fatigue strength coefficient and fatigue strength exponent (slope of the elastic strain-life line), respectively. These parameters were determined by performing a fit using a linear least-squares method, following ASTM standard E739 [29]. Similarly, the plastic strain amplitude, $\frac{\Delta\varepsilon_p}{2}$, as a function of reversals to failure, $2N_f$, was obtained as follow [25]:

$$\frac{\Delta\varepsilon_p}{2} = \varepsilon_f'(2N_f)^c \tag{1.11}$$

where ε_f' is the fatigue ductility coefficient and c is the fatigue ductility exponent (slope of the plastic stain-life line). Therefore, by combining Eqs. (1.10) and (1.11), the total strain amplitude was obtained from the Coffin-Manson relationship as [25]:

$$\frac{\Delta\varepsilon}{2} = \frac{\Delta\varepsilon_e}{2} + \frac{\Delta\varepsilon_p}{2} = \frac{\sigma_f'}{E}(2N_f)^b + \varepsilon_f'(2N_f)^c \tag{1.12}$$

The fatigue parameters in Eqs. (1.10)-(1.12) were calculated from the strain-controlled test at nominal temperature rise (i.e., data in Table 1.1) and presented in Table 1.2. The plots of the elastic, plastic, and total strain amplitude versus reversals to failure for all strain-controlled fatigue tests at nominal temperature and the Coffin-Manson fits are presented in Fig. 1.13(a). As seen, plastic strain amplitudes under uniaxial fully-reversed fatigue tests are greater than elastic strain amplitudes at all strain levels in this study; thus, the transition fatigue life $2N_t$, which is the number of reversals at the intersection between the elastic and plastic strain lines, is not observed. This observation for PEEK is in contrast to other polymeric materials such as a neat polypropylene and polypropylene elastomer blend, as reported by Mellot et al. [10]. Both materials in [10] were subjected to the fully-reversed load-controlled fatigue tests and the relationships between the strain amplitude and fatigue life were determined from the incremental step cyclic deformation tests. Based on their results, the transient life, $2N_t$, was calculated to be 281 and 3,026 reversals for polypropylene and polypropylene elastomer blend, respectively. For PEEK polymer, the strain amplitude of the fatigue tests in Table 1.1 is primarily governed by the plastic strain as illustrated in the stabilized stress strain hysteresis loops in Fig. 1.13(b), which were obtained from specimens S21, S19, S46, S42, and S24. The size of the hysteresis loop and subsequent plastic strain were observed to be larger with increasing in strain amplitude. The elastic strain amplitude values, which were calculated from the stress range at half-life cycle and the modulus of elasticity, are comparatively similar for all tests as depicted in Figs. 1.13(a) and 1.13(b). Additionally, the predicted fatigue lives from the Coffin-Manson approach were compared to those obtained experimentally from both Tables 1.1 and 1.3 (with and

without the frequency effects) as shown in Fig. 1.13(c). In this figure, approximately 77% of total data and 66% of data from the frequency effect tests (i.e., Table 1.3) are within scatter bands of two. The R^2 value of all observed and predicted fatigue lives using the Coffin-Manson approach was calculated to be 0.83. The data that fall outside of the scatter band are primarily the strain-controlled test with varied frequency (i.e., data reported in Table 1.3).

The poor correlation between the Coffin-Manson fits and the experimental data is possibly due to the significant cyclic softening behavior in PEEK. While the calculated plastic strain values used in the Coffin-Manson expression were obtained from stabilized hysteresis loops that essentially represents the deformation in the cyclic stability region, the cyclic deformation during the initial and transient regions may also contribute to the overall fatigue behavior and life, as previously discussed. Consequently, the elastic and plastic strains obtained from the hysteresis loops at earlier stages of cyclic loading should be incorporated into fatigue analysis. Nonetheless, difficulties may arise when attempting to accurately calculate the elastic and plastic strain components due to the propeller like shape of the stress strain hysteresis loop in the initial cycles, as shown in Fig. 1.3(c).

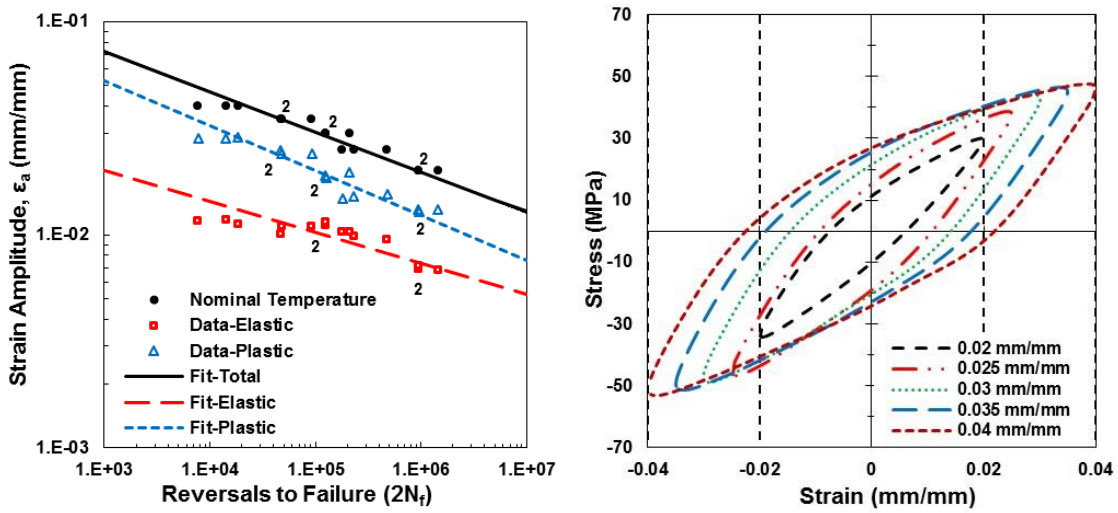

(a) (b)

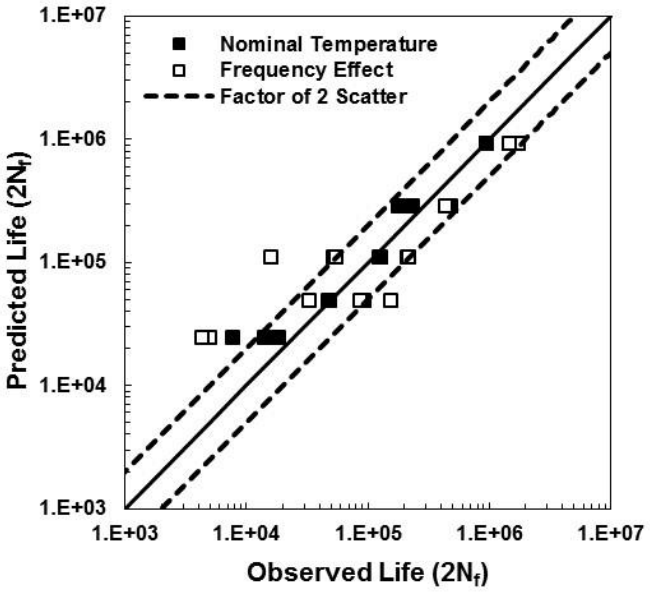

(c)

Figure 1.13 (a) Uniaxial fully-reversed fatigue test data of PEEK in strain amplitude, ε_a,versus reversals to failure, $2N_f$, with nominal temperature rise (Table 1.1) showing elastic, plastic, and total strains and fits, (b) hysteresis stress strain loops at five strain amplitudes, and (c) predicted fatigue lives using the Coffin-Manson model versus experimentally observed fatigue lives for all strain-controlled fatigue data (Tables 1.1 and 1.3).

Numbers in the figure indicate the number of data points on top of each other.

1.4.3.2 Stress-Strain Based Approach

The experimentally obtained data to study the frequency effect in Table 1.3 revealed that the test frequency significantly affects the stress response as well as the evolution of the stress strain hysteresis loop for all tests at different strain amplitudes. Therefore, using a damage parameter that considers the effects of both stress and strain terms, such as the Smith Watson Topper (SWT) parameter, may improve the fatigue life prediction of PEEK. The SWT damage parameter was originally developed to account for both stress and strain amplitudes as well as mean stress/strain effects. The SWT parameter, which is a product of strain amplitude, ε_a (or $\frac{\Delta\varepsilon}{2}$), and maximum tensile stress, σ_{max}, has been used extensively and validated with various experimental results in both low and high cycle fatigue for metals [30]. Additionally, the SWT damage parameter has been found to estimate fatigue damage for materials with strong deformation history effects more accurately than the conventional strain-life approach [31].

For the uniaxial fully-reversed fatigue tests reported in Tables 1.1 and 1.3, the SWT parameter was obtained by multiplying the strain amplitude and the maximum stress, σ_{max}. This parameter can then be related to fatigue life as [32]:

$$\varepsilon_a \sigma_{max} = \frac{(\sigma_f')^2}{E}(2N_f)^{2b} + \sigma_f' \varepsilon_f' E (2N_f)^{b+c} \tag{1.13}$$

where

$$\sigma_{max} = \sigma_m + \sigma_a \tag{1.14}$$

In Eq. (1.14), σ_m and σ_a are mean stress and stress amplitude, respectively. The correlation of SWT parameter, $\varepsilon_a \sigma_{max}$, and the reversals to failure for the PEEK data under strain-controlled tests with nominal temperature rise (Table 1.1) is presented in Fig.

1.14(a) and the predicted lives using Eq. (1.13) are plotted against the experimentally observed fatigue lives for all the strain-controlled fatigue experiments (Tables 1.1 and 1.3) in Fig. 1.14(b). The $\varepsilon_a\sigma_{max}$ values obtained at each strain amplitude were observed to follow the linear relationship with the fatigue life of PEEK in a log-log plot especially at strain amplitudes of 0.02 mm/mm to 0.035 mm/mm, as seen in Fig. 1.14(a). Under the experimental condition where the nominal temperature rise in the specimens was fixed (i.e. Table 1.1), 59% of fatigue life predictions using the SWT parameter fall within scatter bands of two from experimentally observed fatigue lives, as seen in Fig. 1.14(b). However, a poor correlation of fatigue lives using the SWT approach was observed where only 33% of the frequency effect data (from Table 1.3) are within scatter bands of two. The R^2 value of all observed and predicted fatigue lives using the SWT approach was determined to be 0.77. From the results, it can be seen that the Coffin-Manson equation provides a better correlation between the predictive and experimental fatigue lives when compared to the SWT approach.

Since the SWT parameter represents the combined effects that are associated with only the product of two extreme values (strain amplitude and maximum tensile stress), the model does not necessary capture the shape and size of the hysteresis loop that changes throughout the cyclic loading for PEEK polymer. Additionally, because the shape of the hysteresis loop differs with test frequency even for the same strain amplitudes, the SWT parameter cannot accurately correlate the experimental data generated with various frequencies. Nonetheless, in an attempt to incorporate the cyclic softening effects into the SWT fatigue model, the cumulative SWT parameter (i.e., summation of $\varepsilon_a\sigma_{max}$ values for all cycles) was determined for all strain-controlled tests

and correlated to the observed fatigue lives. However, no significant improvement was observed using this approach.

1.4.3.3 Energy Based Approach

Although the SWT parameter that includes both stress and strain terms was considered for PEEK fatigue life prediction, it was not able to provide a good correlation to the experimental data since it only captures the frequency effect based on only the extreme stress and strain values on the hysteresis loop. As seen in Figs. 1.8(a) and 1.9(a), the shape and size of the hysteresis loop that changes throughout cyclic loading is also significantly affected by the test frequency; therefore, the energy based approach that can capture the shape and size of the hysteresis loop may provide better correlations.

The energy based approach for fatigue life estimation is derived based on the strain energy imposed by the external loading that is further separated into elastic (recoverable) and plastic (irrecoverable) parts. The plastic strain energy density, W^P, dissipated in each cycle of loading, can be defined as the area of hysteresis loop, where the elastic strain energy per unit volume associated with the tensile stress, W^E, can be represented by the positive area under the hysteresis loop.

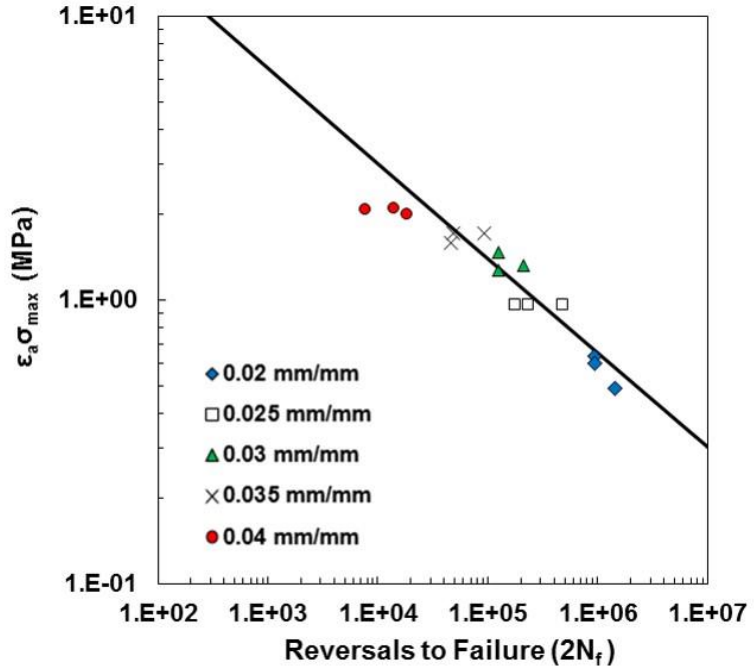

(a)

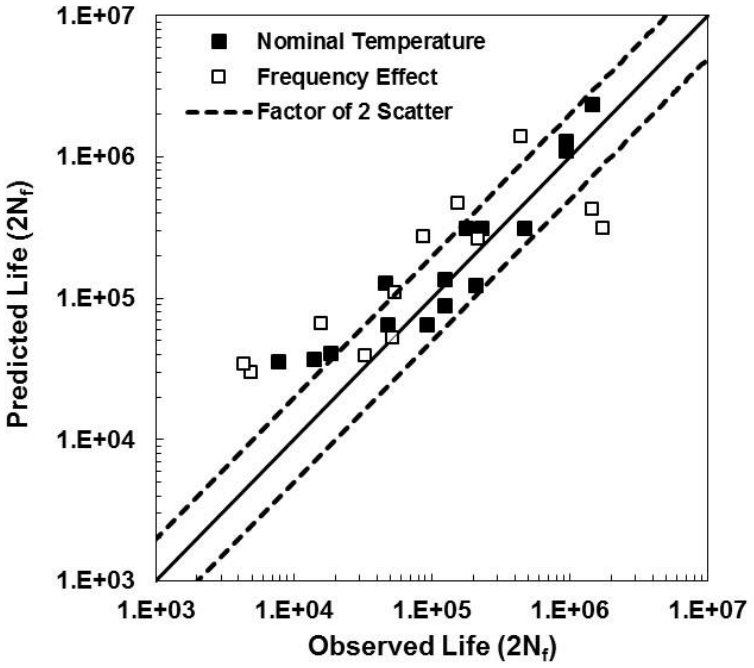

(b)

Figure 1.14 (a) Smith-Watson-Topper (SWT) damage parameter versus reversals to failure, $2N_f$, for the uniaxial fully reversed fatigue tests with nominal temperature rise (Table 1.1), and (b) predicted fatigue lives using the SWT parameter versus experimentally observed fatigue lives for all strain-controlled fatigue data (Tables 1.1 and 1.3).

In the energy-based approach, the dissipated energy associated with the irrecoverable plastic deformation is assumed to be proportional to the damage that occurs in each cycle during fatigue process [33]. However, for the life of a material close to its fatigue limit, the corresponding dissipated energy density value becomes very small and is difficult to measure. Therefore, the total strain energy approach was introduced for fully-reversed fatigue tests and the expression for the total strain energy density, W^T, was proposed by including both plastic and elastic strain energy densities as [33]:

$$W^T = W^P + W^E \tag{1.15}$$

In this study, the plastic strain energy density was determined by calculating the area of the hysteresis loop by integration for each cycle, while the elastic strain energy density was calculated by obtaining the positive area under the hysteresis loop.

Since the majority of PEEK fatigue lives is spent in the cyclic stability region, as illustrated in Fig. 1.3, the plastic and elastic strain energy densities obtained at the half-life cycle in the cyclic stability region were determined and listed in Tables 1.1 and 1.3. The values of the plastic strain energy density, W_{HL}^P, and the total strain energy density, W_{HL}^T,(i.e., sum of both plastic and elastic energy densities) calculated at the half-life cycle were plotted against the reversal to failure for the PEEK data under strain-controlled test with nominal temperature rise (i.e., Table1.1), as shown in Fig. 1.15(a) and Fig. 1.16(a), respectively. Additionally, the predicted fatigue lives using the plastic and total strain energy densities at the half-life cycle were determined for all strain-controlled fatigue tests (i.e., Tables 1.1 and 1.3) and compared to the experimentally observed fatigue lives as illustrated in Figs. 1.15(b) and 1.16(b), respectively. As seen in these figures, about 77% of all the data and 75% of frequency effect test data are within scatter bands of two.

Both R^2 values of all observed and predicted fatigue lives with frequency effect using the plastic and total strain energy densities at the half-life cycle were determined to be 0.87. Due to the minimal differences between Figs. 1.15 and 1.16, one may suggest that the elastic strain energy density has a very small effect on the fatigue behavior of PEEK at the cyclic stability region. A significant plastic strain is typically exists in the hysteresis stress-strain response of PEEK even for the smaller strain amplitude (0.02 mm/mm) tests, as can be seen in Fig. 1.8(a), which might be the reason that elastic strain energy density does not have a significant effect on the fatigue behavior of PEEK.

In Fig. 1.17(a), the cumulative plastic strain energy density was plotted against the reversals to failure for the strain-controlled experiments reported in Table 1.1. The direct proportionality is observed in this figure. In a study performed by Halford [34], the cumulative plastic energy strain density required for the fatigue failure obtained from more than 1,400 fatigue tests of various types of metals was presented. The results showed that the cumulative plastic strain energy increases with fatigue life irrespective to cycling conditions, test temperature, or initial state of the material [34]. Similar results were observed in this study for PEEK, for which the cumulative plastic strain energy density increased with the increase in fatigue life, as can be seen in Fig. 1.17(a). Figure 1.17(b) displays scatter bands of two for correlation between the predicted fatigue lives using the cumulative plastic strain energy density and the experimentally observed fatigue lives for all the strain-controlled test (Tables 1.1 and 1.3).

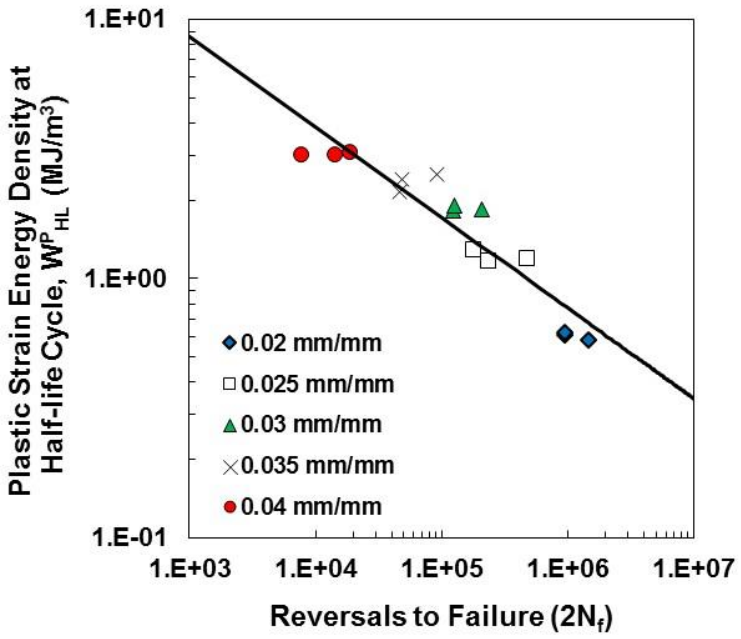

(a)

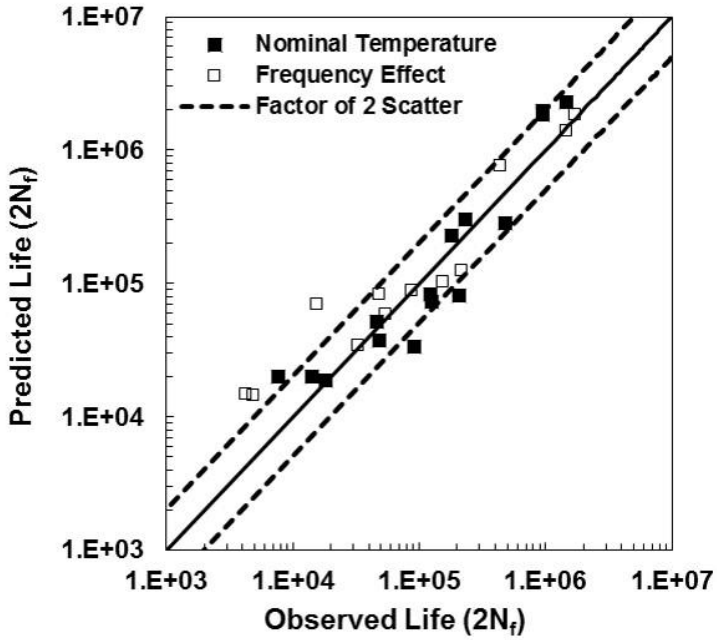

(b)

Figure 1.15 (a) Plastic strain energy density at half-life cycle, W_{HL}^P, versus reversals to failure, $2N_f$, for the uniaxial fully reversed fatigue test with nominal temperature rise (Table 1.1), and (b) predicted fatigue lives using this energy-based approach versus experimentally observed fatigue lives for all strain-controlled fatigue data (Tables 1.1 and 1.3).

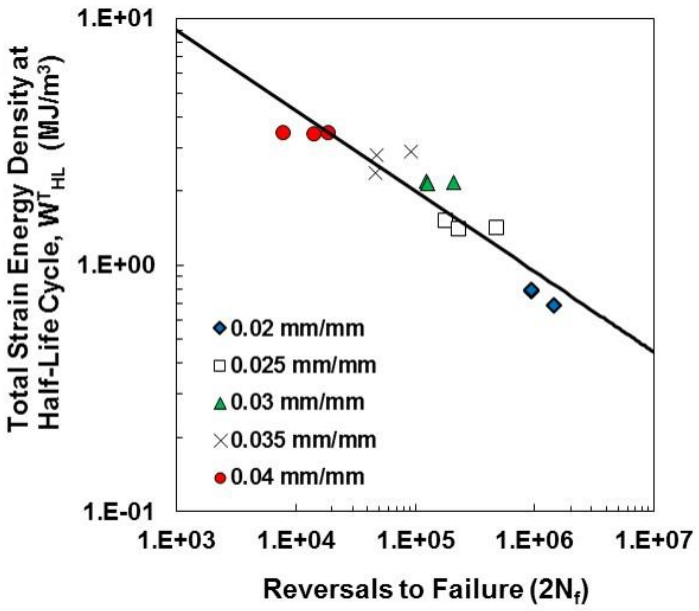

(a)

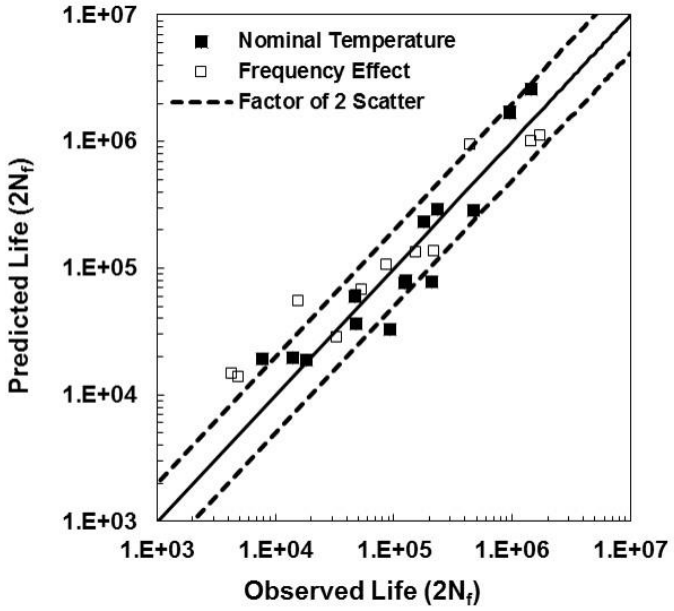

(b)

Figure 1.16 (a) Total strain energy density at half-life cycle, W_{HL}^T, versus reversals to failure, $2N_f$, for the uniaxial fully reversed fatigue test with nominal temperature rise (Table 1.1), and (b) predicted fatigue lives using this energy based approach versus experimentally observed fatigue lives for all strain-controlled fatigue data (Tables 1.1 and 1.3).

Numbers in the figure indicate the number of data points on top of each other.

Good agreement ($R^2 = 0.97$) was observed as all of the experimental data with nominal temperature rise and frequency effects are within the scatter band of two as compared to 77%, 59%, and 77% of those using the Coffin-Manson model, SWT damage parameter, and energy-based approach using the plastic strain energy density at the half-life cycle, respectively. However, it should be noted that, the transient energy-based approach considers sum of all the plastic strain energy density throughout the fatigue life of PEEK. Therefore, the reversals to failure data was embedded in the calculation of the cumulative plastic strain energy density, which may have, to some degree, contributed to the improved fatigue life predictions. It should be also mentioned that a difficulty in using energy based approaches for fatigue life predictions is requiring a constitutive stress-strain model to estimate the hysteresis stress-strain loop. Some further investigations to calibrate/develop a constitutive model capable of predicting cyclic stress-strain behavior of PEEK at different stages of initial, transition and cyclic stability then may be a necessity.

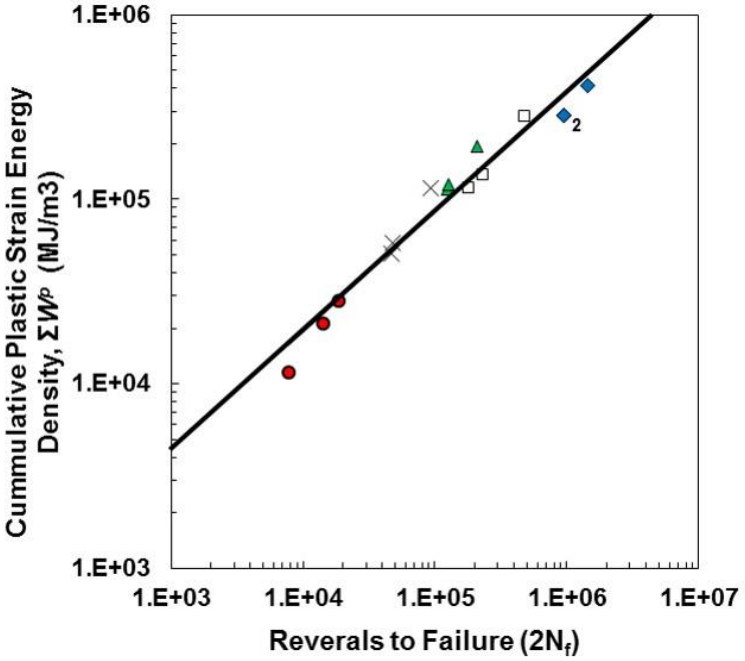

(a)

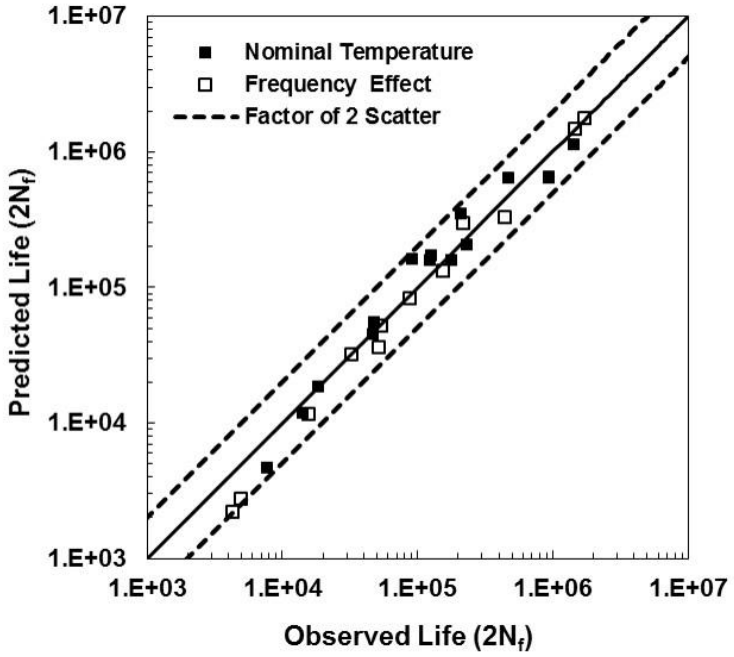

(b)

Figure 1.17 (a) Cumulative plastic strain energy density, $\sum W^P$, versus reversals to failure, $2N_f$, for the uniaxial fully reversed fatigue test with nominal temperature rise (Table 1.1), and (b) predicted fatigue lives using this transient energy-based approach versus observed experimentally observed fatigue lives for all strain-controlled fatigue data (Tables 1.1 and 1.3).

1.5 Conclusions

In this study, an unfilled PEEK thermoplastic was subjected to a series of experiments including uniaxial monotonic and cyclic tests. Three sets of uniaxial fully-reversed cyclic tests under various control modes were performed. These were (1) strain-controlled tests at five strain amplitudes with adjusted test frequencies to maintain the same nominal temperature on the specimen surface in all tests, (2) strain-controlled tests at various test frequencies to study the effects of loading frequency on cyclic deformation, fatigue life, and the change in temperature, and (3) load-controlled tests with the applied loads corresponding to the stress responses obtained from the strain-controlled tests. Three fatigue models; a strain-based (Coffin Manson) model, a strain-stress-based (Smith Watson Topper) model, and an energy-based model, were employed to predict the fatigue life of PEEK under the strain-controlled tests at various loading frequencies. Based on the effort performed in this study, the following conclusions may be drawn:

1. PEEK exhibited significant cyclic softening in both tension and compression when subjected to the uniaxial strain-controlled cyclic loading. Four distinct regions of cyclic stress behavior were identified. These included initial, transition, cyclic stability, and region of crack propagation. It was observed that the magnitude of the stress responses and the number of cycles in the initial region significantly affected the fatigue lifetime. The specimen that experienced the longer number of cycles in the initial region exhibited the shorter fatigue life when compared to those tested at the same strain amplitude and test frequency.

2. The cyclic softening effect of PEEK was more pronounced under cyclic loading at higher strain amplitudes. By keeping the same nominal temperature on the specimen surface in all tests, the specimens at higher strain amplitudes reached the transition region and the subsequent cyclic stability region faster than those tested at the lower strain amplitudes. The faster cyclic softening rate with the increasing strain amplitude was due to the modulus degradation.

3. The frequency effect on the cyclic behavior of PEEK is highly dependent on the strain amplitude level. Based on the test results, under fully-reversed strain-controlled condition, a minimal frequency effect was observed at a lower strain amplitude of 0.02 mm/mm. At higher strain amplitudes, increasing the test frequency resulted in longer fatigue lives. It should be, however, noted that the experimental data obtained from this study may not demonstrate the effects of test frequency on PEEK fatigue behavior with a high level of confidence due to the limited number of experiments conducted. Further studies are required to correlate frequency, temperature rise on the specimen, and strain energy density with the fatigue life.

4. Unlike most metals, the differences between the fatigue behavior of PEEK under uniaxial fully-reversed load-controlled and strain-controlled cyclic tests were significant. With a given applied stress corresponding to those attained from the strain-controlled tests, the strain responses under the load-controlled tests were substantially smaller than expected. It was evident that, under load-controlled cyclic tests, an increase in frequency led to smaller strain responses, which subsequently reflected a longer fatigue life.

5. Mechanical fatigue failure was not observed in all of the fully-reversed load-controlled tests. Instead, at a sufficiently high applied load and frequency, failure occurred due to cyclic necking that was similar to failure in monotonic testing.

6. Based on the experimental results in this study, it was concluded that the fatigue behavior of PEEK obtained under strain-controlled mode could not be directly related to its behavior under load-controlled fatigue loading. Therefore, it was suggested to evaluate fatigue behavior of PEEK components or structures under the operative control modes for the given application.

7. For the strain based fatigue analysis in this study, values for plastic strain were obtained only from the steady state stage, which represents deformation in cyclically stabilized region. However, the initial and transition regions were found to affect the overall fatigue behavior and total life for PEEK. Therefore, the Coffin-Mansion model may provide a better correlation of fatigue life in polymers if the deformation induced during initial and transition stages is incorporated.

8. Since the Smith-Watson-Topper (SWT) damage parameter, $\varepsilon_a \sigma_{max}$, is associated with only the product of two absolute values (strain amplitude and maximum tensile stress), this fatigue parameter did not necessary capture the shape of the hysteresis loop that changed throughout the cyclic loading for PEEK polymer. The shape of the hysteresis loop also differed with test frequency even for the same strain amplitude. Therefore, the SWT parameter could not well correlate the fatigue data in this study.

9. The transient energy-based approach that uses the cumulative plastic strain energy density as the damage parameter provided a better correlation with the PEEK experimental data under strain-controlled mode when compared to the energy based approaches using the plastic and total strain energy densities at the half-life cycle. This is due to the fact that unlike Coffin-Manson and SWT models, the cumulative plastic strain energy density was able to capture the shape of the hysteresis loop for all the cycles including initial, transition, and the cyclic stability regions.

10. Although the energy based approaches were shown to provide better fatigue life predictions than Coffin Manson and SWT models for PEEK, one of the disadvantages of energy based approaches is the fact that they require knowing the cyclic stress-strain behavior of the material. A constitutive cyclic stress-strain model for PEEK is, therefore, required to estimate the hysteresis stress-strain loops at different stages of initial, transition and cyclic stability.

1.6 References

[1] L. Sawyer, D. Grubb, and G. F. Meyers, Polymer microscopy, 3rd ed., Springer, 2008.

[2] S. M. Kurtz and J. N. Devine, "PEEK Biomaterials in Trauma, Orthopedic, and Spinal Implants," Biomaterials, vol. 28, pp. 4845-4869, 2007.

[3] D. P. Jones, D. C. Leach, and D. R. Moore, "Mechanical properties of poly(ether-ether-ketone) for engineering applications," Polymer, vol. 26, pp. 1385-1393, 1985.

[4] R. M. Jones, Mechanics of composite materials, 2nd ed., Taylor & Francis, 1998.

[5] R. W. Hertzberg and J. A. Manson, Fatigue of engineering plastics, 1st ed., Academic Press, 1980.

[6] R. J. Crawford, Plastics engineering, 3rd ed., Oxford: Butterworth-Heinemann, 1998.

[7] D. Kujawski and F. Ellyin, "A unified approach to mean stress effect on fatigue threshold conditions," International Journal of Fatigue, vol. 17, pp. 101-106, 1995.

[8] G. Tao and Z. Xia, "Mean stress/strain effect on fatigue behavior of an epoxy resin," International Journal of Fatigue, vol. 29, pp. 2180-2190, 2007.

[9] M. Shariati, H. Hatami, H. Yarahmadi, and H. R. Eipakchi, "An experimental study on the ratcheting and fatigue behavior of polyacetal under uniaxial cyclic loading," Materials & Design, vol. 34, pp. 302-312, 2012.

[10] S. R. Mellott and A. Fatemi, "Fatigue behavior and modeling of thermoplastics including temperature and mean stress effects," Polymer Engineering & Science, vol. 54, pp. 725-738, 2014.

[11] ASTM E606-04, Standard Practice for Strain-Controlled Fatigue Testing, ASTM International, West Conshohocken, PA, 2004.

[12] J. Zaroulis and M. Boyce, "Temperature, strain rate, and strain state dependence of the evolution in mechanical behaviour and structure of poly (ethylene terephthalate) with finite strain deformation," Polymer, vol. 38, pp. 1303-1315, 1997.

[13] J. Simsiriwong, R. Shrestha, M. Lugo, N. Shamshaei, and R. D. Moser, "Effects of microstructural inclusions on fatigue of poly ether ether ketone (PEEK)," Journal of the Mechanical Behavior of Biomedical Materials, In Press, doi:10.1016/j.jmbbm.2015.07.020.

[14] J. E. Mark, Physical properties of polymers handbook, AIP Press, 1996.

[15] J. A. Sauer and G. C. Richardson, "Fatigue of polymers," International Journal of Fracture, vol. 16, pp. 499-532, 1980.

[16] ASTM D7791-12, Standard Test Method for Uniaxial Fatigue Properties of Plastics, ASTM International, West Conshohocken, PA, 2012.

[17] P. I. Vincent, "The necking and cold-drawing of rigid plastics," Polymer, vol. 1, pp. 7-19, 1960.

[18] G. H. Michler, Electron microscopy of polymers, 1st ed., Springer, 2008.

[19] N. Mills, Plastics Microstructure and Engineering Applications, 3rd ed.: Butterworth-Heinemann, 2005.

[20] F. Rietsch and B. Bouette, "The compression yield behaviour of polycarbonate over a wide range of strain rates and temperatures," European Polymer Journal, vol. 26, pp. 1071-1075, 1990.

[21] J. Richeton, S. Ahzi, L. Daridon, and Y. Rémond, "A formulation of the cooperative model for the yield stress of amorphous polymers for a wide range of strain rates and temperatures," Polymer, vol. 46, pp. 6035-6043, 2005.

[22] S. Rabinowitz and P. Beardmore, "Cyclic deformation and fracture of polymers," Journal of Materials Science, vol. 9, pp. 81-99, 1974.

[23] D. J. Krzypow and C. M. Rimnac, "Cyclic steady state stress–strain behavior of UHMW polyethylene," Biomaterials, vol. 21, pp. 2081-2087, 2000.

[24] G. Tao and Z. Xia, "An experimental study of uniaxial fatigue behavior of an epoxy resin by a new noncontact real-time strain measurement and control system," Polymer Engineering & Science, vol. 47, pp. 780-788, 2007.

[25] R. I. Stephens, A. Fatemi, R. R. Stephens, and H. O. Fuchs, Metal Fatigue in Engineering, 2nd ed. New York: John Wiley & Sons, 2000.

[26] S. Mortazavian and A. Fatemi, "Fatigue behavior and modeling of short fiber reinforced polymer composites: A literature review," International Journal of Fatigue, vol. 70, pp. 297-321, 2015.

[27] A. Bernasconi and R. M. Kulin, "Effect of frequency upon fatigue strength of a short glass fiber reinforced polyamide 6: A superposition method based on cyclic creep parameters," Polymer Composites, vol. 30, pp. 154-161, 2009.

[28] S. Mortazavian, A. Fatemi, S. R. Mellott, and A. Khosrovaneh, "Effect of cycling frequency and self-heating on fatigue behavior of reinforced and unreinforced thermoplastic polymers," Polymer Engineering & Science, 2015, in press.

[29] ASTM E739-10, Standard Practice for Statistical Analysis of Linear or Linearized Stress-Life (S-N) and Strain-Life (ε-N) Fatigue Data, ASTM International, West Conshohocken, PA, 2010.

[30] D. Kujawski, "A deviatoric version of the SWT parameter," International Journal of Fatigue, vol. 67, pp. 95-102, 10 2014.

[31] J. Colin and A. Fatemi, "Variable amplitude cyclic deformation and fatigue behaviour of stainless steel 304L including step, periodic, and random loadings," Fatigue & Fracture of Engineering Materials & Structures, vol. 33, pp. 205-220, 2010.

[32] K. Smith, T. Topper, and P. Watson, "A stress-strain function for the fatigue of metals(Stress-strain function for metal fatigue including mean stress effect)," Journal of materials, vol. 5, pp. 767-778, 1970.

[33] F. Ellyin, Fatigue damage, crack growth and life prediction, 1st ed., Chapman & Hall, 1997.

[34] G. R. Halford, "The energy required for fatigue," Journal of Materials, vol. 1, p. 3, 1966.

CHAPTER II

MEAN STRAIN EFFECTS ON CYCLIC DEFORMATION AND FATIGUE BEHAVIOR OF POLYETHER ETHER KETONE (PEEK)

(Polymer Testing, 2016, 55, 69-77)

2.1 Abstract

In this study, the fatigue behavior of polyether ether ketone (PEEK) thermoplastic was investigated under uniaxial strain-controlled cyclic loading condition with various mean strains ($R_\varepsilon = 0$, 0.2, and 0.25). The mean stress responses of PEEK from all mean strain fatigue tests were found to be fully relaxed. As a result, minimum mean strain effect on fatigue behavior of PEEK was observed. Fractography analyses utilizing a scanning electron microscope were performed on PEEK specimens under tensile mean strain cyclic loading. Two distinct stages of fatigue process, including the crack initiation and the physically small crack growth, were observed on all the fracture surfaces. Moreover, two types of inclusions, unmelted particles and void-like defects, were identified to be the cause of crack initiation. Void-like defects were found to have more detrimental effects on fatigue life of PEEK when compared to particles of similar size. The effect of inclusions on fatigue behavior of PEEK was observed to be more significant than that of the tensile mean strain.

2.2 Introduction

With the advancement in the field of polymer science and engineering, new generation of polymers with tailored properties have been developed to meet specific requirements for various applications. Polymeric materials generally offer a variety of unique characteristics including relatively high strength, good chemical and corrosion resistance, lubricity, ease of processing, and cost effectiveness. In addition, due to a relative high strength to weight ratio, polymers are considered as ideal candidates for structural components in automotive and aerospace industries where light-weighting is required to improve the fuel efficiency [1].

Polyether ether ketone (PEEK), a semi-crystalline, high-performance engineered thermoplastic is the material of interest in this study. Due to its excellent dimensional stability and mechanical properties under extreme conditions, PEEK and its composites are widely used in oil and gas applications as compressor valve plates, seals and gaskets, pipes, etc. [2]. Moreover, selected grades of PEEK polymer are designed to conform to the strict requirements of the Food and Drug Administration to be used in a wide range of biomedical components, from sterilization equipment and temporary dentistry implants to long-term orthopedic implants [3, 4]. As the majority of these PEEK components are typically subjected to cyclic loading, the fatigue characterization of the material is therefore a necessity.

Unlike fatigue in metallic materials, the fundamental understanding underlying the fatigue process in polymers has not been fully realized. This may be due in part to the complexities of polymer structure, which poses a challenge in obtaining the overall failure processes and their correlation with loading conditions [5]. The problem is

compounded by the facts that the fatigue behavior of polymers are sensitive to material variables, such as the crystalline morphology as well as loading variables, including frequency, waveform, temperature, etc. [6]. The dependency on time and frequency is inherent to polymeric materials due to their viscoelastic nature. However, despite the growing use of polymeric materials, only a small number of experimental investigations have been performed to study the fatigue behavior of polymers under mean stress/strain conditions.

Sauer et al. [7] conducted a series of load-controlled fatigue experiments on polystyrene (PS) to obtain the effect of tensile mean stress by varying the alternating stress ratio, A, which is a ratio of alternating stress (or stress amplitude) to mean stress. The alternating stress ratios were adjusted using two approaches; increasing the mean stress while keeping the stress amplitude constant, and varying both the stress amplitude and mean stress with fixed maximum stress value. For a constant stress amplitude, shorter fatigue lives were observed for PS as tensile mean stress increased. On the other hand, for a constant maximum stress, increase of tensile mean stress and decrease of alternating stress resulted in longer fatigue lives. In some cases, the average fatigue life of PS was reported to be three or four times greater than that obtained from the fully-reversed cyclic loading at the same maximum stress value [7]. This may be explained by more influential effect of stress amplitude as compared to mean stress on the fatigue behavior of PS. The presence of tensile mean stress has been also observed to have detrimental effects on fatigue life of other polymers, including acetal [8], epoxy [9], polyoxymethylene [10], and polypropylene (PP) [11].

Fewer studies have been conducted on polymers to obtain their fatigue behavior under strain-controlled condition with a presence of mean strain. Tao and Xia [12, 13] investigated mean strain effects on fatigue life of an epoxy polymer subjected to uniaxial strain-controlled cyclic loading. For the same strain amplitude, the fatigue life of epoxy decreased with increase of mean strain to strain amplitude ratio. Mean stress relaxation was also observed during initial loading cycles in all tests [12]. Chen and Wong [14] studied the fatigue behavior of nylon 6 and PP under nonzero mean strain cyclic tests at various temperatures (e.g. -40ºC, 25ºC, 65ºC, and 125ºC). They reported the tensile mean strain to reduce the fatigue resistance of both investigated polymers at all test temperatures [14].

As mentioned earlier, fatigue behavior of polymers is highly sensitive to loading, material, and environment variables. In this study, an experimental investigation has been conducted to obtain the fatigue behavior of PEEK thermoplastic subjected to strain-controlled cyclic loadings with various mean strains (ratios of minimum to maximum strain, R_ε, of 0, 0.2, and 0.25).The experimental program, including the material description and fatigue test setup, are presented. The effects of mean strain on cyclic deformation and fatigue life of PEEK are then discussed. Fractography results displaying crack initiation sites, inclusions responsible for crack initiation, as well as crack propagation characteristics of PEEK specimens are also presented. Finally, conclusions and recommendations are made based on the experimental observations in this study.

2.3 Material and Experimental Procedure

Neat PEEK polymer (TECAPEEK™ by Ensinger Inc.) with a glass transition temperature of 143°C and a melt temperature of 343°C was selected in this study. Round

specimens with uniform gage section were machined from 12.8 mm diameter extruded PEEK rod using an oil based coolant to reduce heat buildup on specimens. The dimensions and geometry for specimens, as presented in Fig. 1.1, were designed in conformance with ASTM E606/E606M standard [15] with gage section diameter and length of 6.35 mm and 18 mm, respectively. The specimens were further polished in several stages to remove machining marks, resulting in an average surface finish of 3.4 μm in the gage section. The polished specimens were stored in a cool-dry climate-controlled environment prior testing.

In this study, uniaxial strain-controlled fatigue experiments were conducted on PEEK specimens using constant amplitude loading with various R_ε values. Previous studies [16, 6] observed significant plastic deformation in PEEK specimens when subjected to cyclic loading; therefore, strain-controlled tests, which can better characterize the fatigue behavior of a material that exhibits localized plastic deformation as compared to force controlled tests, were performed in this study. Experimental results also indicated that the fatigue behavior of PEEK polymer obtained under strain-controlled condition could not be directly correlate to its behavior under force-controlled condition. As a result, the fatigue behavior of PEEK should be evaluated depending on the loading condition for a given application, many of which are under cyclic deformation.

Moreover, it has been reported that PEEK polymer exhibits self-heating when subjected to cyclic loading due to its low thermal conductivity and high damping characteristics [16, 6]. Consequently, there is a conversion of input energy into heat that causes an initial rise in the specimen temperature, which may be stabilized when the heat

generated equals to the heat transferred to surrounding environment. However, in certain test conditions when the specimen is subjected to a high strain/stress amplitude and/or test frequency, the temperature rise in the specimen, ΔT, does not stabilize; thus, leading to a thermal failure. Therefore, ΔT was monitored throughout testing to avoid thermal failure and ensure mechanical fatigue failure in all specimens.

All fatigue tests were conducted in accordance with ASTM D7791-12 standard [17] at ambient laboratory temperature (~23ºC) and humidity (~50% humidity) using a closed loop servo-hydraulic load frame with a 25 kN load cell. The grip sections of specimens were secured to the load frame using hydraulically operated wedge grips. Tests were performed using a sinusoidal waveform. Axial strain was measured using a mechanical extensometer with 15 mm gage length. The failure criterion was defined as 50% load drop and runout tests were stopped at 10^6 cycles. At least two tests were conducted for each prescribed test condition. A portable laser thermometer (Optris laser thermometer LS LT) was used to monitor the surface temperature of the specimen gage section.

Constant amplitude uniaxial strain-controlled fatigue tests were conducted at strains ranging from zero to 0.06 mm/mm at three R_ε values (0, 0.2, and 0.25). The following tensile mean stain values were used; 0.02, 0.025, and 0.03 mm/mm for $R_\varepsilon = 0$ (pulsating tension) tests, 0.03 mm/mm for $R_\varepsilon = 0.2$ tests, and 0.0375 mm/mm for $R_\varepsilon = 0.25$ tests. The representations of different strain cycles for these tests are illustrated in Fig. 2.1. Test frequencies ranging from 0.5 Hz to 1.5 Hz were selected to maintain similar strain rate and temperature rise (ΔT) on the surface of the specimen gage section. In addition, fracture surfaces of specimens subjected to constant amplitude loading with

mean strains were examined using a scanning electron microscope (SEM). Specimens were first cut, mounted, and sputter coated with a thin layer of gold for SEM analysis. The fracture surfaces were inspected to obtain microstructural inclusion factors (i.e. particles, voids, etc.) for crack initiation and evidence of propagation.

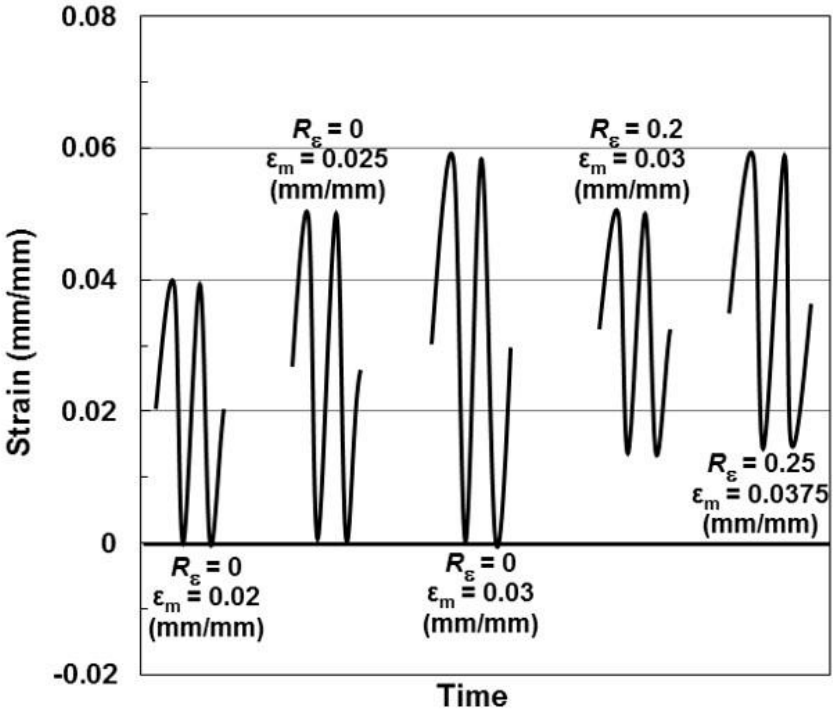

Figure 2.1 Representation of different strain cycles used for mean strain fatigue tests for PEEK thermoplastic in this study.

2.4 Experimental Results and Discussions

2.4.1 Cyclic Deformation and Fatigue Behavior

In this section, the effects of tensile mean strain on cyclic deformation and fatigue behavior of PEEK are discussed. The experimental data from constant amplitude fatigue tests with mean strains are summarized in Table 2.1, which includes strain amplitude, ε_a, mean strain, ε_m, test frequency, f, strain ratio, R_ε, stress amplitude, σ_a, mean stress, σ_m,

reversals to failure, $2N_f$, and the rise in temperature on the specimen gage surface, ΔT. The stress amplitude, σ_a, and mean stress, σ_m, listed in this table, were obtained from the half-life cycle.

The temperature rise in polymer under cyclic loading is due to the self-heating resulting from low thermal conductivity and high damping characteristics, which has been discussed in Section 2. The frequency effect on the fatigue behavior of PEEK with zero mean strain was investigated previously [6]. For tests with non-zero mean strains performed in the present study, test frequencies were adjusted for each combination of strain amplitude and strain ratio to maintain relatively constant strain rate and temperature rise on the specimen's gage section in all tests

Table 2.1 Experimental results for PEEK polymer subjected to uniaxial strain-controlled fatigue loading with mean strains.

Specimen ID	ε_a (mm/mm)	ε_m (mm/mm)	Frequency (Hz)	R_ε Value	σ_a^* (MPa)	σ_m^* (MPa)	$2N_f$ (Reversals)	ΔT (°C)	ΔW_{HL}^P (MJ/m^3)
S86	0.02	0.02	1.5	0	42	-1.98	475,726	31	0.78
S76					47	7.71	696,398	43	0.68
S83					45	0.98	874,850	32	0.74
S78	0.025	0.025	1		46	4.11	318,690	45	1.2
S88					46	1.59	443,580	29	1.2
S84					43	-0.80	535,546	34	1.3
S85	0.03	0.03	0.5		49	2.51	77,892	37	1.9
S87					53	-0.95	83,096	28	1.8
S81					48	1.40	155,458	39	1.7
S92	0.02	0.03	1.5	0.2	45	2.50	578,224	24	0.69
S91					41	4.56	671,842	29	0.74
S89					46	7.50	887,634	26	0.71
S97	0.025	0.0375	1	0.25	47	1.92	231,896	22	0.98
S99					47	2.03	347,108	21	0.98
S90					48	3.84	483,868	24	0.95

*Measured at half-life cycle

The rise in temperature, cyclic deformation, and hysteresis stress-strain responses of PEEK under R_ε = 0 and ε_a = 0.025 mm/mm at 1 Hz condition (specimen S78) are presented in Fig. 2.2(a). The fatigue life of approximately 320,000 reversals and ΔT of 46ºC are obtained for specimen S78. Unlike the cyclic softening for PEEK under fully-reversed (R_ε = -1) fatigue tests, where four distinct regions of stress responses (i.e. initial, transition, cyclic stability, and final failure) were observed [6], the cyclic softening for PEEK with R_ε = 0 was not noticeably evident. The four regions of cyclic softening can be illustrated in Fig. 2.2(b) for specimen S31 subjected to R_ε = -1 and ε_a= 0.025 mm/mm at 1 Hz test condition [6]. Additionally, the stress range during testing for specimen S78 only reduced from approximately 120 MPa to 90 MPa, as compared to its fully-reversed counterpart at similar strain amplitude in Fig. 2.2(b), which had a reduction in stress range from 180 MPa to 90 MPa and a comparable ΔT value of 52 ºC [6].

As presented in Fig. 2.2(a), PEEK thermoplastic under pulsating strain loading exhibited significant mean stress relaxation immediately upon the initial cycling. The mean stress continuously relaxed as cycling progressed and became fully relaxed at approximately 2,000 reversals (less than 1% of total life). Similar behavior was observed in all mean strain tests, where the mean stress response was fully-relaxed in a relatively short time period compared to the total life and the mean stress as well as stress range thereafter held stable for the remaining life. The increasing in the size of the hysteresis loops in this figure indicates the increasing amount of plastic deformation with continued straining up to cyclic stability region. Evolution of the hysteresis loop also indicates the mean stress relaxation phenomenon as the value of mean stress decreases from 58 MPa at initial region to 33 MPa at the transition region, and finally stabilizes to nearly zero at the

cyclic stability region. On the other hands, small compressive mean stress (~ -17 MPa) was observed at the cyclic stability region for specimen S31 tested under R_ε = -1 and ε_a = 0.025 mm/mm test condition in [6], as can be noticed in Fig. 2.2(b). It should be noted that the shape of the hysteresis loops for specimens with zero mean strain are generally symmetric throughout the cyclic process (Fig. 2.2(b)), while the initial irregular shape of the hysteresis loops of specimens with tensile mean strain become more symmetric as the number of cycle increases (Fig. 2.2(a))

Using the PEEK fatigue data with mean strains (i.e. data in Table 2.1), the mean stress values were plotted against number of reversals in Fig. 2.3 to investigate the effect of strain amplitude on the stress relaxation rate. Figure 2.3(a) shows the mean stress evolution for PEEK specimens S83, S88, and S81, which were all tested under R_ε= 0 condition with strain amplitudes of 0.02, 0.025, and 0.03 mm/mm, respectively. As seen in Fig. 2.3(a), the initial mean stress (i.e. up to approximately 200 reversals) relaxed faster for the specimen subjected to a larger strain amplitude. At around 200 reversals, the mean stress values for all specimens in Fig. 2.3(a) reduced to nearly 10% of the mean stress magnitude of the initial loading cycles.

The mean stress continued to decrease, but at a much lower rate, and eventually were fully-relaxed at approximately 2,000 reversals. As a result, one may conclude that, while the rate of relaxation increases by increasing strain amplitude, the mean stress of PEEK relaxes to a stable value close to zero under strain-controlled condition with non-zero mean strain, independent of the strain amplitude level. A similar observation was also reported for an epoxy polymer, where the rate of mean stress relaxation increased with increasing strain amplitude under constant strain ratio [12].

To obtain the effect of strain ratio on the mean stress relaxation, the mean stress of specimens subjected to various R_ε values, but at comparable strain amplitudes, were plotted against number of reversals, $2N$. Figure 2.3(b) presents the mean stress evolution of specimens S83, S91, S99, which were tested under R_ε = 0, 0.2, and 0.25, respectively. The R_ε = 0 and 0.2 experiments were conducted at ε_a = 0.02 mm/mm, while R_ε = 0.25 test was performed at ε_a = 0.025 mm/mm. It was observed that, while almost fully-relaxed mean stress was achieved around 2,000 reversals for all test conditions, the initial mean stress relaxation rate was higher for larger R_ε values at comparable strain amplitudes. The strain-life fatigue behavior of PEEK specimens tested under constant amplitude condition with various mean strains is presented in Fig. 2.4. In addition, the fully-reversed (R_ε = -1) PEEK data [6] are included in this figure. As seen, fatigue lives for PEEK with various mean strains (R_ε = 0, 0.2, and 0.25) were observed to be within a factor of three of those under fully-reversed (R_ε = -1) loading conditions. For examples, the average lives of PEEK specimens tested at 0.02 mm/mm were 1,114,464 reversals for R_ε = -1 [6], 682,324 reversals for R_ε = 0 (specimens S86, S76, and S83 in Table 2.1), and 712,567 reversals for R_ε = 0.2 (specimens S92, S91, and S89 in Table 2.1). The small effect of tensile mean strain on fatigue behavior of PEEK observed in this study may be attributed to the fully-relaxed mean stress response, as illustrated in Figs. 2.2 and 2.3.

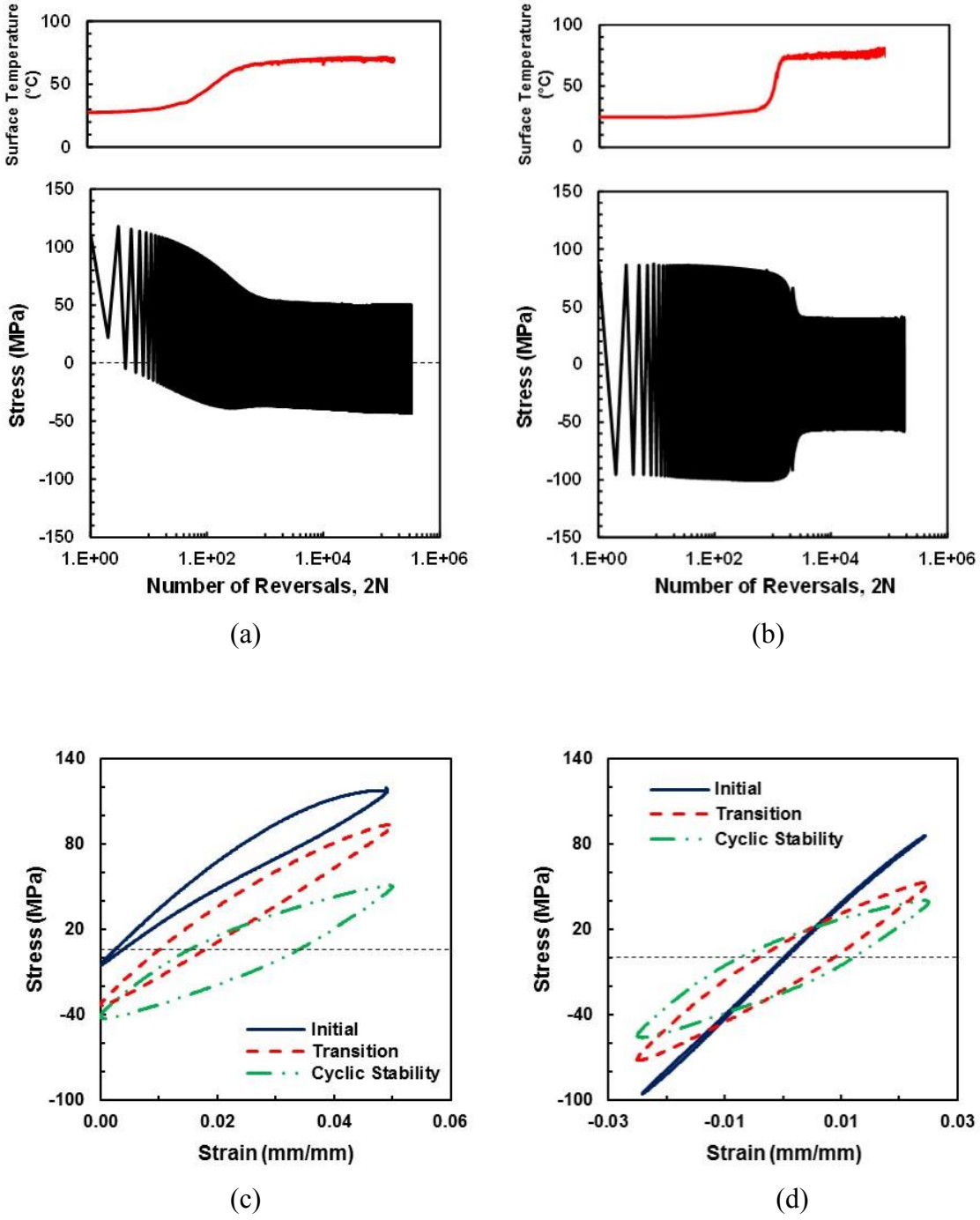

Figure 2.2 Surface temperature, stress responses and hysteresis loops at different stages of cyclic deformation of fatigue tests at ε_a= 0.025 mm/mm and 1 Hz for (a) specimen S78 with R_ε = 0 and (b) specimen S31 with R_ε = -1 [6].

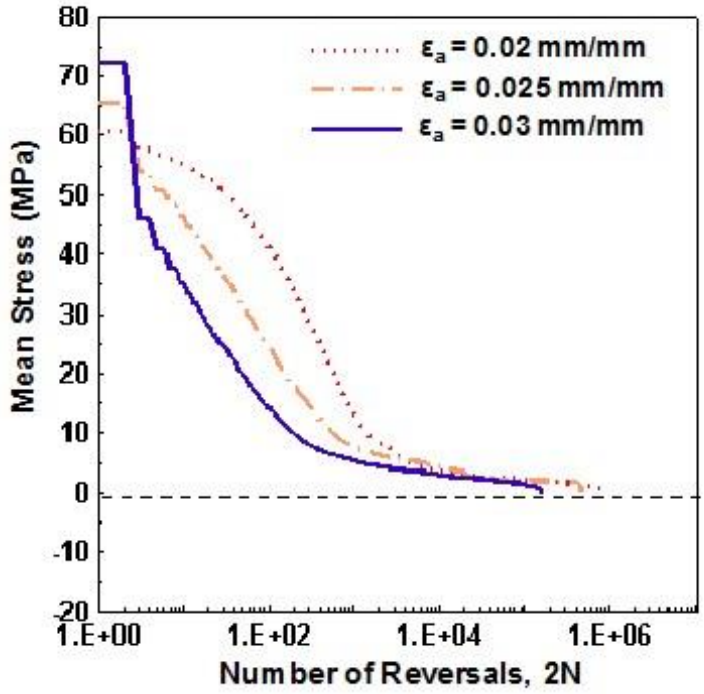

(a)

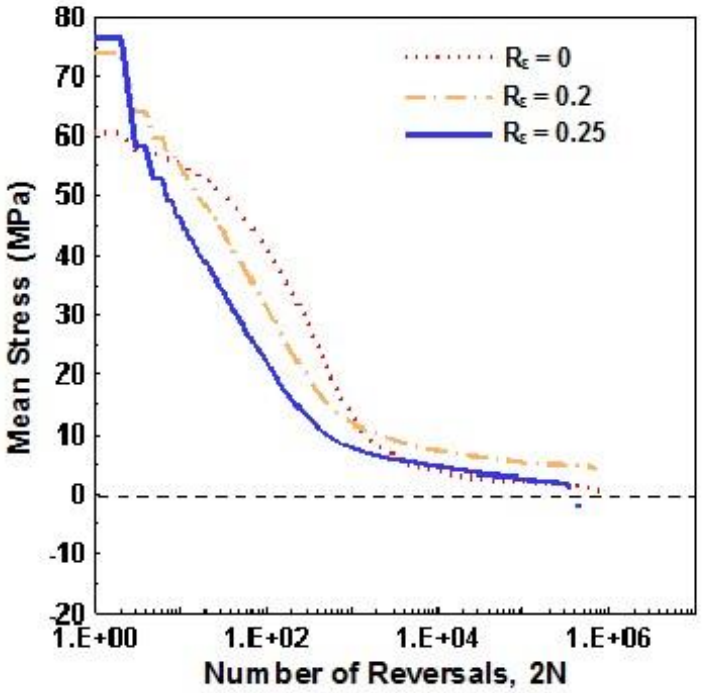

(b)

Figure 2.3 Mean stress versus number of reversals of PEEK fatigue specimen for (a) tests at various strain amplitudes and $R_\varepsilon = 0$, and (b) tests at 0.02 mm/mm and various R_ε values.

Furthermore, as seen in Fig. 2.4, slightly shorter or longer fatigue lives for PEEK with a presence of mean strain were observed. For example, shorter fatigue lives were noticed for specimens subjected to 0.02 mm/mm and 0.03 mm/mm with tensile mean strain when compared to specimens under fully-reversed loading condition at comparable strain amplitudes. On the other hand, some beneficial effect of tensile mean strain was obtained for specimens tested at 0.025 mm/mm. As a result, one may conclude that the presence of tensile mean strain may not necessary result in shorter fatigue lives for PEEK.

Although the rate of cyclic softening (amount of cyclic softening per cycle) may be slightly different, it should be noted that similar level of cyclic softening and hysteresis stress-strain responses at the cyclic stability region for specimens with zero and non-zero mean strain were observed, as previously illustrated in Fig. 2.2. In addition, it has been shown in [6] that the number of cycles spent in the initial region of cyclic softening may affect the fatigue life of PEEK specimens, where the PEEK specimen with greater number of cycles in the initial region of cyclic softening exhibited the shortest fatigue life when compared to those subjected to the identical test condition. It can be noticed that specimens with tensile mean strain, as shown in Fig. 2.2, typically have shorter number of cycles in the initial region of cyclic softening when compared to those without mean strain. In addition, some tensile mean stress, which is generally detrimental to fatigue life, can be observed during the initial cycles. Therefore, the combination of these two (number of cycles in the initial region of cyclic softening and the presence of tensile mean stress) may result the specimens with tensile mean strain to exhibit slightly shorter or longer fatigue lives as compared to the fully-reversed ones.

The combined effects of frequency and rise in temperature on dissipated strain energy was investigated for the uniaxial strain-controlled fully-reversed (R_ε = -1) test in an earlier study [6]. Similar approach is conducted in the present work to obtain the relationship between frequency, f, rise in temperature, ΔT, and dissipated plastic strain energy density at half-life cycle, W_{HL}^P, for PEEK specimens subjected to cyclic loading in presence of mean strains. The energy parameter W_{HL}^P was measured by determining the area of hysteresis stress-strain loop at half-life cycle using an integration method. A linear relationship expressed by Eq. (2.1) was proposed by Bernasconi and Kulin [18] for short glass fiber reinforced polyamide 6:

$$\frac{\Delta T}{f} = BW_{HL}^P \tag{2.1}$$

where B is a material constant and W_{HL}^P, reported in Table 2.1 for all constant amplitude fatigue tests, is the plastic strain energy density represented by the area of the hysteresis loop at half-life cycle. Using the linear relation expressed by Eq. (2.1), the ratio of rise in temperature to the test frequency, $\Delta T/f$, is plotted against the dissipated plastic strain energy at half-life cycle, W_{HL}^P, in Fig. 2.5(a) for all the specimens under constant amplitude fatigue loading with mean strains (i.e. data in Table 2.1). The fully-reversed (R_ε = -1) fatigue data from [6], which include both nominal temperature rise tests as well as those conducted to study the frequency effect, are also included in this figure. As seen, while better correlation is obtained for tests with lower $\Delta T/f$ values, some scatter is noticeable at higher $\Delta T/f$ values (i.e. higher strain amplitude tests). Nonetheless, an acceptable correlation, indicated by the R^2 = 0.89 between $\Delta T/f$ and W_{HL}^P, can be realized

in this figure for all tests with zero and non-zero mean strains and at different frequencies.

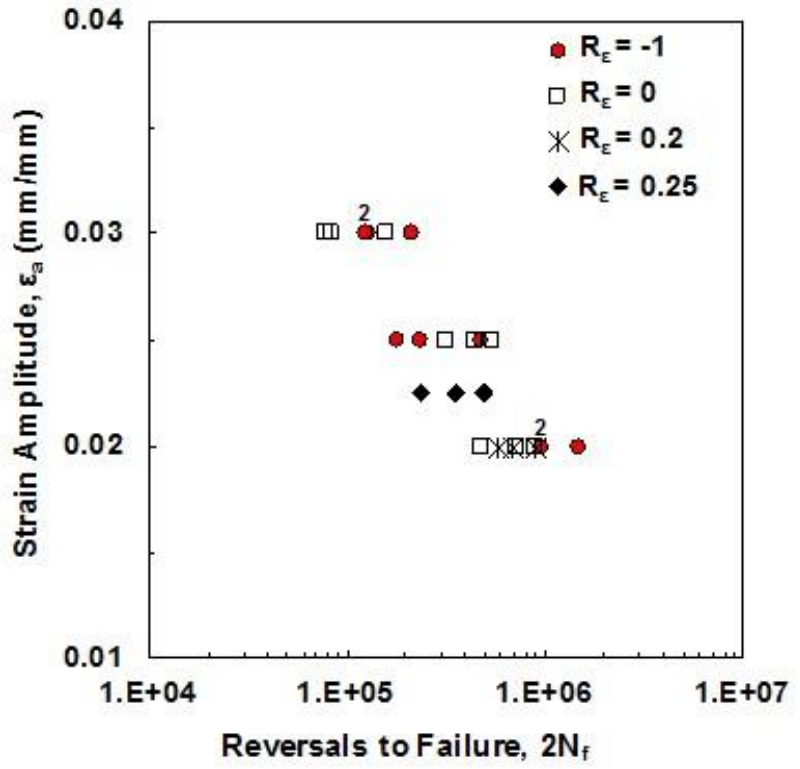

Figure 2.4 Strain-life fatigue behavior of PEEK specimens under strain-controlled fully-reversed (R_ε = -1) [6] and tensile mean strains (R_ε = 0, 0.2, and 0.25) cyclic loadings in Table 2.1.

A different approach to correlate the temperature rise in specimen under cyclic loading to test frequency, proposed by Krause [19], was also employed in this study. Krause's model was initially developed for glass fiber reinforced laminates [19] and recently has been validated for reinforced and unreinforced PP, as well as PP blended with 25 wt% elastomer and filled with 30% magnesium silicate [20]

Based on this model, the ratio of temperature rise in the specimen to cycling frequency can be expressed as:

$$\frac{\Delta T}{f} = C\sigma_a(\varepsilon_a)^2 \tag{2.2}$$

where C is a material constant. Using the data in Table 2.1, the correlation for $\Delta T/f$ and $\sigma_a(\varepsilon_a)^2$ is presented in Fig. 2.5(b) for all fatigue data with tensile mean strain. Similar to Fig. 2.5(a), PEEK fatigue data reported in [6] for fully-reversed (R_ε = -1) condition with various frequencies are also included in this figure. Although some scatter is noticeable at higher $\Delta T/f$ values, a reasonable correlation, expressed by R^2 = 0.84, is obtained. Based on the results shown in Fig. 2.5, one may suggest that fatigue prediction models utilizing energy-based approaches may be suitable for PEEK polymer subjected to mean strain cyclic loading.

2.4.2 Fractography Analysis

The fractography analysis was conducted on fatigue specimens subjected to various R_ε values to determine microstructural inclusions responsible for fatigue crack initiation, as well as to observe crack propagation behavior of PEEK. Under fully-reversed (R_ε = -1) cyclic loading, two distinct stages of fatigue process were observed for PEEK polymer [16]. These include (1) crack initiation stage, which consists of crack incubation (i.e. nucleation period of a crack) and microstructural small crack (MSC), and (2) physically small crack (PSC) stage

The fracture surface of specimen S86 subjected to 0.02 mm/mm and R_ε = 0 loading condition is illustrated in Fig. 2.6, which also represents a typical fatigue fracture surface observed for all PEEK specimens with mean strains (i.e. specimens in Table 2.1).

Both crack initiation and PSC stages are noticeable in this figure. In addition, Simsiriwong et al. observed two different types of inclusions, including particles (i.e. unmelted particles) and void-like defects as respectively displayed in Figs. 2.6 and 2.7 of their paper [16], to be responsible for crack initiation in PEEK. Similar inclusions were also found to be responsible for fatigue crack initiation in specimens with tensile mean strains in this study. For specimen S86 in Fig. 2.6, a subsurface particle with the approximated size of 34 μm, determined from the square root of the projected area of the particle as described in [21], caused the crack initiation Figure 2.7 displays SEM images of the fracture surface of specimens S86 ($2N_f$ = 475,726 reversals), S76 ($2N_f$ = 696,398 reversals), and S83 ($2N_f$ = 874,850 reversals), which were all subjected to pulsating cyclic loading ($R_\varepsilon = 0$) with 0.02 mm/mm strain amplitude. The crack initiation site (i.e. incubation + MSC region) was also identified for each specimen and the area of crack initiation site was obtained from SEM images using an image processing software. Fatigue crack in all specimens in Fig. 2.7 was initiated from a subsurface particle of a similar size

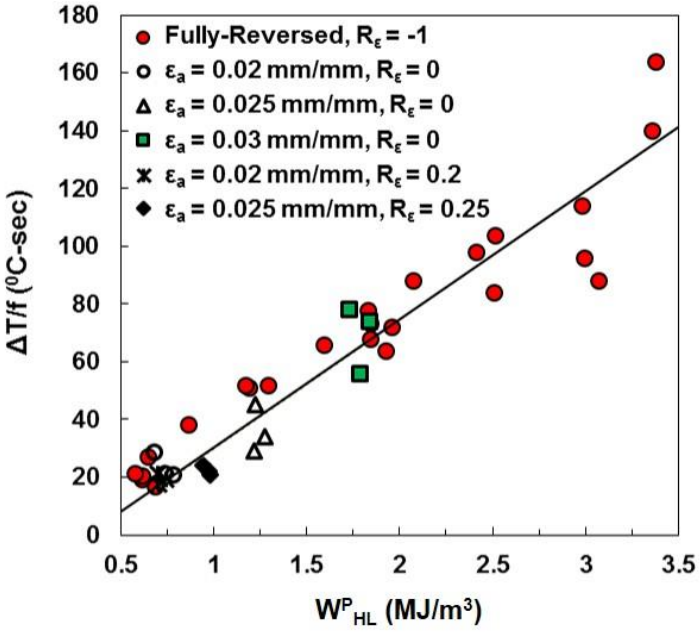

(a)

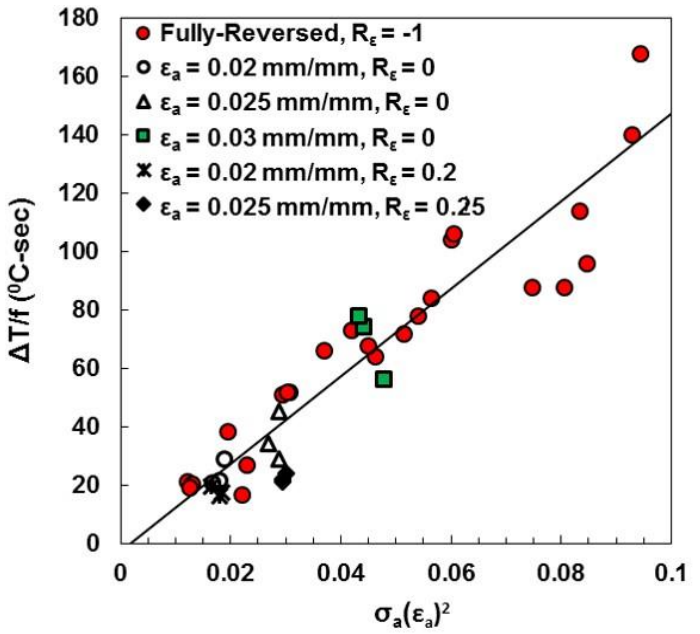

(b)

Figure 2.5 (a) The ratio of the rise in temperature to test frequency, $\Delta T/f$, versus the plastic strain energy density at half-life (cyclic stability region), W_{HL}^P, and (b) the ratio of $\Delta T/f$ versus $\sigma_a(\varepsilon_a)^2$ for strain-controlled fatigue data with and without tensile mean strains.

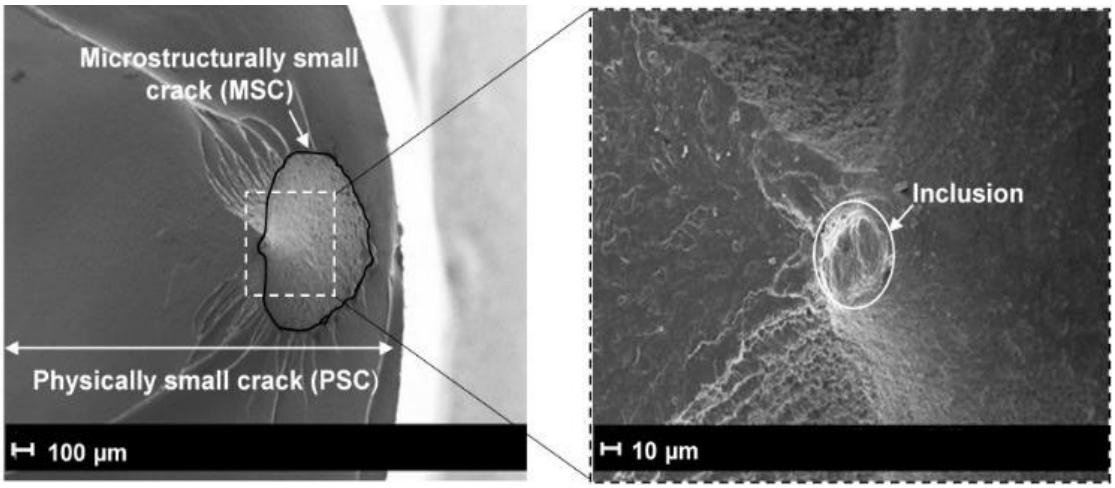

Figure 2.6 SEM images of the fracture surface of PEEK specimen S86 tested at 0.02 mm/mm strain amplitude with $R_\varepsilon = 0$, showing (a) an overview of fatigue failure stages including crack initiation, microstructurally small crack (MSC), and physically small crack (PSC), and (b) the inclusion caused the crack initiation.

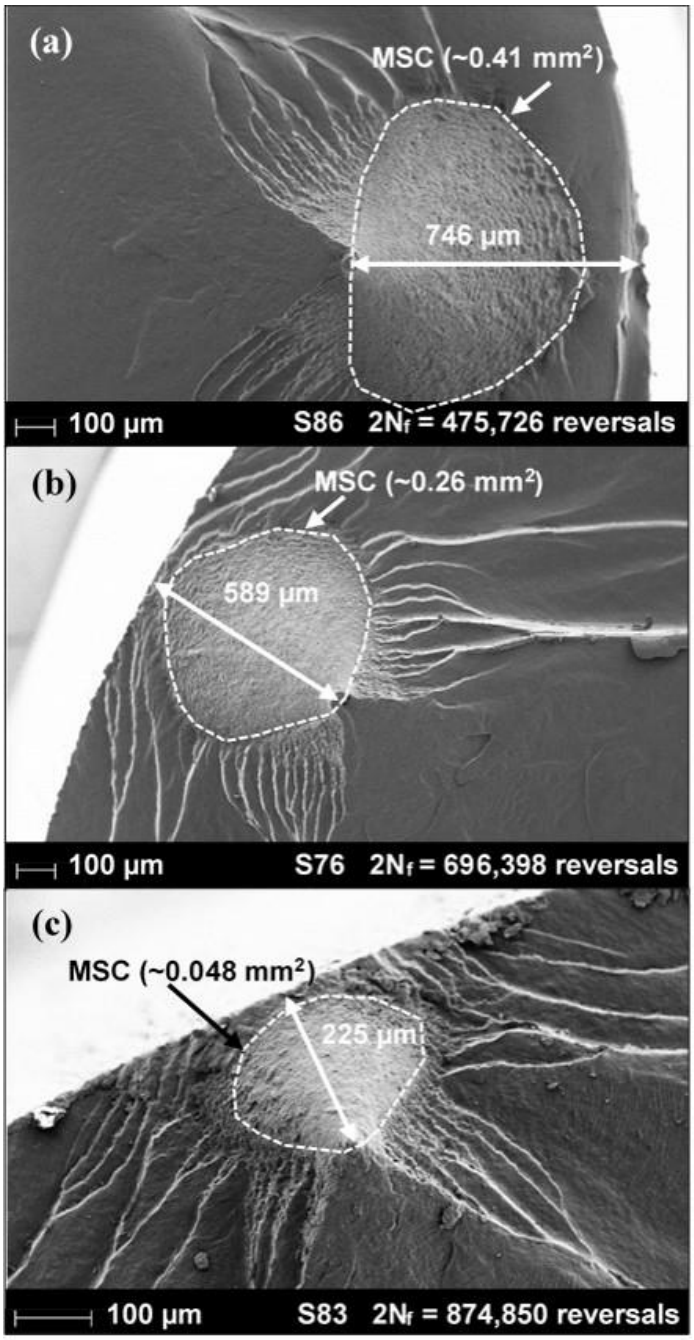

Figure 2.7 Fracture surfaces of fatigue specimen (a) S86, (b) S76, and (c) S83, showing the variations of the location of micro-particles responsible for the crack initiation, and the size of microstructurally small crack (MSC) region.

All specimens were subjected to 0.02 mm/mm strain amplitude and $R_\varepsilon = 0$ test condition.

As seen in this figure, the particle responsible for crack initiation in specimens S86, S76, and S83 located at approximately 746, 589, and 225 μm away from the surface, respectively. The crack initiation site in specimens S86, S76, and S83 was also determined to be approximately 0.41, 0.26, 0.048 mm^2, respectively. From this observation, it appears that the location of the particle relative to the specimen surface may influence the size of the initiation site (i.e. the farther the distance from the particle to the specimen surface, the larger the area of the crack initiation site). In addition, it may be concluded from Fig. 2.7 that, under the same test condition, specimens with inclusions furthest away from the outer surface yielded larger crack initiation sites and shorter fatigue lives. Furthermore, cracks in the MSC region of these specimens were observed to be on an inclined plane and propagated toward the surface of specimens prior transitioning to the loading plane in the PSC region.

Figure 2.8 presents SEM images of fracture surfaces of specimens S76, S91, and S90, which were tested at 0.02 mm/mm with $R_\varepsilon = 0$, 0.02 mm/mm with $R_\varepsilon = 0.2$, and 0.025 mm/mm with $R_\varepsilon = 0.25$, respectively. In addition, the fracture surface of specimen subjected to $R_\varepsilon = -1$ in [16] at 0.02 mm/mm strain amplitude is also displayed in this figure. It can be observed that, although the presence of mean strain did not significantly affect the fatigue behavior of PEEK, the size of the crack initiation site in PEEK specimens generally decreased with an increase in strain ratio, R_ε. The crack initiation site in specimens with tensile mean strain were observed to be subsurface, which is in contrast to most specimens under fully-reversed ($R_\varepsilon = -1$) condition reported in [16], where the crack initiation typically occurred at the specimens' surface. The particles responsible for crack initiation in the specimens in Fig. 2.8 were also found to be at a

greater distance away from the specimen surface as the strain ratio, R_ε, increased. In an attempt to explain such observations for specimens in Fig. 2.8 under different strain ratios, the surface roughness of all of these specimens was measured. An increase in the surface roughness was noticed as the strain ratio, R_ε, increased. This may indicate that, despite the fact that specimens in Fig. 2.8 appear to have the preferential crack nucleation at or near the surface, the surface roughness (intrusion/extrusion mechanism) may not be the cause of fatigue failure in PEEK polymer.

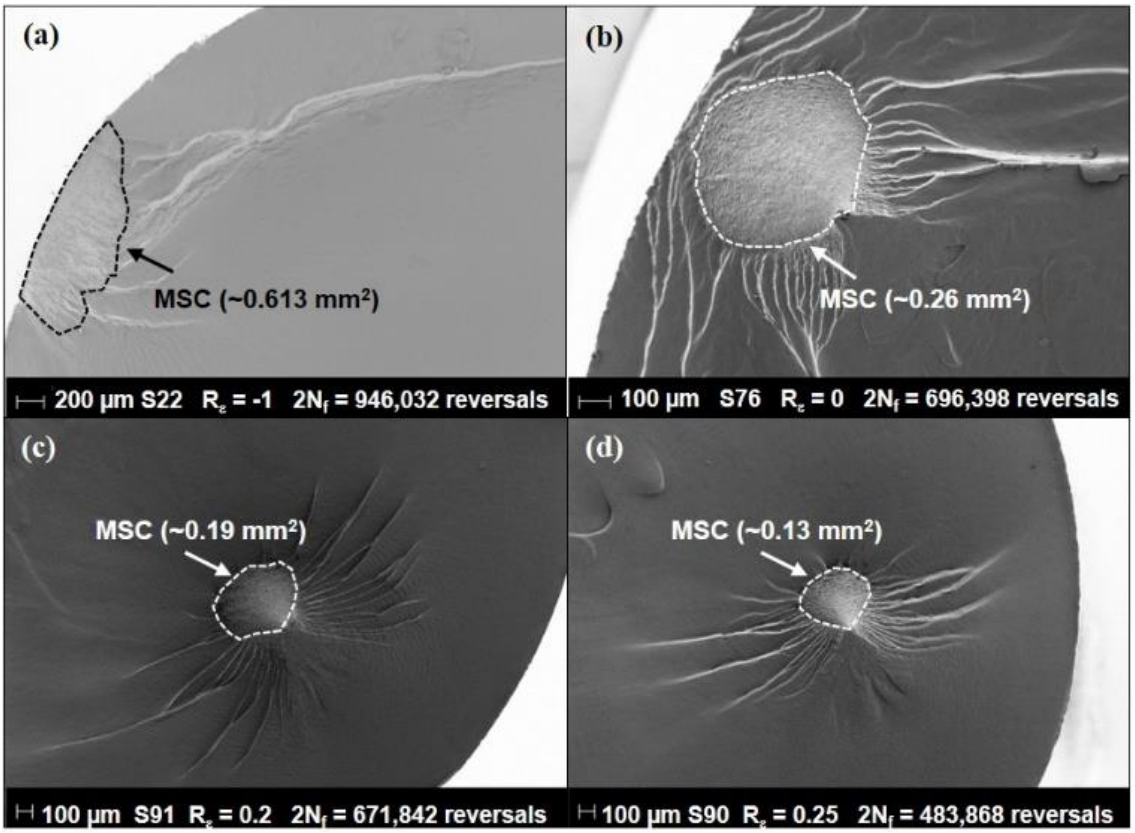

Figure 2.8 Fracture surfaces of fatigue specimen (a) S22 under R_ε = -1 and ε_a= 0.02 mm/mm [16], (b) S78 under R_ε = 0 and ε_a= 0.02 mm/mm, (c) S91 under R_ε = 0.2 and ε_a = 0.02 mm/mm, and (d) S90 under R_ε = 0.25 and ε_a= 0.025 mm/mm, showing the effect of strain ratio on the size of microstructurally small crack (MSC) region.

The effect of crack initiation factor (i.e. particles or void-like defect) size on fatigue life for all specimens with tensile mean strain and in fully-reversed [6] condition is presented in Fig. 2.9. The size of crack initiation factors shown in Fig. 2.9 is categorized by the diameter: 1-10 μm, 11-15 μm, 16-20 μm, 21-30 μm, and 31-40 μm. Solid and hollow features in this figure represent particles and void-like defects, respectively. It should be noted that the fatigue cracks in most PEEK specimens with non-zero mean strain initiated from particles, while only a few specimens had void-like defects that caused the crack initiation. As seen in Fig. 2.9, for all the combinations of R_ε values and strain amplitude levels, PEEK fatigue lives decreased with an increase in size of inclusion factors. Moreover, specimens with void as crack initiation factor exhibited much lower fatigue resistance than those with particles of similar size. Such observation indicated that voids had more influence on PEEK fatigue behavior when compared to particles. Figure 2.9 also reveals that the scatter in fatigue lives of PEEK is largely attributed to the size and type of inclusion responsible for crack initiation, while minimal effect of tensile mean strain was observed. As a result, one can conclude that the effect of the size/type of the crack initiation factors on fatigue life of PEEK may be more significant than the mean strain effect.

Although the formation of inclusions within the material, such as voids or unmelted particles that are typically introduced during the manufacturing process, is unavoidable, there are some manufacturing techniques that may potentially reduce the inclusions in polymers. Some examples include using high curing pressure to avoid air entrapment during the curing process, utilizing preform mold with less complex geometry, as well as optimizing the flow rate of the resin, mold temperature, and resin

injection temperature [22]. By minimizing the presence of inclusions, fatigue performance of PEEK polymer may be improved.

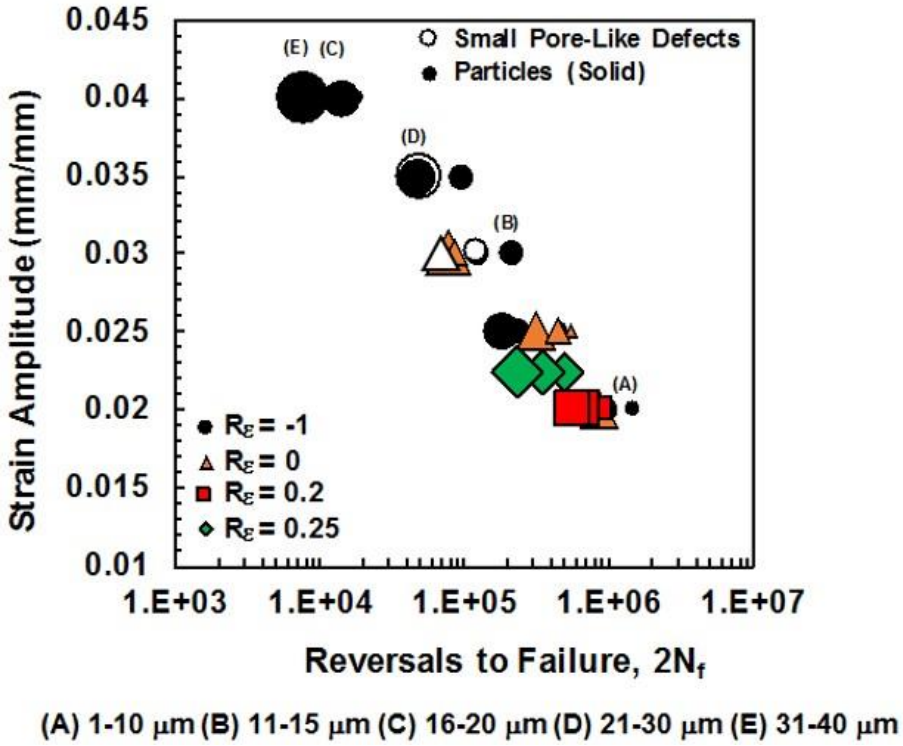

Figure 2.9 Strain amplitude versus reversals to failure for PEEK subjected to constant amplitude fully-reversed (R_ε = -1) [6] and mean strain tests (R_ε = 0, 0.2, and 0.25), showing the effect of size and type of inclusion responsible for crack initiation on the fatigue behavior.

2.5 Conclusions

In this study, uniaxial strain-controlled tests with various strain ratios were utilized to study the mean strain effect on fatigue behavior of a neat PEEK thermoplastic Based on the experimental results, the following conclusions can be drawn:

1. PEEK exhibited significant mean stress relaxation under uniaxial strain-controlled loading with tensile mean strains. The mean stress for tests at $R_\varepsilon = 0$, 0.2, and 0.25 was observed to be fully-relaxed and minimally affect the PEEK fatigue life.

2. The mean stress relaxation rate for PEEK significantly depends on the strain amplitude and R_ε value. It was observed that the mean stress relaxation rate was initially higher for tests subjected to larger strain amplitudes and/or a larger R_ε values (i.e. larger mean strains).

3. Unlike those without mean strain, PEEK subjected to cyclic loading with tensile mean strain did not clearly exhibit the multiple stages of cyclic softening behavior, most likely due the concurrent mean stress relaxation in the material. The initial irregular shape of hysteresis stress-strain loops of specimens with mean strains were observed to become more symmetric as the number of cycle increased.

4. For all fatigue tests with zero and non-zero mean strains, a linear relationship can be assumed between the ratio of the temperature rise in the specimen gage section (due to cyclic loading) to the test frequency, $\Delta T/f$, and (1) the dissipated plastic strain energy density, W_{HL}^{P}, or (2) $\sigma_a(\varepsilon_a)^2$. As a result, energy-based fatigue models may be suitable to correlate PEEK data under cyclic loading with and without mean strains at different test frequencies.

5. The fractography analysis revealed two fatigue stages observed on the fracture surface of PEEK specimens under tensile mean strain cyclic loading. These are crack initiation stage that consists of crack incubation and microstructurally small crack (MSC), as well as physically small crack (PSC) growth stage. Two types of inclusions, including particles and void-like defect, were found to be responsible for crack initiation in PEEK specimens. Moreover, the incubating inclusions in most specimens under fully-reversed loading were observed to be on the outer surface, while they appeared to be subsurface inclusions for specimens under non-zero mean strains.

6. At comparable strain amplitudes and strain ratios, presence of a larger inclusion (particles or void-like defects) generally resulted in a shorter fatigue life of the PEEK specimen. Furthermore, specimens with void-like defects, serving as the source of crack initiation, were found to have shorter fatigue lives as compared to the specimens containing particles of similar size.

2.6 References

[1] Ward I.M, Sweeney J. Mechanical Properties of Solid Polymers, John Wiley and Sons, 2012.

[2] Jones D, Leach D, Moore D. Mechanical properties of poly (ether-ether-ketone) for engineering applications. Polymer 1985;26:1385–93.

[3] Kurtz SM, Devine JN. PEEK biomaterials in trauma, orthopedic, and spinal implants. Biomaterials 2007;28:4845–69.

[4] Kurtz SM, Lanman TH, Higgs G, MacDonald DW, Berven SH, Isaza JE, et al. Retrieval analysis of PEEK rods for posterior fusion and motion preservation. European Spine Journal 2013;22:2752–9.

[5] Ravi Chandran K, Mechanical fatigue of polymers: A new approach to characterize the S-N behavior on the basis of macroscopic crack growth mechanism. Polymer 2016;91:222-238.

[6] Shrestha R, Simsiriwong J, Shamsaei N, Moser RD. Cyclic deformation and fatigue behavior of polyether ether ketone (PEEK). International Journal of Fatigue 2016;82:411–27.

[7] Sauer J, McMaster A, Morrow D. Fatigue behavior of polystyrene and effect of mean stress. Journal of Macromolecular Science Part B Physics 1976;12:535–62.

[8] Crawford RJ, Benham PP. Some fatigue characteristics of thermoplastics. Polymer 1975;16:908–14.

[9] Tao G, Xia Z. Ratcheting behavior of an epoxy polymer and its effect on fatigue life. Polymer testing 2007;26(4):451-60.

[10] Shariati M, Hatami H, Yarahmadi H, Eipakchi HR. An experimental study on the ratcheting and fatigue behavior of polyacetal under uniaxial cyclic loading. Mater and Design 2012;34:302–12.

[11] Mellott SR, Fatemi A. Fatigue behavior and modeling of thermoplastics including temperature and mean stress effects. Polymer Engineering and Science 2014;54:725–38.

[12] Tao G, Xia Z. Mean stress/strain effect on fatigue behavior of an epoxy resin. International Journal of Fatigue 2007;29:2180–90.

[13] Tao G, Xia Z. An experimental study of uniaxial fatigue behavior of an epoxy resin by a new noncontact real-time strain measurement and control system. Polymer Engineering and Science 2007;47:780–8.

[14] Chen P, Wong S-C. Strain-controlled fatigue life and modeling of conduit polymers. Journal of Material Science 2011;46:1902–12.

[15] ASTM E606/E606M, Standard practice for strain-controlled fatigue testing, ASTM International, West Conshohocken, PA, 2012.

[16] Simsiriwong J, Shrestha R, Shamsaei N, Lugo M, Moser RD. Effects of microstructural inclusions on fatigue life of polyether ether ketone (PEEK). Journal of the Mechanical Behavior of Biomedical Materials 2015;51:388–97

[17] ASTM D7791-12, Standard test method for uniaxial fatigue properties of plastics, ASTM International, West Conshohocken, PA, 2012.

[18] Bernasconi A, Kulin RM. Effect of frequency upon fatigue strength of a short glass fiber reinforced polyamide 6: A superposition method based on cyclic creep parameters. Polymer Composites 2009;30:154–61.

[19] Krause O. Frequency effects on lifetime. Optimat Blades Project, DLR, do. OB_TX_N003 rev. 1, Wieringerwerf, The Netherlands; 2002

[20] Mortazavian S, Fatemi A, Mellott SR, Khosrovaneh A. Effect of cycling frequency and self-heating on fatigue behavior of reinforced and unreinforced thermoplastic polymers. Polymer Engineering & Science 2015;55;2355-2367.

[21] Murakami Y. Metal fatigue: Effects of small defects and nonmetallic inclusions. Elsevier; 2012.

[22] Xueshu LI, Fei C. A review of void formation and its effects on the mechanical performance of carbon fiber reinforced plastic, Engineering Transactions 2016; 64(1):33-51

CHAPTER III

LOAD HISTORY AND SEQUENCE EFFECTS ON CYCLIC DEFORMATION AND FATIGUE BEHAVIOR OF A THERMOPLASTIC POLYMER

(Polymer Testing, 2016, In press, DOI: 10.1016/j.polymertesting.2016.09.026)

3.1 Abstract

In this study, the effect of load history and sequence on the cyclic deformation and fatigue behavior of polyether ether ketone (PEEK) thermoplastic was experimentally investigated. Various uniaxial strain-controlled multi-block fatigue tests were conducted, including (1) fully-reversed (R_ε = -1) two-, three-, and four-block loadings with adjusted frequencies to maintain a nominal temperature rise on the specimen gage surface, (2) fully-reversed two-block loading to study the frequency effect, and (3) pulsating tension (R_ε = 0) two-block loading to investigate the combine effect of pre-loading and mean stress/strain on cyclic deformation and fatigue behavior of PEEK. For all fatigue tests under fully-reversed (R_ε = -1) multi-block loadings, cyclic stability of PEEK specimens was achieved at approximately the same reversals and with similar stress amplitudes as those without pre-loading under identical test condition. Additionally, for tests with R_ε= -1, pre-loading was found to have a significant beneficial effect on PEEK fatigue resistance irrespective to the load sequence (i.e. high-low or low-high). However, no obvious load history and sequence effect on fatigue behavior of PEEK was observed for

pulsating tension ($R_\varepsilon = 0$) block loading tests. Experimental results also revealed that increasing test frequency generally leads to higher fatigue lives.

3.2 Introduction

Polymeric materials have been extensively used in various applications, from common household products to advanced prosthetic hip devices. This is due to their unique advantageous characteristics, such as high strength to weight ratio, ease of processing, and tailorability, allowing the material properties to be altered to meet specific requirements by utilizing a wide range of additives such as fillers, reinforcements, stabilizers, and plasticizers [1]. Despites these advantages, the mechanical behavior of most polymers is known to be complex and depend significantly on time, temperature, and loading rate, specifically when it is influenced by the presence of some fluctuating loads (i.e. fatigue) [2]. Since polymers and polymer-based materials (i.e. polymer matrix composites) are often used for load-bearing purposes where cyclic loadings are typically experienced, an adequate understanding of their fatigue resistance and in service performance is necessary.

Unlike the relatively advanced, state-of-the-art understanding of progressive damage evolution processes in metals under cyclic loading, those in polymeric materials, including crazing and shear banding, as well as fatigue crack initiation and propagation, are not yet well understood [3]. Only a small number of studies have been conducted to obtain their correlations to material structure, material composition, and loading conditions [4-11]. The problem is also compounded by the fact that realistic loading conditions in most applications typically involve non-constant amplitude loading. As a result, additional loading variables, including level of mean force (or mean deformation),

presence of periodic overloading, and load interaction/sequence, etc., should be taken into consideration in analysis and design of these structures and components.

To circumvent the high cost and time-consuming nature of realistic loading experiments, a number of laboratory test methods have been developed to simulate non-constant amplitude service histories. Among them, block testing with multiple high-low and low-high sequences has been widely utilized to obtain the effects of load history and sequence on the material's mechanical behavior under cyclic loading [12]. However, in spite of the growing use of polymers in structural applications, very few studies involving fatigue testing with block loading on polymers have been conducted. Eftekhari et al. [13] performed load-controlled two-block cyclic tests with both zero and nonzero mean stresses to evaluate the effects of load sequence and periodic overload histories on notched and un-notched polypropylene (PP) polymer specimens. They concluded that, similar to the observation for metals, less detrimental effect on fatigue life of both types of PP specimens was observed for low-high loading as compared to high-low loading. In addition, a factor of 2.5 reduction in fatigue life was reported for PP in presence of periodic overload.

The objective of this study is to experimentally investigate the effects of mean strain, frequency, as well as load history and sequence on the fatigue behavior of a thermoplastic polymer subjected to block loading. The material of interest in this study is polyether ether ketone (PEEK), an engineering grade, high performance polymer. PEEK thermoplastic has gained popularity in various structural and nonstructural applications due to its highly stable chemical structure that results in exceptional chemical, high temperature, and hydrolysis resistance [14]. Furthermore, PEEK polymer possesses

processing versatility, allowing parts to be manufactured by various techniques, such as extrusion, compression molding, injection molding, thermoforming [15], or additive manufacturing [16]. Common applications that utilize PEEK polymer include aerospace, automotive, oil and gas, and biomedical [15].

In this study, the fatigue behavior of PEEK polymer is evaluated under different types of strain-controlled multi-block cyclic loading. The loading conditions examined in this study include (1) fully-reversed (ratios of minimum to maximum strain, R_ε, of -1) two, three-, and four-block loadings with adjusted frequencies to maintain a nominal temperature rise on the specimen gage surface, (2) fully-reversed two-block loading to study the frequency effect, and (3) pulsating tension ($R_\varepsilon = 0$) two-block loading to investigate the effect of pre-loading in presence of mean strain/stress. The experimental program, entailing the material, specimen geometry, and test procedure, is presented. The experimental results regarding the effects of load sequence on cyclic deformation and fatigue life of PEEK with various strain ratios and test frequencies are given and discussed, followed by conclusions and recommendations.

3.3 Material and Experimental Procedures

In this study, a series of experiment was performed on unfilled PEEK polymer (TECAPEEK™ by Ensinger Inc.) with a glass transition and melt temperatures of 143°C and 343°C, respectively. To prepare the fatigue specimens, extruded PEEK rod was machined to round specimens with uniform gage section of 6.35 mm in diameter and 18 mm in length, using an oil based coolant to minimize heat buildup on specimens. The dimensions and geometry of the specimens were designed in accordance to ASTM E606-

04 standard [17] and can be found in [7]. The specimens were further polished to achieve an average surface finish of 3.4 μm in the gage section.

Fatigue tests were conducted in conformance to ASTM D7791-12 standard [18] at ambient laboratory temperature (~23ºC) with relative humidity of ~45%. All tests were performed using an MTS closed-loop servo-hydraulic load frame with a 25 kN load cell. A mechanical extensometer with 15 mm gage length and sinusoidal waveform was utilized. Runout tests were stopped at 10^6 cycles. In addition, the surface temperature of the specimens' gage section was monitored using a portable laser thermometer. The purpose of the temperature monitoring throughout testing was to ensure that specimens underwent mechanical failure and not the failure due to excessive temperature rise on the specimen during cycling (i.e. self-heating), resulting from inherent high damping and low thermal conductivity characteristics of polymers. Such failure due to self-heating in PEEK polymer under cyclic loading has been reported in [19-20].

PEEK specimens were subjected to strain-controlled low-high (L-H) and high-low (H-L) block loading at R_ε values of -1 and 0. Two sets of experiments were conducted under R_ε = -1 test condition. Experiments were first performed using the frequencies at each level that were similar to those used in [6], which were selected to maintain a nominal temperature rise on the specimen surface, ΔT, in fully-reversed constant amplitude fatigue tests. Therefore, any tests conducted using these frequencies will be referred to as "tests with nominal temperature rise" throughout this paper. The second set of block loading fatigue tests with R_ε = -1 were conducted using various frequencies to study the effect of test frequency on PEEK specimens under block loading. The applied frequencies for these tests are identical to those conducted in [6], which were

used to study the effect of test frequency on fatigue behavior for PEEK subjected to constant amplitude fully-reversed cyclic loading. For $R_\varepsilon = 0$ test condition, the applied frequencies at each strain amplitude level were similar to those used for constant amplitude tests with mean strains in [7].

The number of cycles applied in the first loading block was approximately equal to half of the average fatigue lives at the same level that was reported in [6-7]. Following the initial loading, the specimens were subjected to subsequent loading block until failure. In $R_\varepsilon = -1$ tests, 0.02 or 0.03 mm/mm was selected as the lower strain amplitude and 0.04 mm/mm was taken as the higher strain amplitude. Similarly, for tests with $R_\varepsilon = 0$, 0.02 and 0.03 mm/mm were taken as the lower and higher strain amplitudes, respectively.

The strain histories for fatigue tests with two-block loading (i.e. L-H and H-L) with $R_\varepsilon = -1$ are presented in Figs. 3.1(a) and 3.1(b), respectively. Similar strain histories with zero minimum strain were used for two-block loading fatigue tests at $R_\varepsilon = 0$ condition. Additionally, three- and four-block loading tests with $R_\varepsilon = -1$ were also conducted to further study the fatigue behavior and cyclic deformation of PEEK under zero mean strain, multi-block loading. The L-H-L and H-L-H strain histories for three-block loading tests are illustrated in Figs. 3.1(c) and 3.1(d), respectively, while the four-block loading, H-L-H-L, is displayed in Fig. 3.1(e).

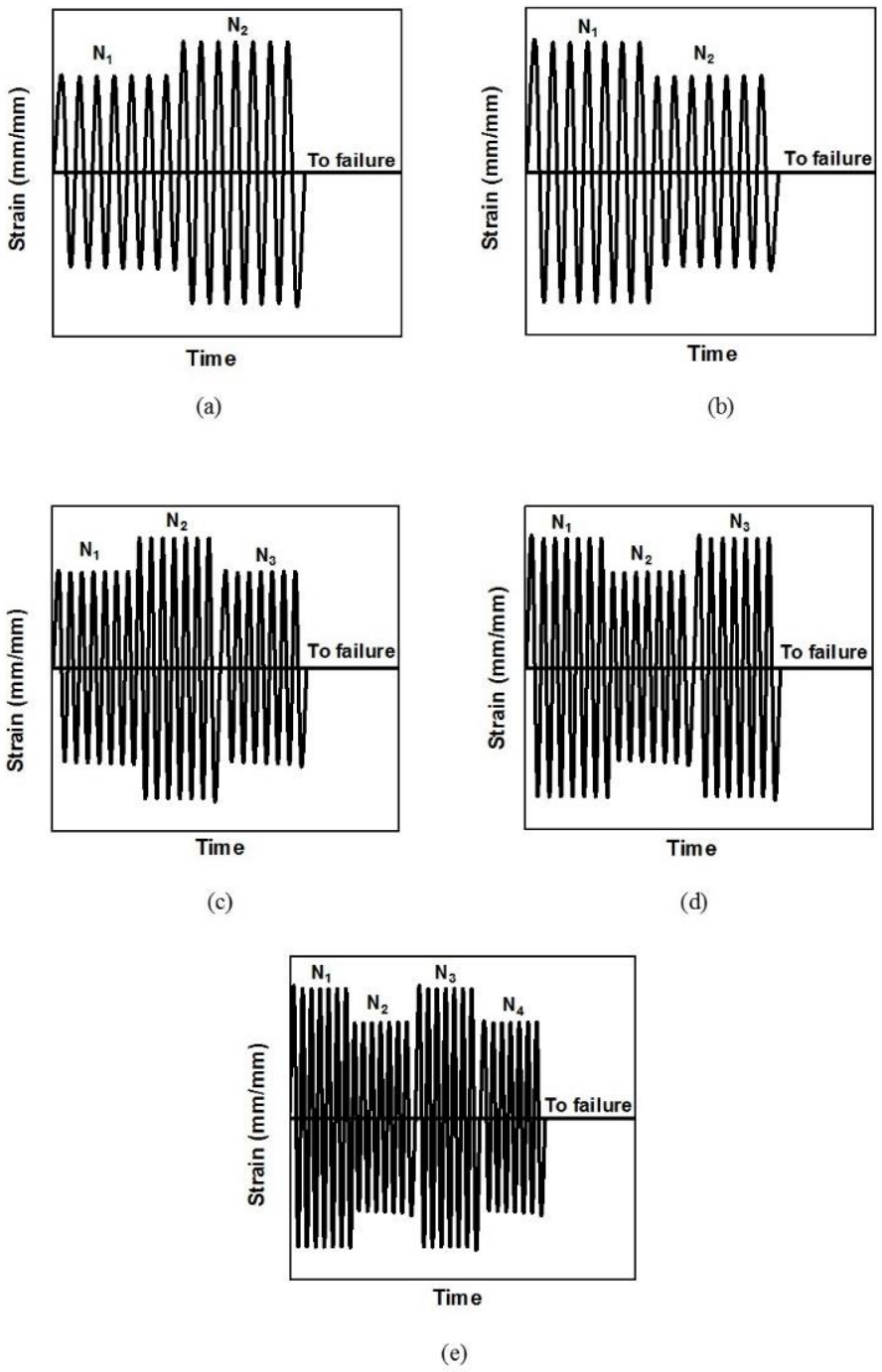

Figure 3.1 Loading history for multi-block loading fatigue tests with R_ε = -1 including (a) two-block L-H, (b) two-block H-L, (c) three block L-H-L, (d) three block H-L-H, and (e) four-block H-L-H-L.

3.4 Experimental Results and Discussions

The effect of loading sequence on cyclic deformation and fatigue behavior of PEEK specimens subjected to multi-block loading is presented in this section. In addition, mean strain and frequency effects on cyclic deformation and fatigue behavior of PEEK under multi-block loading are discussed.

3.4.1 Fully-Reversed Block Loading with Nominal Temperature Rise

The results obtained from the two-block loading fatigue tests under fully-reversed strain cycles, using the frequencies similar to those presented in an earlier work [6] for the constant amplitude conditions, are summarized in Table 3.1. The data in Table 3.1 include the strain amplitude, ε_a, cyclic frequency, f, temperature rise on the specimen gage surface, ΔT, and reversals to failure, $2N_f$. The stress amplitude, σ_a, and mean stress, σ_m, values obtained at half-life cycle (i.e. stabilized cycle) are also given in this table. It should be reminded that test frequencies employed for these tests were selected to maintain a similar nominal temperature rise on the gage section of the specimen, ΔT. In Table 3.1, the test data associated to the first and second loading blocks are denoted by subscripts 1 and 2, respectively.

Table 3.1 Experimental results for uniaxial fully-reversed (R_ε = -1) strain-controlled fatigue tests of PEEK with two-block loading with adjusted frequencies to maintain a nominal temperature rise on the specimens.

Specimen ID	$\varepsilon_{a1}/\varepsilon_{a2}$ (mm/mm)	f_1/f_2 (Hz)	$\Delta T_1/\Delta T_2$ (°C)	$2N_1/2N_2$ (Reversals)	$\sigma_{a1}/\sigma_{a2}{}^*$ (MPa)	$\sigma_{m1}/\sigma_{m2}{}^*$ (MPa)
High-Low						
S123	0.04/0.02	0.5/3	20/36	6,000/2,130,352#	49/30	14/16
S101			31/37	6,000/1,371,616	47/30	-12/-9
S105	0.04/0.03	0.5/0.75	26/28	6,000/296,276	49/47	-11/-9
S102			28/27	6,000/412,318	47/47	-12/-10
S108			31/30	6,000/459,890	51/49	-12/-10
Low-High						
S103	0.03/0.04	0.75/0.5	27/31	100,000/33,542	51/51	-10/-11
S109			29/31	100,000/50,136	47/48	-10/-11
S106			22/29	100,000/53,076	50/49	-10/-11

*Measured at half-life cycle
Runout test

The stress response for tests with H-L loading for specimen S105 and L-H loading for specimen S109 from Table 1 are presented in Figs. 3.2 and 3.3, respectively. Fully-reversed strain amplitude of 0.04 mm/mm at 0.5 Hz was taken as the high load and fully-reversed strain amplitude of 0.03 mm/mm at 0.75 Hz was chosen as the low load. As expected, cyclic stress responses in the first loading block for both H-L (first 6,000 reversals) and L-H (first 100,000 reversals) loadings, shown in Figs. 3.2(a) and 3.3(a), were similar to those observed in [6] for the fully-reversed constant amplitude cyclic tests at the same strain amplitude and frequency, where distinct stages of stress responses, including initial, transition, and cyclic stability were observed.

Furthermore, the stress response of the second loading block is compared to that obtained from the test conducted using an identical strain amplitude and frequency, but without pre-loading in [6]. This can be seen in Figs. 3.2(b) and 3.2(c) for H-L loading (specimen S105), and Figs. 3.3(b) and 3.3(c) for L-H loading (specimen S109). By comparing Figs. 3.2(b) and 3.2(c), it can be noticed that the stress response of specimen

S105 in the second loading block did not distinctly display the initial stage of cyclic softening and immediately decreased upon cycling into transition stage. Similar behavior can be also seen for specimen S109 with L-H loading, as illustrated in Fig. 3.3(b). Overall, higher stress amplitudes (~ 15% higher) at the initial cycles of the specimens without pre-loading were observed as compared to those with pre-loading. It has been reported that the duration of the initial region of cyclic softening for polymers significantly depends on the initial state of material microstructure as well as the applied strain/stress amplitude [21]. During the initial stage of cyclic softening, some molecular rearrangement may occur which can cause the movement and formation of mobile defects (i.e. voids) in polymeric materials. The materials will begin to soften (i.e. enter the transition stage of cyclic softening) when the mobile defect population reaches its critical value.

Some polymers, such as nylon and acrylonitrile butadiene styrene, do not exhibit an initial stage of cyclic softening under constant amplitude cyclic loading, which is believed to be associated to the presence of a larger mobile defect population in the initial material state [21]. As a result, an absence of the initial stage of cyclic softening in PEEK specimens with pre-loading may be explained by an increased mobile defects as compared to the virgin material. However, despite the differences in the initial cyclic deformation, the stress response of PEEK specimens with pre-loading irrespective of loading sequence (i.e. L-H or H-L) was stabilized at approximately the same loading cycle as the specimens without pre-loading. Furthermore, the pre-loading effect on the stress amplitude at the cyclic stability region was not noticeable.

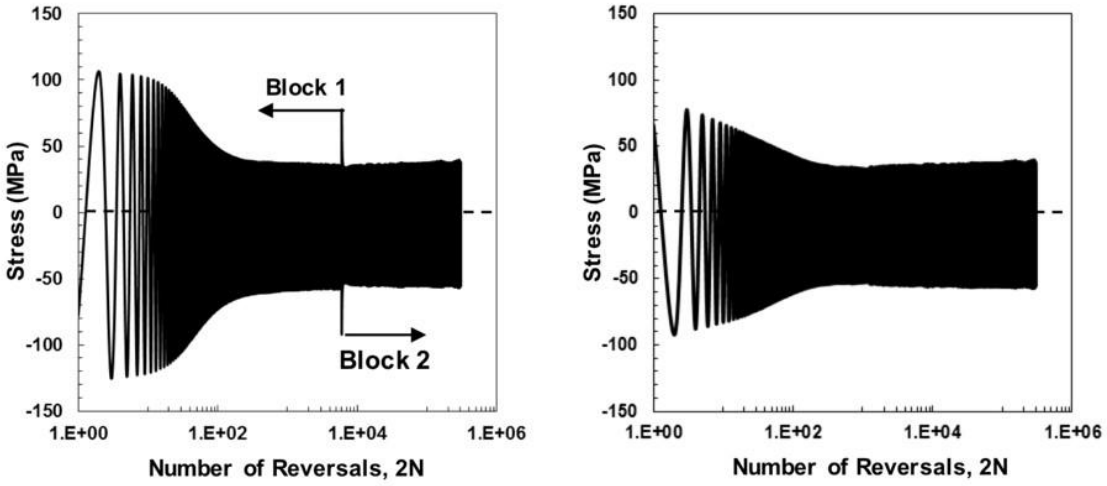

(a) (b)

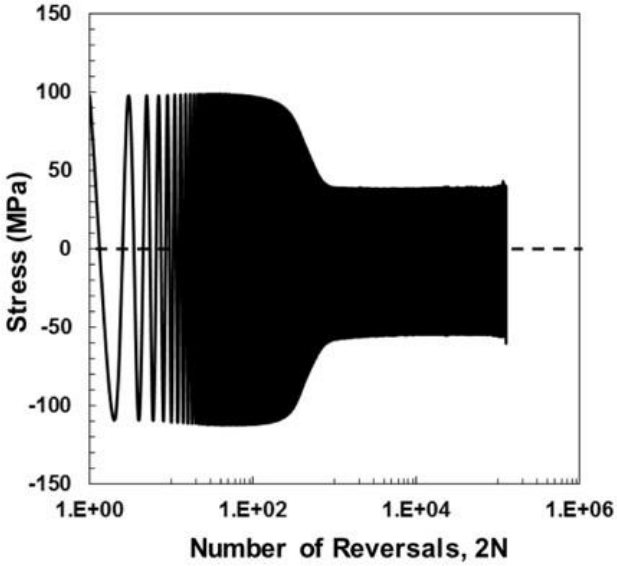

(c)

Figure 3.2 (a) Overall PEEK stress response of specimen S105 subjected to fully-reversed strain-controlled H-L block loading (ε_{a1} = 0.04 mm/mm at 0.5 Hz and ε_{a2} = 0.03 mm/mm at 0.75 Hz), as well as the comparison between the stress responses of (b) the second loading block of specimen S105 and (c) the specimen subjected to constant amplitude loading of 0.03 mm/mm at 0.75 Hz without pre-loading reported in [6].

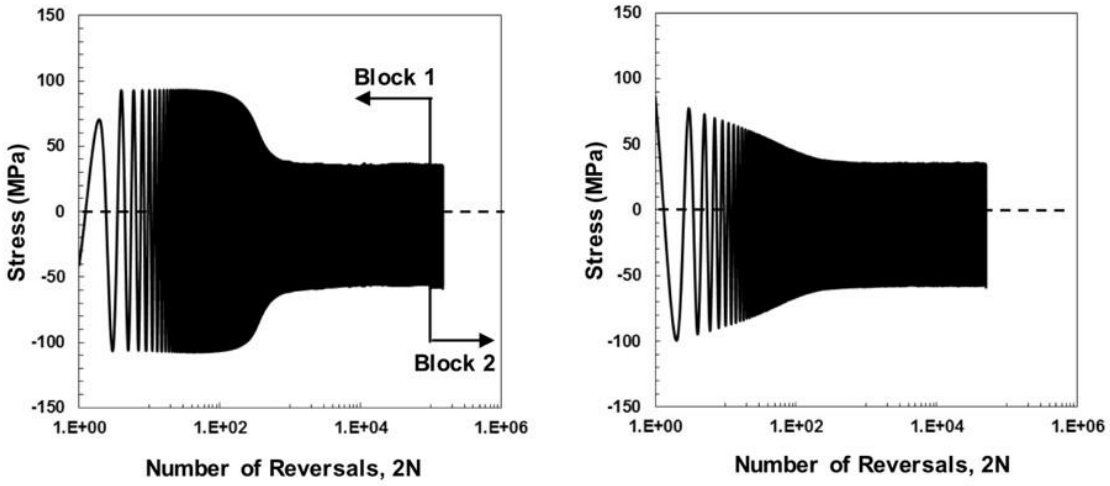

(a) (b)

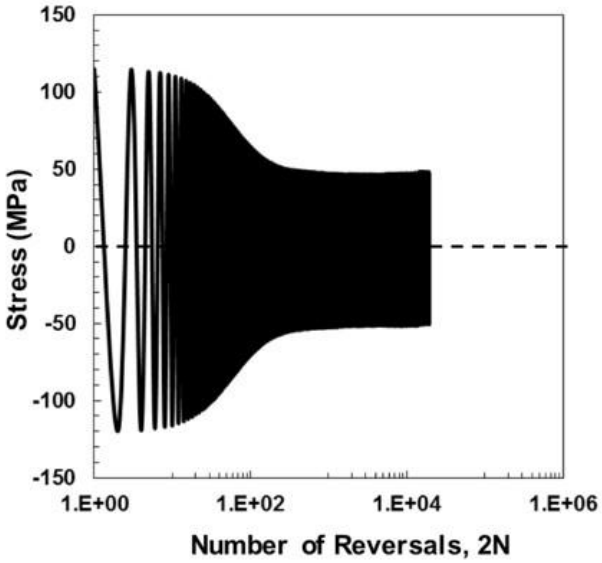

(c)

Figure 3.3 (a) Overall PEEK stress response of specimen S109 subjected to fully-reversed strain-controlled L-H block loading (ε_{a1} = 0.03 mm/mm at 0.75 Hz and ε_{a2} = 0.04 mm/mm at 0.5 Hz), as well as the comparison between the stress responses of (b) the second loading block of specimen S109 and (c) the specimen subjected to constant amplitude loading of 0.04 mm/mm at 0.5 Hz without pre-loading, reported in [6].

Fatigue lives obtained from the second loading block (i.e. data in Table 1) were compared to the experimental results from the constant amplitude fully reversed tests (i.e.

without any pre-loading) with nominal temperature rise [6], as presented in Fig. 3.4. Numbers in this figure represents the number of data points lie on top of each other. Although the damage caused by the first loading block is approximated to be 50% of the overall fatigue tolerance of the material, PEEK specimens exhibited significantly longer fatigue lives by pre-loading with either lower or higher strain amplitudes, when compared to those without any pre-loading. For example, the average fatigue life for specimens subjected to 0.04 mm/mm at 0.5 Hz without pre-loading was 13,464 reversals [6], while the average fatigue life for PEEK specimens under fully-reversed 0.04 mm/mm strain amplitude (specimens S103, S109, and S106 in Table 3.1) increased to 45,585 reversals after being subjected to a prior loading block of 0.03 mm/mm strain amplitude for 100,000 reversals. Similarly, in the case of 0.03 mm/mm at 0.75 Hz, the average fatigue life (specimens S105, S102, and S108) increased from 152,927 reversals without pre-loading [6] to 389,495 reversals when a loading block with strain amplitude of 0.04 mm/mm was first applied for 6,000 reversals.

Although some compressive mean stresses are noticeable in two-block loading tests in Table 3.1, PEEK specimens under constant amplitude loading also exhibited some compressive mean stresses, but at slightly less values [6]. Furthermore, while specimen S123 in Table 3.1 exhibited a tensile mean stress at half-life cycle, it had a longer fatigue life (>2,000,000 reversals) than specimen S101 (1,370,000 reversals) with some compressive mean stress. Therefore, the presence of compressive mean stress may not be the main contributor to the increased fatigue resistance observed in PEEK thermoplastic when subjected to pre-loading.

Under cyclic loading, polymeric materials may experience some microstructural rearrangements that consist of the realignments and entanglements of individual polymer molecules, leading to a molecular directional hardening [22]. A small increase (~ 1%) in density for polycarbonate and nylon polymers was reported after being subjected to fully-reversed strain-controlled cyclic loading at room temperature [23]. Hence, a decrease in the material's internal free volume may possibly affect the fatigue behavior of PEEK with pre-loading. Further microstructural investigations, however, are needed to better understand the mechanisms involved in the fatigue failure of PEEK polymer with and without pre-loading.

The next set of fatigue experiment with nominal temperature rise was conducted using three- (H-L-H and L-H-L) and four-block (H-L-H-L) loadings with zero mean strain (R_ε = -1). Strain amplitudes of 0.04 mm/mm at 0.5 Hz and 0.03 mm/mm at 0.75 Hz were chosen as the high and low loads, respectively. The experimental details and results for three- and four-block tests are presented in Table 3.2.

The stress response for specimen S126, which was subjected to three-block H-L-H loading is presented in Fig. 3.5. As expected, the overall cyclic deformation for the first two loading blocks shown in Fig. 3.5(a) was similar to that of the specimen with H-L loading (i.e. specimen S105 in Fig. 3.2(a)). Furthermore, the initial stage of cyclic deformation (i.e. the stage with constant stress response prior to transitioning to the cyclic stability stage) was not evident in either the second (Fig. 3.5(b)) or the third (Fig. 3.5(c)) loading blocks. Specimen S126 in the third loading block (Fig. 3.5(c)) underwent a similar number of cycles (~1,000 reversals) to the specimen without pre-loading before achieving cyclic stability. Minimum effect of pre-loading was also observed on the

stabilized mean stress and stress amplitude values in the third loading block, when compared to the cyclic stability stage of fully-reversed constant amplitude 0.04 mm/mm strain amplitude test without pre-loading in [6].

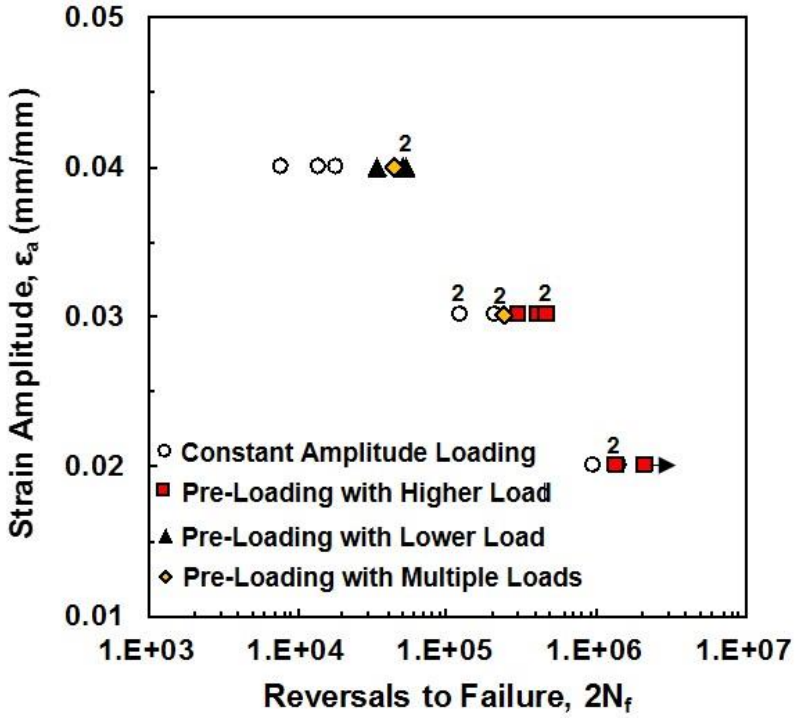

Figure 3.4 Comparison of fatigue lives obtained from the last loading block for two- (Table 3.1), three-, and four-block loading tests (Table 3.2) along with the fatigue results from the fully-reversed constant amplitude strain-controlled tests without any pre-loading [6], all with nominal temperature rise.

Regardless of the damage caused by the first two blocks in the specimen under three-block loading, which is close to the overall fatigue tolerance of the material, significant increase in the number of reversals to failure of the last loading block was observed for these specimens as compared to those without pre-loading, as illustrated in Fig. 3.4. For example, the average life of PEEK specimens at strain amplitude of 0.03

mm and 0.75 Hz without pre-loading was reported to be 152,927 reversals [6]. However, the number of reversals for the third loading block of specimen S127 increased to 239,800 after pre-loading by two-block loading of 100,000 reversals at 0.03 mm/mm strain amplitude and 20,000 reversals at 0.04 mm/mm strain amplitude. Similar improvement in fatigue life under 0.04 mm/mm fully-reversed strain amplitude at 0.5 Hz from 13,464 without pre-loading [6] to 44,098 reversals after two-block of H-L pre-loading was observed for specimen S126 in Table 3.2.

Similarly, despite the fact that the overall cumulative damage exceeds 100% of the material's fatigue tolerance based on the constant amplitude case, the beneficial effect of pre-loading on PEEK fatigue life in the last loading block was observed for the specimen subjected to four-block loading. This can be seen for the specimen tested at the strain amplitude of 0.03 mm/mm at 0.75 Hz under fully-reversed condition, where an increase in fatigue life from 153,927 reversals without pre-loading [6] to 237,786 reversals after three-block of H-L-H pre-loading for specimen S128 in Table 4.2 was obtained. Again, it should be emphasized that further investigations at lower-length scales are needed to understand the mechanisms involved in fatigue failure of polymers to explain the beneficial effects of pre-loading on fatigue resistance of PEEK.

Table 3.2 Experimental results for uniaxial fully-reversed (R_ε = -1) strain-controlled fatigue tests of PEEK with three- and four-block loadings with adjusted frequencies to maintain a nominal temperature rise on the specimens.

Specimen ID	$\varepsilon_{a1}/\varepsilon_{a2}/\varepsilon_{a3}$ (mm/mm)	$f_1/f_2/f_3$ (Hz)	$\Delta T_1/\Delta T_2/\Delta T_3$ (°C)	$2N_1/2N_2/2N_3$ (Reversals)	$\sigma_{a1}/\sigma_{a2}/\sigma_{a3}$* (MPa)	$\sigma_{m1}/\sigma_{m2}/\sigma_{m3}$* (MPa)
High-Low-High						
S126	0.04	0.5	22	6,000	51	-11
	0.03	0.75	26	180,000	47	-9
	0.04	0.5	21	44,098	59	10
Low-High-Low						
S127	0.03	0.75	30	100,000	47	-7
	0.04	0.5	32	20,000	48	-9
	0.03	0.75	31	239,800	46	-10
Specimen ID	$\varepsilon_{a1}/\varepsilon_{a2}/\varepsilon_{a3}/\varepsilon_{a4}$ (mm/mm)	$f_1/f_2/f_3/f_4$ (Hz)	$\Delta T_1/\Delta T_2/\Delta T_3/\Delta T_4$ (°C)	$2N_1/2N_2/2N_3/2N_4$ (Reversals)	$\sigma_{a1}/\sigma_{a2}/\sigma_{a3}/\sigma_{a4}$* (MPa)	$\sigma_{m1}/\sigma_{m2}/\sigma_{m3}/\sigma_{m4}$* (MPa)
High-Low-High-Low						
S128	0.04	0.5	26	6,000	47	-10
	0.03	0.75	26	180,000	46	-8
	0.04	0.5	31	20,000	48	-8
	0.03	0.75	29	237,786	47	-6

*Measured at half-life cycle

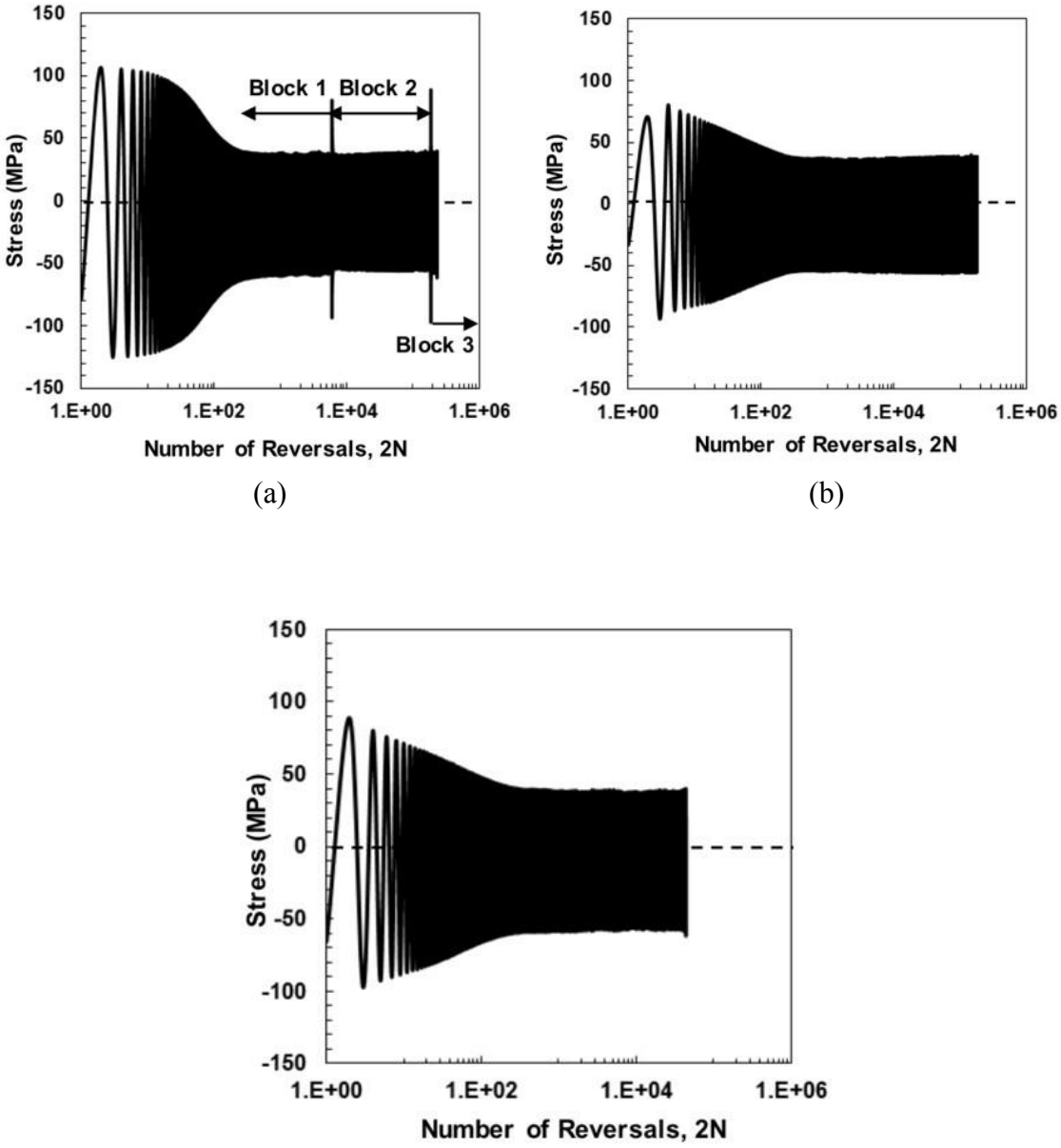

Figure 3.5 (a) Overall PEEK stress response of specimen S126 subjected to fully-reversed strain-controlled H-L-H block loading (ε_{a1}= 0.04 mm/mm at 0.5 Hz, and ε_{a2} = 0.03 mm/mm at 0.75 Hz, ε_{a3} = 0.04 mm/mm at 0.5 Hz), as well as the stress response of (b) the second loading block at ε_a = 0.03 mm/mm, 0.75 Hz, and (c) the third loading block at ε_a = 0.04 mm/mm, 0.5 Hz.

3.4.2 Fully-Reversed Block Loading to Study Frequency Effects

Table 3.3 contains the experimental results from the fully-reversed fatigue tests under two-block loading with frequencies lower than those used in the previous test conditions (i.e. data in Table 3.1). The stress response of specimen S114 in Table 3.3 under H-L loading sequence is shown in Fig. 6(a). For this test, 0.04 mm/mm strain amplitude at 0.25 Hz was considered as the high load and 0.03 mm/mm strain amplitude at 0.5 Hz was taken as the low load. When comparing the stress response for the first loading block (first 2,000 reversals) of specimen S114 to that of specimen 105 (first 6,000 reversals with ε_a= 0.04 mm/mm and f = 0.5 Hz) in Fig. 3.2(a), the stress amplitudes in the initial region of cyclic response are comparable, while slightly higher stress amplitude (~ 23% higher) in the stabilized cyclic region was observed for specimen S114 with lower frequency. Such observation, where an increase in test frequency resulted in a lower stabilized stress amplitude, was also reported for PEEK polymer in [6].

In addition, the stress responses for the second loading block under H-L test (specimen S114) and constant amplitude test with an identical loading condition (i.e. 0.03 mm/mm strain amplitude at 0.5 Hz) [6] are presented in Figs. 3.6(b) and 3.6(c), respectively. Again, no initial region of cyclic response was observed for specimen with pre-loading. However, the stress amplitude in the initial cycles for the second loading block (Fig. 3.6(b)) was lower (~ 40%) than that of the specimen without pre-loading (Fig. 3.6(c)). Nonetheless, the stress amplitudes at the cyclic stability region for both cases were observed to be comparable.

Similarly, specimens S111 and S113 in Table 3.3, which were subjected to L-H loading with lower test frequencies, exhibited no initial region of cyclic softening in the

second loading block. The initial stress amplitude in the second loading block of these specimens was also much lower than the one for the specimen without pre-loading in [6], while the stress amplitudes at the cyclic stability region were observed to be comparable.

Fatigue lives obtained from the second loading block for specimens listed in Table 3.3 are plotted in Fig. 3.7. The test data under constant amplitude loading at similar strain amplitude and test frequency without pre-loading [6] are also included in this figure. As seen, fatigue lives of the second loading block increased significantly for specimens subjected to pre-loading (i.e. either H-L or L-H) when compared to those under constant amplitude loading. The average fatigue life of PEEK without pre-loading at 0.03 mm/mm strain amplitude and 0.5 Hz was 33,594 reversals [6]. However, when PEEK was first subjected to the prior higher strain amplitude of 0.04 mm/mm at 0.25 Hz, the average fatigue life for the second loading block of specimens S124 and S114 were 191,104 reversals.

Table 3.3 Experimental results for uniaxial fully-reversed (R_ε = -1) strain-controlled fatigue tests of PEEK with two-block loading for frequency effect study.

Specimen ID	$\varepsilon_{a1}/\varepsilon_{a2}$ (mm/mm)	f_1/f_2 (Hz)	$\Delta T_1/\Delta T_2$ (°C)	$2N_1/2N_2$ (Reversals)	σ_{a1}/σ_{a2}* (MPa)	σ_{m1}/σ_{m2}* (MPa)
High-Low						
S124	0.04/0.03	0.25/0.5	9/15	2,000/140,582	64/55	14/15
S114			37/30	2,000/241,626	64/55	-8/-7
Low-High						
S111	0.03/0.04	0.5/0.25	17/14	30,000/46,000	54/61	-10/-11
S113			17/14	30,000/53,434	55/61	-7/-7

*Measured at half-life cycle

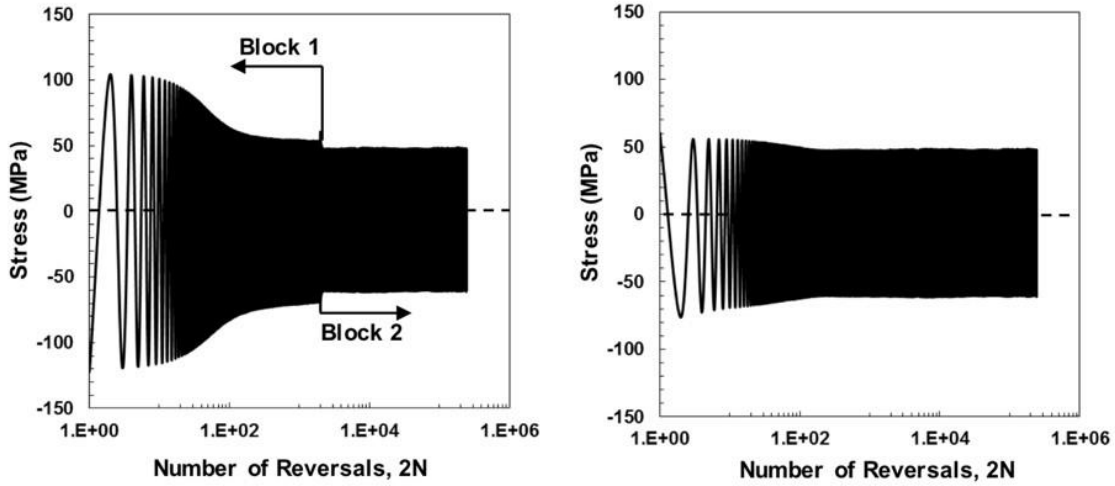

(a) (b)

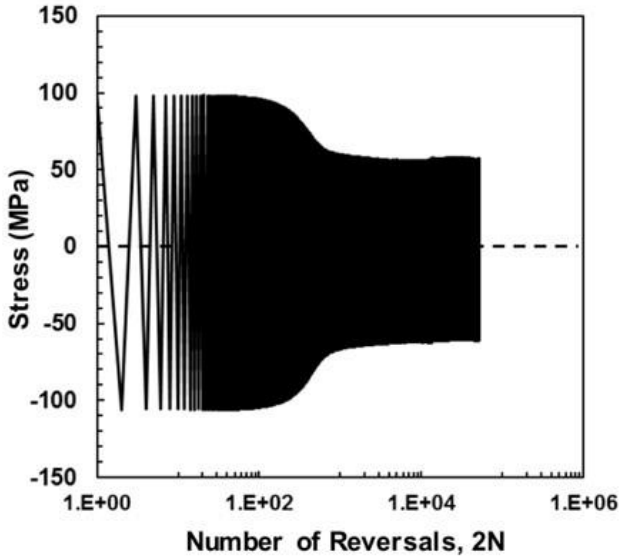

(c)

Figure 3.6 (a) Overall PEEK stress response of specimen S114 subjected to fully-reversed strain-controlled H-L block loading (ε_{a1}= 0.04 mm/mm at 0.25 Hz, and ε_{a2} = 0.03 mm/mm at 0.5 Hz), as well as the comparison between the stress responses of (b) the second loading block of specimen S114 and (c) the specimen subjected to constant amplitude loading of 0.03 mm/mm at 0.5 Hz without pre-loading, reported in [6].

Similar increase in fatigue lives were also observed for specimens with pre-loading at a lower strain amplitude. Therefore, it can be concluded that, under uniaxial fully-reversed strain-controlled cyclic loading regardless of the loading frequency, the fatigue behavior of PEEK polymer demonstrates a strong strain history dependence, which needs to be taken into consideration by an appropriate cumulative damage parameter.

In addition, it is worth mentioning that the frequency effect on fatigue behavior of PEEK under fully-reversed constant amplitude loading was observed to be highly dependent on strain level [6]. At smaller strain amplitude (i.e. 0.02 mm/mm), an increase in test frequency led to shorter fatigue lives of PEEK. In contrast, at higher strain amplitudes (i.e. 0.025-0.04 mm/mm), an increase in frequency resulted in longer fatigue lives. In this study, a similar trend of frequency effect on fatigue behavior of PEEK was observed under fully-reversed block loading to the ones under constant amplitude loading at 0.03 and 0.04 mm/mm, where a decrease in frequency reduced the fatigue resistance of this polymer.

3.4.3 Pulsating Tension Block Loading

The results obtained from pulsating tension ($R_\varepsilon = 0$) two-block loading fatigue experiments, using the frequencies similar to those presented in [7] for the constant amplitude conditions with $R_\varepsilon = 0$, are summarized in Table 3.4. For these tests, 0.03 mm/mm strain amplitude at 0.5 Hz and 0.02 mm/mm strain amplitude at 1.5 Hz were taken as the high and low loads, respectively. The overall stress response for specimen S116 under H-L loading in Table 3.4 is presented in Fig. 3.8(a). Additionally, the stress response of the second loading block of specimen S116 and the stress response of

specimen subjected to pulsating tension loading ($R_\varepsilon = 0$) without pre-loading (i.e. constant amplitude condition) at similar strain amplitude and frequency [7], are displayed in Figs. 3.8(b) and 3.8(c), respectively. As seen in Fig. 3.8(b), although there was some compressive mean stress at initial cycles of the second loading block for specimen S116, it gradually relaxed from -22.5 MPa to -1.5 MPa. On the other hand, tensile mean stress (55 MPa) was initially observed in Fig. 3.8(c) for the PEEK specimen without pre-loading prior to becoming stabilized at approximately -5 MPa.

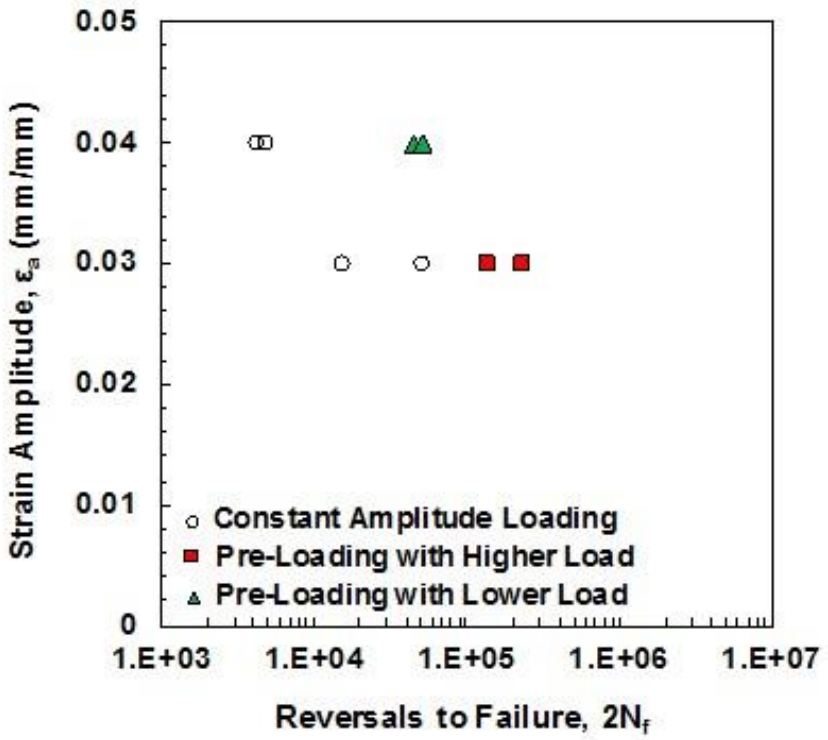

Figure 3.7 Comparison of fatigue lives obtained from the second loading block of H-L and L-H tests (Table 3.3) with the fatigue results from the fully-reversed constant amplitude strain-controlled tests without pre-loading [6], both from the frequency effect study.

Fully-relaxed mean stresses in Figs. 3.8(b) and 3.8(c) were achieved at similar number of reversals, and stress amplitudes at the cyclic stability region in both specimens were also comparable. Similar behavior was observed for all the specimens under pulsating tension L-H loading condition in Table 3.4.

Table 3.4 Experimental results for uniaxial pulsating tension ($R_\varepsilon = 0$) strain-controlled fatigue tests of PEEK with two-block loading.

Specimen ID	$\varepsilon_{a1}/\varepsilon_{a2}$ (mm/mm)	f_1/f_2 (Hz)	$\Delta T_1/\Delta T_2$ (°C)	$2N_1/2N_2$ (Reversals)	σ_{a1}/σ_{a2}* (MPa)	σ_{m1}/σ_{m2}* (MPa)
High-Low						
S120	0.03/0.02	0.5/1.5	14/16	60,000/312,756	55/44	24/19
S116			21/31	60,000/645,088	52/42	1/-3
Low-High						
S121	0.02/0.03	1.5/0.5	20/18	300,000/65,032	45/54	24/24
S118			26/31	300,000/99,310	44/53	-0.2/1

*Measured at half-life cycle

The strain-life fatigue data of the second loading block from block loading tests with $R_\varepsilon = 0$ (i.e. specimens in Table 3.4), as well as the fatigue data for constant amplitude pulsating tension ($R_\varepsilon = 0$) loadings in [7], are compared in Fig. 3.9. As seen, the pre-loading minimally affected fatigue life of PEEK and generally resulted in slightly shorter lives when compared to those without pre-loading. For example, specimen S116 in Table 3.4 failed at 645,088 reversals after pre-loading with a higher strain amplitude for 60,000 reversals. The number of reversals to failure of specimen S116 is similar to the average fatigue life of specimens subjected to pulsating tension constant amplitude loading with $\varepsilon_a = 0.02$ mm/mm without pre-loading, which was reported to be 682,324 reversals in [7]. Therefore, the significant beneficial effect of pre-loading on fatigue lives was primarily observed for the specimens under fully-reversed cyclic loading and not pulsating tension loading.

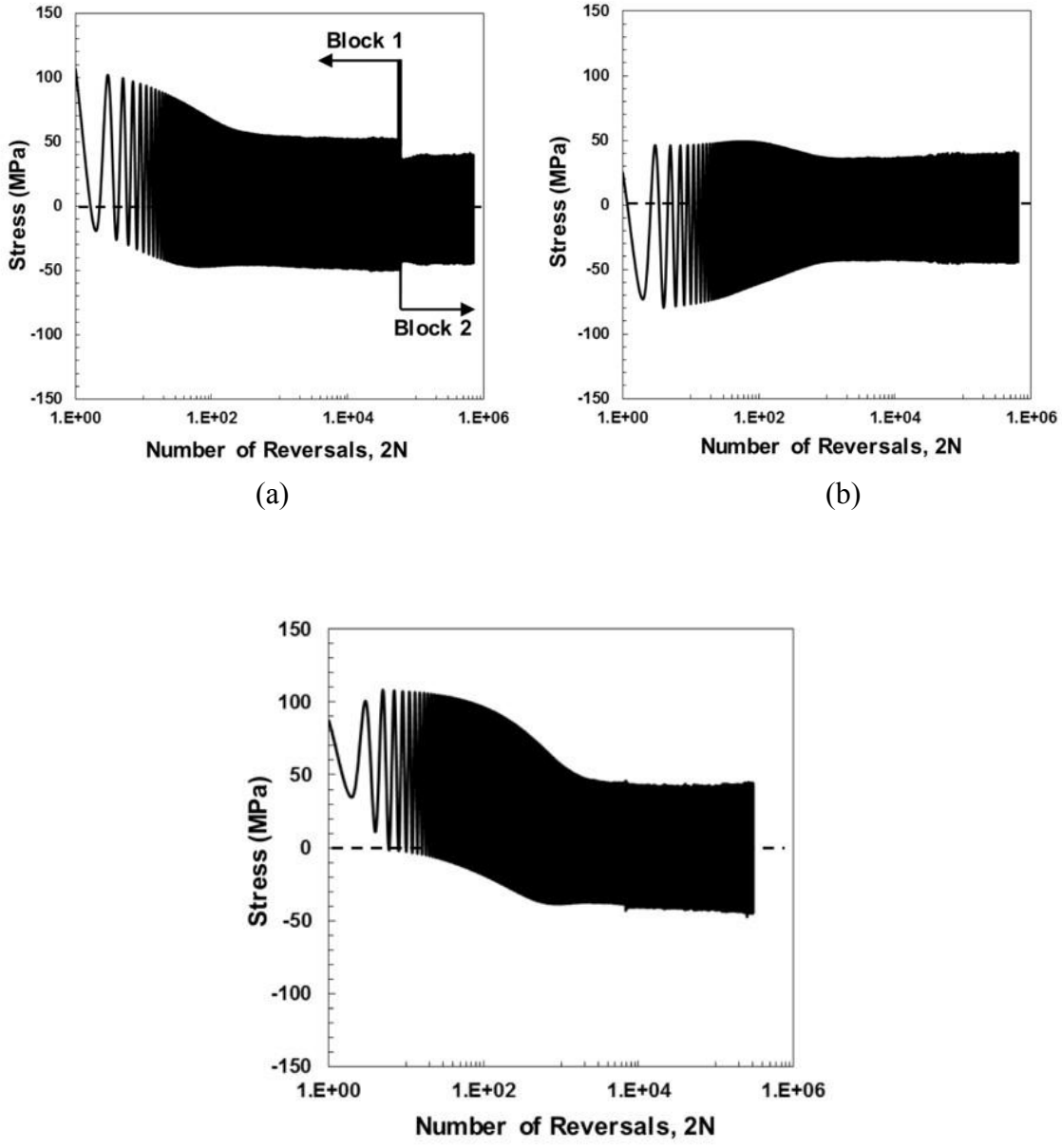

Figure 3.8 (a) Overall PEEK stress response of specimen S116 subjected to strain-controlled H-L block loading with mean strain, $R_\varepsilon = 0$ ($\varepsilon_{a1} = 0.03$ mm/mm at 0.5 Hz, and $\varepsilon_{a2} = 0.02$ mm/mm at 1.5 Hz), as well as the comparison between the stress responses of (b) the second loading block of specimen S116 and (c) the specimen subjected to constant amplitude loading of 0.02 mm/mm at 1.5 Hz with $R_\varepsilon = 0$ without pre-loading in [7].

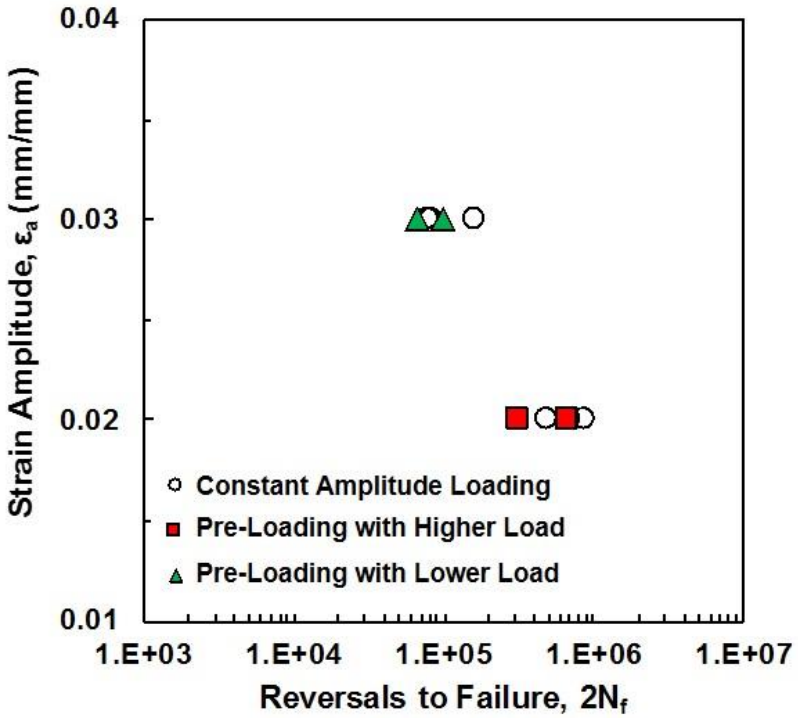

Figure 3.9 Comparison of fatigue lives obtained from the second loading block of H-L and L-H tests with $R_\varepsilon = 0$ (Table 3.4) with the fatigue results from the constant amplitude pulsating tensile loading tests ($R_\varepsilon = 0$) without pre-loading [7].

3.5 Conclusions

A series of uniaxial strain-controlled cyclic tests under various multi-block loading conditions were employed in this study to investigate the load sequence effects on fatigue behavior of a neat PEEK thermoplastic. The fatigue tests conducted in this study include multi-block fully-reversed loading with various frequencies and multi-block loading with mean strains. Based on the experimental results, the following conclusions and recommendations can be made:

1. In general, PEEK specimens with fully-reversed (R_ε = -1) pre-loading (with higher or lower strain amplitude) did not exhibit the initial stage of cyclic softening. The cyclic stability of the pre-loaded specimens was achieved at approximately the same reversals as those without pre-loading under identical test condition. Furthermore, the stress amplitudes at the cyclic stability region were also comparable. Such cyclic deformation behavior was observed for all specimens under two-, three-, or four-block loading with R_ε = -1.

2. Pre-loading for specimens under fully-reversed (R_ε = -1) condition was found to have a significant beneficial effect on PEEK fatigue resistance irrespective to the load sequence (i.e. high-low or low-high).

3. Similar to fatigue tests without pre-loading for higher strain amplitudes (i.e. $\varepsilon_a \geq$ 0.025 mm/mm), increasing the test frequency resulted in longer fatigue lives in both low-high and high-low loading block tests.

4. Load history and sequence minimally affected fatigue behavior of PEEK under pulsating tension condition (R_ε = 0). Only some slight decreases in fatigue lives of specimens under block-loading (high-low or low-high with R_ε = 0) were observed as compared to those under constant amplitude loading.

5. The experimental results in this study revealed a distinctive fatigue behavior of PEEK under multi-block loading. However, due to the unavailability of published studies in polymer fatigue involving both upper-length scale non-constant (i.e. variable) amplitude loading and lower-length scale micro/nanostructure analysis, the mechanisms causing such behaviors are not fully realized. Therefore, there is a need for further fatigue related multi-scale studies to better understand the underlying fatigue damage mechanisms of polymers.

While the present work deals with the experimental investigation to obtain the effect of load history and sequence on PEEK fatigue behavior, the knowledge gained based on this study can be used to develop appropriate cumulative fatigue damage models that are essential for life prediction of polymeric components under realistic service loadings.

3.6 References

[1] Crawford RJ. Plastics engineering. Butterworth-Heinemann, 1998.

[2] Tomkins B, Biggs WD. Low endurance fatigue in metals and polymers. Journal of Materials Science, 1969;4:532-53.

[3] Vinogradov AM, Jenkins CH, Winter RM. Cyclic loading effects on durability of polymer systems. Long Term Durability of Structural Materials, 2001;29:159-70.

[4] Arbeiter FJ, Frank A, Pinter G. Influence of molecular structure and reinforcement on fatigue behavior of tough polypropylene materials. Journal of Applied Polymer Science, 2016;133;43948.

[5] Simsiriwong J, Shrestha R, Shamsaei N, Lugo M, Moser RD. Effects of microstructural inclusions on fatigue life of polyether ether ketone (PEEK). Journal of the mechanical behavior of biomedical materials, 2015;51:388-97.

[6] Shrestha R, Simsiriwong J, Shamsaei N, Moser RD. Cyclic deformation and fatigue behavior of polyether ether ketone (PEEK). International Journal of Fatigue, 2016;82:411–27.

[7] Shrestha R, Simsiriwong J, Shamsaei N. Mean strain effects on cyclic deformation and fatigue behavior of polyether ether ketone (PEEK). Polymer Testing, 2016;55:69-77

[8] Chudnovsky A, Zhou Z, Zhang H, Sehanobish K. Lifetime assessment of engineering thermoplastics. International Journal of Engineering Science, 2012;59:108-39.

[9] Medel FJ, Pena P, Cegoñino J, Gómez-Barrena E, Puertolas JA. Comparative fatigue behavior and toughness of remelted and annealed highly crosslinked polyethylenes. Journal of Biomedical Materials Research Part B: Applied Biomaterials, 2007;83(2):380-90.

[10] Wainstein J, Chapetti M, Montemartini PE, Frontini P. Fatigue crack propagation evaluation of several commercial grade propylene polymers. International Journal of Polymeric Materials, 2005;54:575-87.

[11] Jones NA, Lesser AJ. Morphological study of fatigue-induced damage in isotactic polypropylene. Journal of Polymer Science Part B: Polymer Physics, 1998;36:2751-60.

[12] Stephens RI, Fatemi A, Fuchs HO, Stephens RR. Metal fatigue in Engineering, John Wiley & Sons, 2000.

[13] Eftekhari M, Fatemi A, Khosrovaneh A. Fatigue behavior of neat and short glass fiber reinforced polymers under two-step loadings and periodic overloads. SAE International Journal of Materials and Manufacturing, 2016;01-0373.

[14] Olabisi O, Adewale K. Handbook of thermoplastics, CRC press, 2016.

[15] Thomas S, Visakh PM. Handbook of engineering and specialty thermoplastics: volume 3: polyethers and polyesters, John Wiley & Sons, 2011.

[16] Schmidt M, Pohle D, Rechtenwald T. Selective laser sintering of PEEK. CIRP Annals-Manufacturing Technology, 2007;56(1):205-8.

[17] ASTM E606/E606M, Standard practice for strain-controlled fatigue testing, ASTM International, West Conshohocken, PA, 2012.

[18] ASTM D7791-12, Standard test method for uniaxial fatigue properties of plastics, ASTM International, West Conshohocken, PA, 2012.

[19] Berer M, Major Z, Pinter G, Constantinescu DM, Marsavina L. Investigation of the dynamic mechanical behavior of polyetheretherketone (PEEK) in the high stress tensile regime. Mechanics of Time-Dependent Materials, 2014;18;663-84.

[20] Berer M, Tscharnuter D, Pinter G. Dynamic mechanical response of polyetheretherketone (PEEK) exposed to cyclic loads in the high stress tensile regime. International Journal of Fatigue, 2015;80:397-405.

[21] Rabinowitz S., Beardmore P. Cyclic deformation and fracture in polymer. Journal of Materials Science, 1974; 9:81-99.

[22] Hertzberg RW, Manson J. Fatigue of engineering plastics, Academic press, 1980.

[23] Beardmore, P., Rabinowitz S. Treatise on materials science and technology - vol. 6, Academic Press, 1975.

CHAPTER IV

FATIGUE MODELING OF POLYETHER ETHER KETONE (PEEK) UNDER MEAN STRAIN AND MULTI-BLOCK LOADINGS

4.1 Abstract

In this study, the applicability of several fatigue models for polyether ether ketone (PEEK) under constant amplitude with mean strain and multi-blocks loadings was evaluated. The models examined in this study were correlated to the experimental data for PEEK under various cyclic loading conditions, including (1) constant amplitude loading with non-zero mean strains, (2) two-block loading with zero and non-zero mean strain, and (3) three- and four-block loading with zero mean strain. A strain-based, a strain-stress-based, and an energy-based models were employed to correct for the effect of mean strain on fatigue behavior of PEEK. Among these models, the fatigue life prediction using the energy based approach, which considered the deformation response of the material throughout its entire life, was found to provide a better correlation to PEEK experimental data in the presence of mean strain. For specimens under block loading, the linear damage rule was employed to evaluate its applicability for PEEK. In addition, a direct cumulative damage (DCD) approach using an energy-based parameter was proposed to account for the load history and sequence effect on PEEK fatigue behavior. The proposed DCD method was found to provide acceptable fatigue life

predictions for PEEK under multi-block loading with various strain ratios and frequencies.

4.2 Introduction

Polyether ether ketone (PEEK), a high performance thermoplastic polymer, has been widely used in various applications, such as aerospace, automotive, and biomedical, due to its excellent mechanical properties, high dimensional stability, as well as good chemical and wear resistance. In addition, PEEK generally provides good resistance to damage due to hydrolysis, radiation, and lipid exposure (i.e. *in vivo* degradation) when compared to traditional metallic counterparts [1]. As a result, an emergence of PEEK in various biomedical applications has significantly increased in the past decades as an alternative spinal-related implant material to replace metals. The mechanical properties of PEEK can also be tailored, enabling the material to be conformed to specific requirements of a given application. For example, the modulus of elasticity of PEEK can be tailored to closely match that of cortical bones by reinforcing the material with carbon fiber, allowing more uniform stress distribution between the natural bone and the implant material. Successful clinical studies of PEEK have been reported for dental implants [2] and spinal cages used in cervical spinal fusion [3], while there is also a growing interest in a number of PEEK-based orthopedic components, such as fracture fixation plate [4] and hip joint endoprosthesis [1].

Despite an increasing demand of polymer-based components in aforementioned applications, not many studies have been performed to obtain the mechanical behavior of polymers under cyclic (fatigue) loading. Additionally, the cyclic loading under realistic service conditions is generally complex in nature and seldom involves constant amplitude

loading. Consequently, the effects of loading history and sequence, which resulted from the changes in stress/strain amplitude, stress/strain ratio, test frequency, etc., on cyclic deformation and fatigue life of a material must be considered in component design. The damage accumulated in a material under such loading should also be carefully quantified using appropriate and reliable methodologies.

Considerable efforts have been made in the past decades to develop cumulative fatigue damage and life prediction models for metals and their alloys as discussed in a comprehensive review paper by Fatemi and Yang [5]. However, despite the growing use of polymers, significant less studies regarding their cumulative fatigue damage have been performed on neat (unfilled) polymers. As a result, their fatigue behavior under non-constant amplitude cyclic loading is not fully understood. Nonetheless, a number of experimental studies have indicated that fatigue and fracture behavior in polymer matrix composites (PMCs) are generally governed by micro-mechanical response of the matrix material and its interface with reinforced fillers [6]. It has been shown that the damage process in PMCs under cyclic loading initiates from cracks in the polymer matrix [7].

The Palmgren-Miner Linear Damage Rule (referred to as LDR or Miner's rule) has been dominantly used to quantify the cumulative fatigue damage in PMCs. In [8], a series of tension-tension load-controlled fatigue tests were conducted on a short glass fiber reinforced styrene maleic anhydride. High-low (H-L) and low high (L-H) block loading were employed and the data were analyzed using the LDR shown in Eq. (4.1) [8].

$$D = \sum \frac{N_i}{N_{f_i}} \tag{4.1}$$

where D is the cumulative damage or the sum of all damage induced in the specimen from each cycle. In Eq. (4.1), N_i is the number of cycles at a stress level of i and N_{f_i} is the

total number of cycles to failure at the same stress level of i, which is obtained from the stress-life (S-N) curve under constant amplitude load-controlled test. The failure was predicted when the value of D approaches unity. The cumulative damage using Eq. (4.1) ranging from 0.40 to 1.14 were obtained for all tests in [8].

The fatigue process in short fiber reinforced composites can be described as a two-stage process as defined in [9]. As a result, a two-stage linear cumulative damage rule was proposed by combining the damage induced in each stage using the LDR, and validated for short carbon fiber-reinforced PEEK under rotating-bending cyclic block loading [9]. Moreover, Zago and colleagues [10, 11] proposed a nonlinear cumulative damage model for short glass fiber-reinforced copolyamide subjected to block loading that consisted of random load cycles [10, 11].

On the other hand, the cumulative damage rule using the residual strength as the damage parameter was introduced by Yao et al. [12], and validated for glass/epoxy cross-ply laminates [13] and carbon fiber-reinforced composites [14]. Similarly, Lee and Jen [15, 16] also proposed and verified the cumulative damage model based on the residual strength for AS-4/PEEK laminates.

Due to its simplicity, the LDR is still commonly used to determine fatigue damage accumulation in non-constant amplitude loadings tests. As previously discussed, reasonable cumulative damage predictions for different types of PMCs were obtained utilizing various nonlinear and modified LDRs. However, the damage parameters employed in these studies, such as residual strength, are typically difficult to obtain. On the other hand, it has been recently shown that the energy-based fatigue models provided satisfactory life predictions for PEEK under various types of uniaxial fully-reversed

strain-controlled constant amplitude loading conditions [17]. Therefore, a cumulative damage approach with an energy-based damage parameter may provide a better prediction for PEEK fatigue behavior under block loading.

In this study, an analytical investigation is carried out to obtain appropriate fatigue life prediction models for PEEK polymer subjected to different cyclic loading conditions based on the experimental results presented in the previous studies [18, 19]. In these studies, neat PEEK polymer was subjected to a series of cyclic loadings, including constant amplitude loading with mean strains, and multi block (two-, three-, and four-blocks) loading with various strain ratios and frequencies. In the present study, a strain-based approach, a strain-stress-based approach, and an energy based fatigue approach are employed to predict fatigue lives of PEEK polymer under constant amplitude loading with mean strains. For block loading fatigue tests with zero and non-zero mean strain, the LDR, with either strain amplitude or strain energy density as the damage parameter, is used to evaluate its applicability for the damage prediction for PEEK. Furthermore, an alternative method for cumulative damage prediction utilizing an energy-based parameter is proposed and validated. Finally, some conclusions based on prediction models are presented.

4.3 Fatigue Modeling for Mean Strain Condition

In this section, three types of fatigue models, including the Coffin-Manson model, SWT model, and an energy based fatigue model, are used to predict the fatigue behavior of PEEK polymer in a presence of mean strain. The strain-based Coffin-Manson model and the strain-stress-based SWT model are employed in this study since they have been commonly used in both low and high cycle fatigue for metals. On the other hand, the

energy based approach was previously shown to provide reasonable fatigue life predictions for PEEK under uniaxial fully-reversed strain-controlled cyclic loading at various frequencies [17]; therefore, its capability in predicting fatigue lives of PEEK in a presence of mean strain is also examined.

4.3.1 Strain-Based Approach

For the strain-based Coffin-Manson model, the total strain amplitude, $\frac{\Delta\varepsilon}{2}$, from the stabilized hysteresis loop (i.e., hysteresis loop at half-life) can be separated into elastic and plastic strain components, represented by $\frac{\Delta\boldsymbol{\varepsilon_e}}{\mathbf{2}}$ and $\frac{\Delta\boldsymbol{\varepsilon_p}}{\mathbf{2}}$, respectively. These components at the half-life cycle were determined using Eqs. (4.2) and (4.3), respectively [20].

$$\frac{\Delta\varepsilon_e}{2} = \frac{\Delta\sigma}{2E} \tag{4.2}$$

$$\frac{\Delta\varepsilon_p}{2} = \frac{\Delta\varepsilon}{2} - \frac{\Delta\sigma}{2E} \tag{4.3}$$

where $\frac{\Delta\sigma}{2}$ is the stress amplitude obtained at the half-life cycle and E is the modulus of elasticity. The elastic and plastic strain amplitudes were determined using Eqs. (4.2) and (4.3), based on the experimental data for PEEK under fully-reversed (ratios of minimum to maximum strain, R_ε, of -1) loading with nominal rise in temperature (i.e. tests with adjusted frequencies to maintain a similar nominal temperature rise on the gage section of the specimen) presented in [17]. These elastic and plastic strain components were plotted against the reversals to failure, $2N_f$, in a log-log scale to obtain the linear relationship between each strain component and fatigue life as [20]:

$$\frac{\Delta\varepsilon_e}{2} = \frac{\sigma_f'}{E}(2N_f)^b \tag{4.4}$$

$$\frac{\Delta\varepsilon_p}{2} = \varepsilon_f'(2N_f)^c \tag{4.5}$$

where σ_f', ε_f', b, and c are the fatigue strength coefficient, fatigue ductility coefficient, fatigue strength exponent, and fatigue ductility exponent, respectively. These fatigue parameters were obtained using a linear least square fit method following the ASTM standard E739-10 method [21] and reported in [17]. By combining Eqs. (4.4) and (4.5), the total strain amplitude was determined using the Coffin-Manson relationship as [20]:

$$\frac{\Delta\varepsilon}{2} = \frac{\Delta\varepsilon_e}{2} + \frac{\Delta\varepsilon_p}{2} = \frac{\sigma_f'}{E}(2N_f)^b + \varepsilon_f'(2N_f)^c \tag{4.6}$$

The experimental results and the Coffin-Manson fit for PEEK polymer under constant amplitude fully-reversed (R_ε = -1) fatigue loading with nominal rise in temperature [17] are displayed in Fig 4.1(a). In addition, the experimental data for tests with non-zero mean strains (R_ε = 0, 0.2, and 0.25) with nominal temperature rise from the earlier work [18], which are tabulated in Table 4.1, are also superimposed in this figure. As seen, a satisfactory correlation was observed for all tests with various R_ε. Additionally, the predicted fatigue lives using the Coffin-Manson model were compared to the experimental data for all constant amplitude loading tests with nominal temperature rise as depicted in Fig. 4.1(b). It can be seen that all data, except the zero mean strain data at 0.04 mm/mm, are within scatter bands of two with R^2 = 0.76.

As displayed in Fig. 4.1(b), the strain-based model of zero mean strain (R_ε = -1) test data alone was able to reasonably correlate PEEK fatigue lives with non-zero mean strains. Such observation can be attributed to the mean stress relaxation phenomenon reported in [18], in which the presence of tensile mean strains in PEEK resulted in an

initial tensile mean stress prior to becoming fully-relaxed in a relatively short time period as compared to the total life

Despite these facts, it has been demonstrated in [18] that the change in shape and size of hysteresis stress-strain loop throughout various cyclic softening stages (i.e. initial, transition, and cyclic stability) significantly influenced the fatigue life of PEEK polymer. Since the Coffin-Manson model only utilizes the cyclic response at the half-life cycle, it may not be the most suitable model for PEEK under various strain ratios (zero and non-zero mean strains) as illustrated in Fig. 4.1(b).

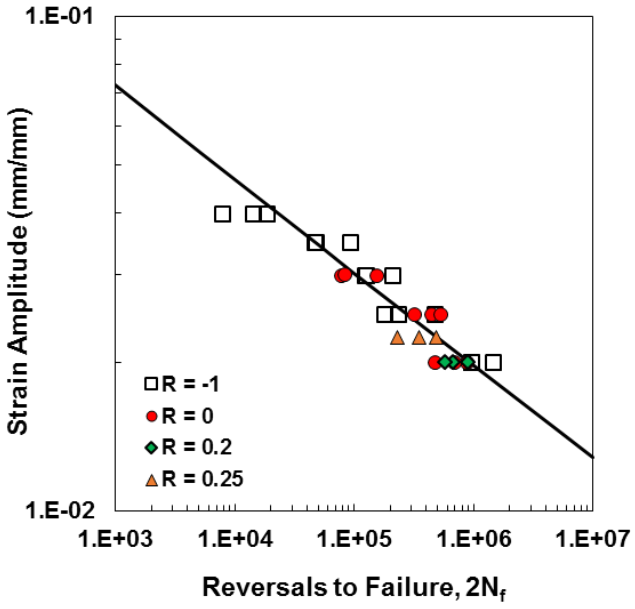

(a)

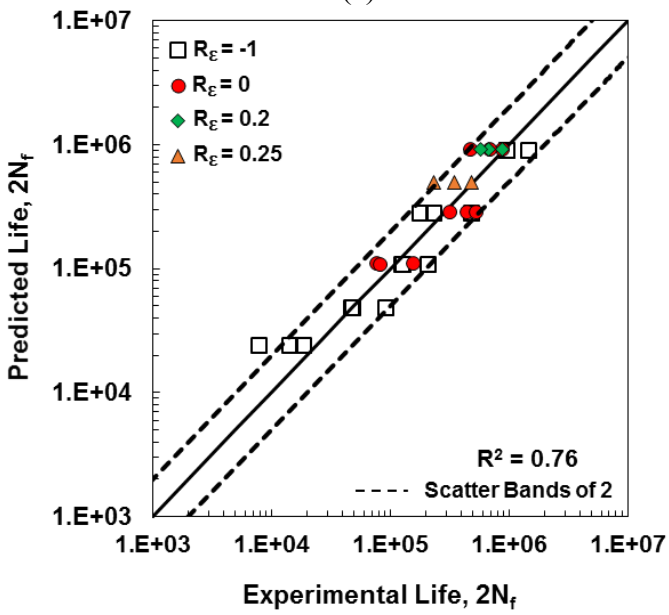

(b)

Figure 4.1 (a) Strain amplitude versus reversals to failure, $2N_f$, for PEEK under uniaxial strain-controlled constant amplitude fatigue tests with zero [18] and non-zero (Table 4.1) mean strains with nominal rise in temperature, and (b) predicted fatigue lives using the Coffin-Manson model versus experimentally observed fatigue lives.

4.3.2 Strain-Stress-Based Approach

The SWT fatigue model incorporates mean stress/strain effects by including the maximum tensile stress, σ_{max}, within its damage parameter as [22]:

$$\varepsilon_a \sigma_{max} = \frac{\left(\sigma_f'\right)^2}{E}(2N_f)^{2b} + \sigma_f'\varepsilon_f'(2N_f)^{b+c} \tag{4.7}$$

where

$$\sigma_{max} = \sigma_m + \sigma_a \tag{4.8}$$

where, $\varepsilon_a$is the strain amplitude and N_f is the number of cycles to failure. The mean stress, σ_m, and stress amplitude, σ_a, are obtained from the stabilized hysteresis loop (i.e. half-life cycle). These stress components for constant amplitude fatigue tests with various tensile mean strains (R_ε = 0, 0.2, and 0.25) and nominal temperature rise [18] are summarized in Table 4.1.

The correlation between the SWT damage parameter, $\varepsilon_a \sigma_{max}$ (i.e. the left hand side of Eq. (4.7)), and the corresponding experimentally observed reversals to failure, $2N_f$, for all tests with tensile mean strains (i.e. data in Table 4.1) is displayed in Fig. 4.2(a). The fully-reversed (R_ε = -1) PEEK data with nominal rise in temperature [17] are also included in this figure. Interestingly, the SWT damage parameters are not well correlated to zero and non-zero mean strain fatigue data of PEEK. Again, the scatter appears to be mostly for the fully-reversed (R_ε = -1) data at 0.04 mm/mm. In Fig. 4.2(b), PEEK fatigue lives were determined using Eq. (4.7) and plotted against the experimentally observed fatigue lives. Scatter bands of two were also superimposed in this figure. As depicted in Fig. 4.2(b), 11 out of 30 fatigue data for PEEK with zero and non-zero mean strains are outside of the scatter bands. The predicted lives for specimens

with mean strains are generally underestimated (i.e. conservative predictions), while the predictions for zero mean strain condition using the SWT model are slightly overestimated. Poor correlation indicated by $R^2 = 0.65$ was obtained as seen in Fig. 4.2(b).

Table 4.1 Experimental results [18] for PEEK polymer and the corresponding energy densities for uniaxial constant amplitude strain-controlled fatigue tests with mean strains.

Specimen ID	ε_a (mm/mm)	ε_m (mm/mm)	Frequency (Hz)	R_ε Value	σ_a^* (MPa)	σ_m^* (MPa)	$2N_f$ (Reversals)	ΔT (°C)	ΔW_{HL}^P (MJ/m^3)	ΔW_{HL}^E (MJ/m^3)	$\sum W^T$ (MJ/m^3)
S86	0.02	0.02	1.5	0	42	-1.98	475,726	31	0.78	0.27	248,987
S76					47	7.71	696,398	43	0.68	0.54	400,771
S83					45	0.98	874,850	32	0.74	0.39	467,617
S78	0.025	0.025	1		46	4.11	318,690	45	1.2	0.42	262,781
S88					46	1.59	443,580	29	1.2	0.38	352,939
S84					43	-0.80	535,546	34	1.3	0.28	417,132
S85	0.03	0.03	0.5		49	2.51	77,892	37	1.9	0.49	91,105
S87					53	-0.95	83,096	28	1.8	0.52	93,544
S81					48	1.40	155,458	39	1.7	0.51	173,921
S92	0.02	0.03	1.5	0.2	45	2.50	578,224	24	0.69	0.37	304,513
S91					41	4.56	671,842	29	0.74	0.34	360,697
S89					46	7.50	887,634	26	0.71	0.42	501,458
S97	0.025	0.0375	1	0.25	47	1.92	231,896	22	0.98	0.39	158,243
S99					47	2.03	347,108	21	0.98	0.48	236,173
S90					48	3.84	483,868	24	0.95	0.45	330,107

*Measured at half-life cycle

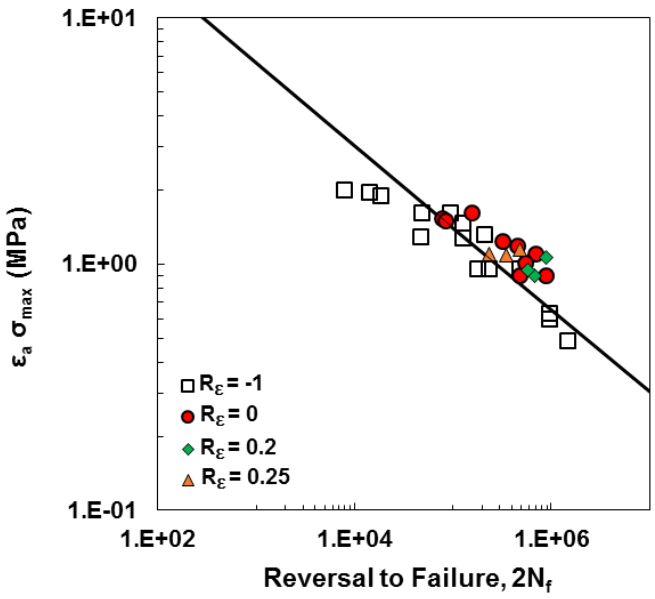

(a)

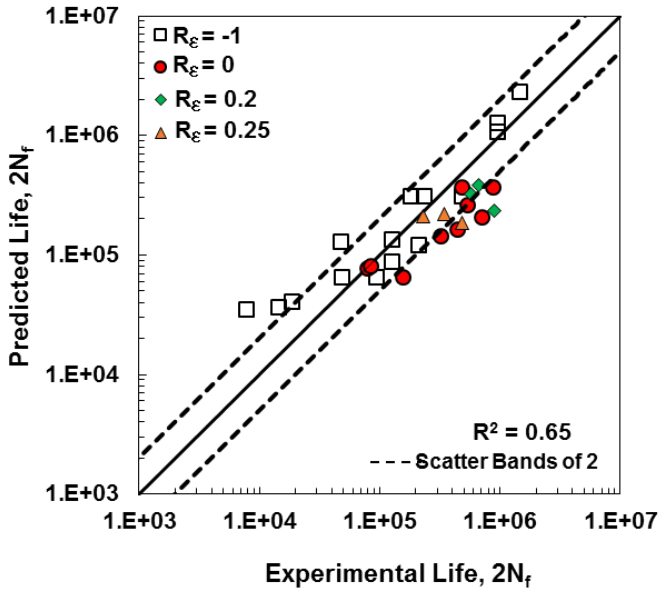

(b)

Figure 4.2 (a) Smith-Watson-Topper (SWT) damage parameter versus reversals to failure, $2N_f$, for PEEK under uniaxial strain-controlled constant amplitude fatigue tests with zero [18] and non-zero (Table 4.1) mean strains with nominal rise in temperature, and (b) predicted fatigue lives using the SWT parameter versus experimentally observed fatigue lives.

The presence of the stress component in the fatigue parameter appears to have a detrimental effect on the fatigue life prediction of PEEK, as compared to the strain-based model (i.e. the Coffin-Manson model). Furthermore, when plotting σ_{max}versus $2N_f$ for all tests with zero and non-zero mean strains, a large scatter of the data was observed, which may explain an inadequacy of the SWT model to capture the mean strain effect of PEEK polymer. In addition, PEEK exhibited both stress relaxation and cyclic deformation under mean strain test condition, resulting in the hysteresis stress-strain loop to evolve, specifically at the beginning of the test [18]. Since SWT model only employs the stress and strain responses at half-life cycle, it does not take the variation of cyclic deformation into account. Therefore, the SWT model may not be an appropriate model for mean strain effect on the fatigue behavior of PEEK.

4.3.3 Energy-Based Approach

The imposed strain energy resulted from an external loading can generally be divided into two parts: a recoverable elastic strain energy and an irrecoverable plastic strain energy [23]. The dissipated plastic strain energy density, ΔW^P, is defined by the area of the hysteresis stress-strain loop, while the elastic strain energy density, ΔW^E, is defined as the positive area under the hysteresis loop. In the energy based approach, the irrecoverable plastic strain energy density, ΔW^P, has been used as a damage parameter for fully-reversed or nearly fully-reversed fatigue tests. However, ΔW^P is not suitable for fatigue tests with mean strain/stress since, it is generally not sensitive to stress relaxation or ratchetting behavior [23]. Additionally, for high cycle fatigue tests or tests at small strain amplitudes, ΔW^P becomes very small and can be difficult to determine. Therefore,

the total strain energy density, ΔW^T, which is defined as the sum of elastic and plastic strain energy densities, has been proposed as a damage parameter [24], which can be used to combine the damages in both high cycle and low cycle fatigue in a single model [23].

As the majority of PEEK fatigue lives is spent in the cyclic stability region [17, 18], the total strain energy density calculated at the half-life cycle in the cyclic stability region, ΔW_{HL}^T, can be considered as a damage parameter, which is given as:

$$\Delta W_{HL}^T = \Delta W_{HL}^P + \Delta W_{HL}^E \tag{4.9}$$

where ΔW_{HL}^P and ΔW_{HL}^E are the plastic and elastic strain energy densities obtained at the half-life cycle, respectively. These values for constant amplitude fatigue tests with mean strains conducted in [18] were determined by integration method and listed in Table 4.1. It should be noted that, unlike the strain-based and stress-strain-based approaches, the energy-based approach takes the shape and size of the hysteresis loop into account. Thus, it inherently incorporates the stress and strain responses from an entire loading cycle, and not only at the extreme points (i.e. maximum or minimum values).

The total strain energy density at half-life, ΔW_{HL}^T, versus reversals to failure, $2N_f$, for all of the uniaxial strain-controlled fatigue tests with zero (R_ε = -1) [17] and non-zero mean strains (R_ε = 0, 0.2, 0.25) [18] with nominal temperature rise is presented in Fig. 4.3(a). An acceptable correlation of the fatigue life data was observed in this figure. Moreover, the predicted fatigue lives using the energy-based method with ΔW_{HL}^T as a damage parameter are plotted against the experimentally observed fatigue lives in Fig. 4.3(b). As seen, all fatigue lives under cyclic loading with R_ε values of -1, 0.2, and 0.25 are within scatter bands of two, while three out of nine fatigue life data under pulsating tension loading (R_ε = 0) are merely outside scatter bands. Nonetheless, a better predictive

ability of the energy-based model using ΔW_{HL}^{T} are obtained by $R^2 = 0.78$ when compared to the strain-stress based SWT model ($R^2 = 0.65$). The correlation using this energy approach with ΔW_{HL}^{T} is also found to be comparable to that of the strain-based Coffin-Manson model ($R^2 = 0.76$).

The cumulative total strain energy density, $\sum W^T$, is also considered in this study to account for both mean stress relaxation that results in vertical shifting in the stress-strain hysteresis loops as well as the cyclic softening effects that significantly incurred during the initial cycling, as discussed in [17]. The value of $\sum W^T$ is determined from the following:

$$\sum W^T = \sum W^P + \sum W^E \tag{4.10}$$

where $\sum W^P$ and $\sum W^E$ are the cumulative plastic and elastic strain energy densities, respectively, which represent the sum of plastic/elastic strain energy density for all cycles. The $\sum W^T$ values for all constant amplitude loading tests with mean strains were calculated and tabulated in Table 4.1.

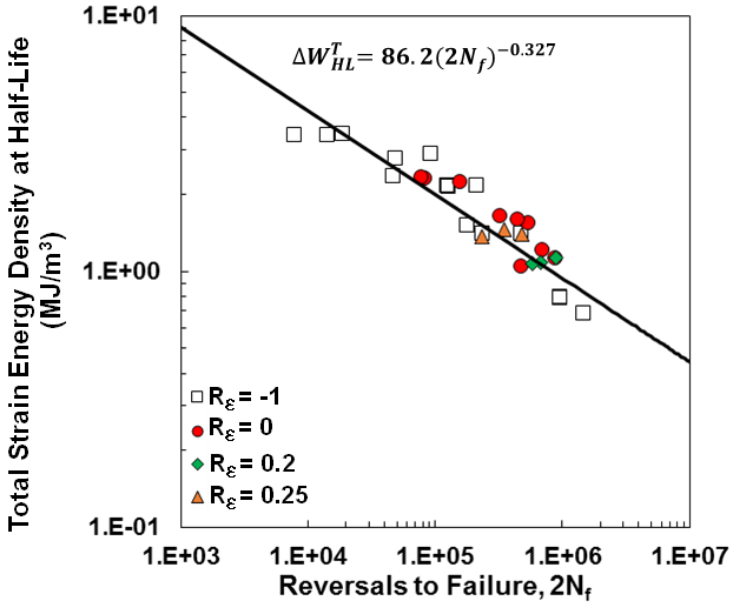

(a)

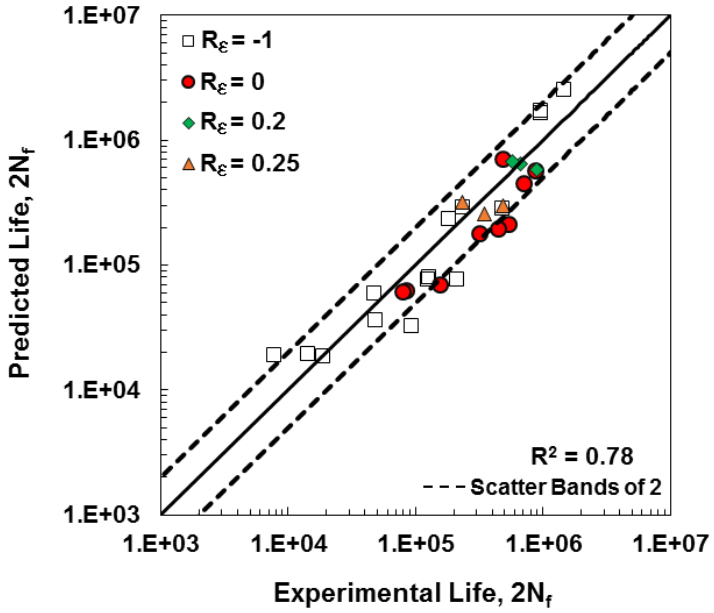

(b)

Figure 4.3 (a) Total strain energy density at half-life, ΔW_{HL}^{T}, versus reversals to failure, $2N_f$, for PEEK under uniaxial strain-controlled constant amplitude fatigue tests with zero [18] and non-zero (Table 4.1) mean strains with nominal rise in temperature, (b) predicted fatigue lives using energy-based approach with ΔW_{HL}^{T} versus experimentally observed fatigue lives.

The cumulative total strain energy density, $\sum W^T$, versus reversals to failure, $2N_f$, for all constant amplitude strain-controlled fatigue tests with various mean strains (R_ε = 0, 0.2, and 0.25) [18], and fully-reversed loading (R_ε = -1) [17] with nominal temperature rise are plotted in Fig. 4.4(a). In addition, the predicted fatigue lives using $\sum W^T$ are plotted against the experimentally observed fatigue lives for all uniaxial strain-controlled test with and without mean strain as displayed in Fig. 4.4(b). Scatter bands of two are also included in this figure. A good correlation (R^2 = 0.88) was observed for the energy-based fatigue model using $\sum W^T$ as damage parameter, when compared to those of the strain-based Coffin-Manson model (R^2 = 0.76), the strain-stress based SWT model (R^2 = 0.65), and the energy-based model using ΔW_{HL}^T (R^2 = 0.78). Therefore, it is evident that the energy-based model utilizing $\sum W^T$ may be an appropriate model to correlate fatigue data of PEEK under strain-controlled loading conditions in presence of mean strains.

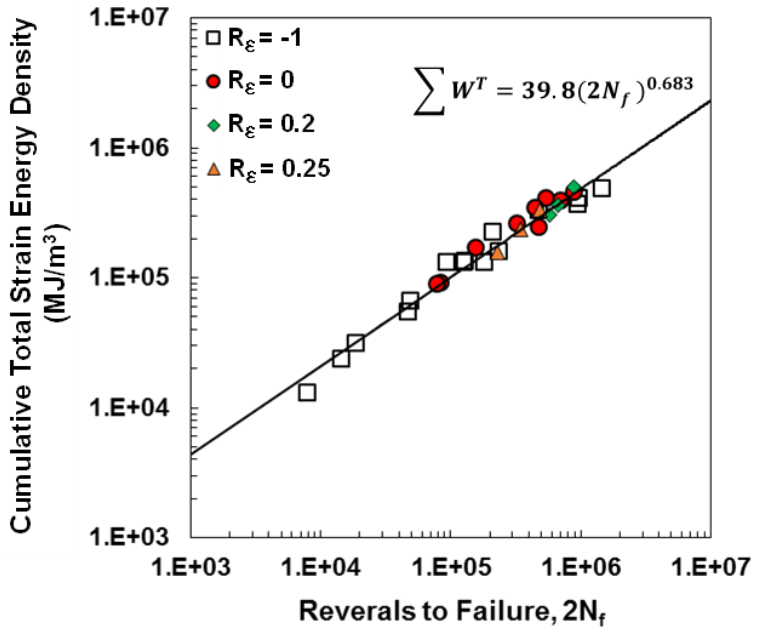

(a)

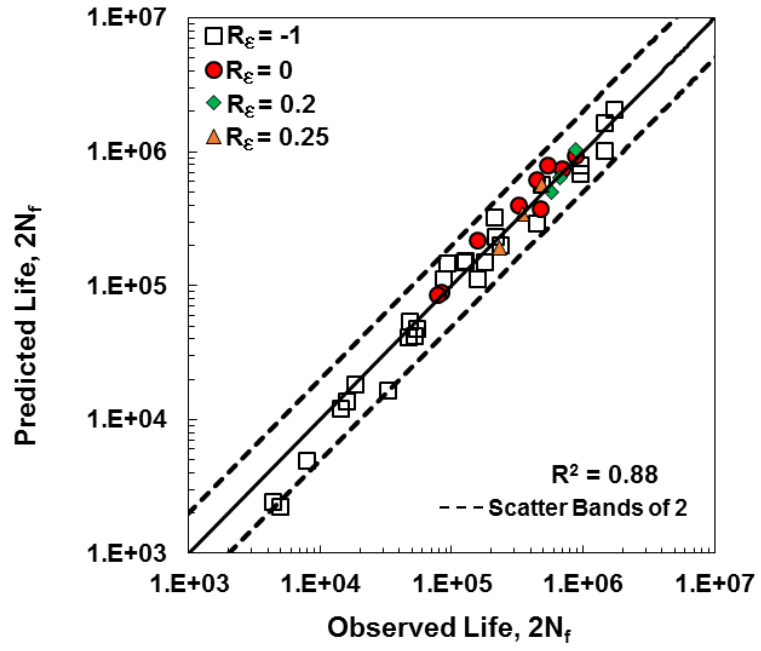

(b)

Figure 4.4 (a) Cumulative total strain energy density, $\sum W^T$, versus reversals to failure, $2N_f$, for PEEK under uniaxial strain-controlled constant amplitude fatigue tests with zero [18] and non-zero (Table 4.1) mean strains with nominal rise in temperature, (b) predicted fatigue lives using energy-based approach with $\sum W^T$ versus experimentally observed fatigue lives.

4.4 Fatigue Modeling for Block Loading Condition

This section presents the analysis and modeling of several cumulative fatigue damage approaches for PEEK specimens under multi-block loading condition with zero and non-zero mean strains at various frequencies. The Palmgren-Miner LDR is first employed using either strain or energy-based parameter to assess its applicability for PEEK polymer. Due to the satisfactory life predictions using $\sum W^T$ for specimens under constant amplitude loading in the previous section, a direct cumulative damage method based on an energy parameter is also proposed.

In this study, the validity of the selected cumulative damage models is evaluated using the experimental data for PEEK polymer under various uniaxial strain-controlled multi-block loading conditions [19]. The experimental results employed in this study were obtained using the following test conditions [19]:

I. fully-reversed (R_ε = -1) two-block loading with nominal temperature rise (i.e. data in Table 4.2),

II. fully-reversed (R_ε = -1) two-block loading to study the frequency effect (i.e. data in Table 4.3),

III. pulsating tension (R_ε = 0) two-block loading with nominal temperature rise, (i.e. data in Table 4.4), and

IV. fully-reversed (R_ε = -1) three- and four- block loadings with nominal temperature rise (i.e. data in Table 4.5).

The fatigue tests under two-block loading were conducted using either H-L or L-H loading sequence, while three-block loading experiments were performed using high-

low-high (H-L-H) or low-high-low (L-H-L) sequence. The high-low-high-low (H-L-H-L) loading was conducted for four-block loading fatigue tests [19].

.

Table 4.2 Experimental results [19] and calculated cumulative damages for uniaxial fully-reversed (R_ε = -1) strain-controlled fatigue tests of PEEK with two-block loading with adjusted frequencies to maintain the nominal temperature rise on the specimens (i.e. test condition (I)).

Specimen ID	$\varepsilon_{a1}/\varepsilon_{a2}$ (mm/mm)	f_1/f_2 (Hz)	ΔT (°C)	$2N_1/2N_2$ (Reversals)	σ_{a1}/σ_{a2}* (MPa)	σ_{m1}/σ_{m2}* (MPa)	LDR using ε_a		LDR using ΔW_{HL}^T		DCD Method using $\sum W^T$
							D_1/D_2	D	D_1/D_2	D	
High-Low											
S123	0.04/0.02	0.50/3	20 36	6,000/2,130,352#	49/30	14/16	0.44/1.4	1.8	0.44/2.1	2.5	0.74
S101			31 37	6,000/1,371,616	47/30	-12/-9	0.44/0.9	1.5	0.44/0.3	0.72	1.6
S105	0.04/0.03	0.5/0.75	26 28	6,000/296,276	49/47	-11/-9	0.44/3.7	4.1	0.44/4.1	4.6	0.59
S102			28 27	6,000/412,318	47/47	-12/-10	0.44/5.1	5.5	0.44/5.6	6.1	0.53
S108			31 30	6,000/459,890	51/49	-12/-10	0.42/5.7	6.1	0.44/5.59	6	0.51
Low-High											
S103	0.03/0.04	0.75/0.5	27 31	100,000/33,542	51/51	-10/-11	0.65/3.4	4	0.65/2.6	3.3	0.72
S109			29 31	100,000/50,136	47/48	-10/-11	0.65/5.1	5.7	0.65/2.8	3.4	0.64
S106			22 29	100,000/53,076	50/49	-10/-11	0.65/5.4	6	0.65/4.1	4.7	0.63

*Measured at half-life cycle
#Runout

Table 4.3 Experimental results [19] and calculated cumulative damages for uniaxial fully-reversed (R_ε = -1) strain-controlled fatigue tests of PEEK with two-block loading for frequency effect study (i.e. test condition (II)).

Specimen ID	$\varepsilon_{a1}/\varepsilon_{a2}$ (mm/mm)	f_1/f_2 (Hz)	ΔT (°C)	$2N_1/2N_2$ (Reversals)	σ_{a1}/σ_{a2}* (MPa)	σ_{m1}/σ_{m2}* (MPa)	LDR using ε_a		LDR using ΔW_{HL}^T		DCD Method using $\sum W^T$
							D_1/D_2	D	D_1/D_2	D	
High-Low											
S124	0.04/0.03	0.25/0.5	9 15	2,000/140,582	64/55	14/15	0.43/1.7	2.2	0.43/5.2	5.6	0.53
S114			37 30	2,000/241,626	64/55	-8/-7	0.43/3	3.4	0.43/3.9	4.3	0.61
Low-High											
S111	0.03/0.04	0.5/0.25	17 14	30,000/46,000	54/61	-10/-11	0.89/4.6	5.5	0.89/4.9	5.8	0.56
S113			17 14	30,000/53,434	55/61	-7/-7	0.89/5.4	6.3	0.89/3.9	4.8	0.56

*Measured at half-life cycle

Table 4.4 Experimental results [19] and calculated cumulative damages for uniaxial pulsating tension ($R_\varepsilon = 0$) strain-controlled fatigue tests of PEEK with two-block loading (i.e. test condition (III)).

Specimen ID	$\varepsilon_{a1}/\varepsilon_{a2}$ (mm/mm)	f_1/f_2 (Hz)	ΔT (°C)	$2N_1/2N_2$ (Reversals)	σ_{a1}/σ_{a2}* (MPa)	σ_{m1}/σ_{m2}* (MPa)	LDR using ε_a		LDR using ΔW_{HL}^T		DCD Method using $\sum W^T$
							D_1/D_2	D	D_1/D_2	D	
High-Low											
S120	0.03/0.02	0.5/1.5	14 16	60,000/312,756	55/44	24/19	0.57/0.2	0.77	0.57/0.96	1.5	0.76
S116			21 31	60,000/645,088	52/42	1/-3	0.56/0.4	0.98	0.57/0.62	1.2	1.1
Low-High											
S121	0.02/0.03	1.5/0.5	20 18	300,000/65,032	45/54	24/24	0.44/0.8	1.2	0.44/3.1	3.5	0.5
S118			26 31	300,000/99,310	44/53	-0.19/0.88	0.44/1.2	1.6	0.44/1.7	2.1	1

*Measured at half-life cycle

Table 4.5 Experimental results [19] and calculated cumulative damages for uniaxial fully-reversed (R_ε = -1) strain-controlled fatigue tests of PEEK with three- and four-block loadings (i.e. test condition (IV)).

Specimen ID	$\varepsilon_{a1}/\varepsilon_{a2}/\varepsilon_{a3}$ (mm/mm)	$f_1/f_2/f_3$ (Hz)	ΔT (°C)	$2N_1/2N_2/2N_3$ (Reversals)	$\sigma_{a1}/\sigma_{a2}/\sigma_{a3}$* (MPa)	$\sigma_{m1}/\sigma_{m2}/\sigma_{m3}$* (MPa)	LDR using ε_a		LDR using ΔW_{HL}^T		DCD Method using $\sum W^T$
							$D_1/D_2/D_3$	D	$D_1/D_2/D_3$	D	
High-Low-High											
S126	0.04	0.5	22	6,000	51	-11	0.44	5.4	0.44	3.6	0.58
	0.03	0.75	26	180,000	47	-9	0.46		0.46		
	0.04	0.5	21	44,098	59	10	4.4		2.7		
Low-High-Low											
S127	0.03	0.75	30	100,000	47	-7	0.65	4.1	0.65	4.1	0.54
	0.04	0.5	32	20,000	48	-9	0.44		0.44		
	0.03	0.75	31	239,800	46	-8	3		3		

Specimen ID	$\varepsilon_{a1}/\varepsilon_{a2}/\varepsilon_{a3}/\varepsilon_{a4}$ (mm/mm)	$f_1/f_2/f_3/f_4$ (Hz)	ΔT (°C)	$2N_1/2N_2/2N_3/2N_4$ (Cycles)	$\sigma_{a1}/\sigma_{a2}/\sigma_{a3}/\sigma_{a4}$* (MPa)	$\sigma_{m1}/\sigma_{m2}/\sigma_{m3}/\sigma_{m4}$* (MPa)	LDR using ε_a		LDR using ΔW_{HL}^T		DCD Method using $\sum W^T$
							$D_1/D_2/D_3/D_4$	D	$D_1/D_2/D_3/D_4$	D	
High-Low-High-Low											
S128	0.04	0.5	26	6,000	47	-10	0.44	4.3	0.44	4.6	0.5
	0.03	0.75	26	180,000	46	-8	0.46		0.46		
	0.04	0.5	31	20,000	48	-8	0.45		0.45		
	0.03	0.75	29	237,786	47	-6	2.9		3.2		

*Measured at half-life cycle

4.4.1 The Linear Damage Rule

According to the Palmgren-Miner LDR, which is the most widely used and commonly accepted for fatigue life prediction of metals, the damage induced in each loading block is given as [25]:

$$D_i = \frac{N_i}{N_{fi}} \tag{4.11}$$

where i represents the number of loading blocks, D_i is the damage produced by N_i cycles for a specific block of loading i, and N_{fi} is the number of cycles to failure at particular strain or stress level as applied in the loading block i. The damage D_i can be defined as a cycle ratio or a fraction of life that is removed from the material. Depending on the damage parameter chosen, N_{fi} can be obtained from the fatigue data under constant amplitude loading. Fatigue damage, D_i, determined using Eq. (4.11) is added linearly to predict fatigue failure, which occurs when the cumulative damage, D, equals to unity:

$$\mathrm{D} = \sum D_i = 1 \tag{4.12}$$

The validity of the LDR, in conjunction with strain or energy-based parameter, is evaluated and discussed in the subsequent sections.

4.4.1.1 Strain-Based LDR

The LDR with strain amplitude as a damage parameter was first employed to obtain the cumulative damage for PEEK specimens under two- , three-, and four-block loadings. The damage induced in each loading block, D_i, was determined using Eq. (4.11) in which N_i represents the number of cycles applied in each loading block, and N_{fi} was obtained from the best fit (i.e. the Coffin-Manson fit in Fig. 4.1(a)) on strain-life fatigue data under constant amplitude fully-reversed (R_ε = -1) loading. Once D_i was determined,

the cumulative damage, D, was obtained using Eq. (4.12). The damage, D_i, for each loading block and the cumulative damage, D, for the test conditions I-IV are presented in Tables 4.2-4.5, respectively

Despite the fact that the strain-based approach was able to provide reasonable correlations of PEEK fatigue lives under constant amplitude loading (i.e. the correlation in Fig. 4.1(b)), mostly conservative damage predictions were obtained for block-loading using the strain-based LDR, as illustrated by the cumulative damage values, D, ranging from 0.77 to 6.3 in Tables 4.2-4.5. Typically, for most metals in H-L loading, micro-cracks can initiate during the high loading level and continue to grow during a low loading level. On the other hand, in L-H loading, the possibility of cracks to initiate during a low loading level is generally limited; hence, longer fatigue lives are often observed for L-H loading as compared to H-L loading. In addition, the corresponding cumulative damage using the LDR is typically less than one when the material is subjected to a H-L loading sequence, and greater than one for L-H loading sequence [22].

However, for the loading condition I in which PEEK specimens were subjected to two-block loading with nominal temperature rise, the loading sequence appears to have minimum influence on the cumulative damage using the strain-based LDR as seen in Table 4.2. However, for the loading conditions II in Table 3 and the loading condition III in Table 4, lower cumulative damage using the strain-based LDR can be observed for all specimens subjected to H-L loading, as compared to those under L-H loading with identical strain amplitude and frequency.

Furthermore, to illustrate the applicability of the strain-based LDR for damage prediction in term of cycle ratio, N_1/N_{f1} is plotted against N_2/N_{f2} for all two-block

loading tests (i.e. test conditions I-III) as shown in Fig. 4.5(a). For three-block loading, $N_1/N_{f1} + N_2/N_{f2}$ is plotted against N_3/N_{f3}, while, for four-block loading $N_1/N_{f1} + N_2/N_{f2} + N_3/N_{f3}$ is plotted against N_4/N_{f4} as illustrated in Fig 4.5(b). The ratio N_1/N_{f1} (or $N_1/N_{f1} + N_2/N_{f2}$) for three-block loading or $N_1/N_{f1} + N_2/N_{f2} + N_3/N_{f3}$ for four-block loading) corresponds to the damage induced in the initial block(s), while N_2/N_{f2} (or N_3/N_{f3}) for three-block loading and N_4/N_{f4} for four-block loading) represents the remaining damage tolerance based on the LDR.

In addition, the LDR prediction lines, the straight lines intersecting unity on both x- and y-axes, as well as the bands representing the factor of two of the LDR prediction line, are also displayed in these figures. As seen, poor correlations can be observed for the majority of the data in Figs. 4.5(a) and 4.5(b), except data under test condition III (i.e. data in Table 4.4) for pulsating tension ($R_\varepsilon = 0$) two-block loading with nominal temperature rise.

Conservative predictions can be attributed to the fact that the LDR assumes that the damage accumulates in a linear fashion and may not be able of incorporating the load history and sequence effect. Hence, the LDR with strain amplitude as the damage parameter may not be able to capture the beneficial effect of pre-loading on the fatigue life of PEEK when subjected to zero mean strain loading (i.e. loading conditions I, II, and IV), as reported in [19]. On the other hand, for the test conducted under pulsating tension loading (i.e. loading condition III), minimal effect of pre-loading on fatigue life was reported [19]. This may explain an acceptable correlation of the fatigue data under pulsating tension loading (i.e. loading condition III), using the strain-based LDR, while

the strain-based LDR failed to correlate fatigue life data under fully-reversed (R_ε = -1) loading.

4.4.1.2 Energy-Based LDR

Due to the fact that the strain-stress SWT parameter was not able to adequately correlate PEEK fatigue lives under constant amplitude loading and strain-based LDR resulted in very conservative damage prediction for PEEK under block loading, the LDR based on the total strain energy density at half-life, ΔW_{HL}^{T}, was considered.

In this approach, the damage due to each loading block, D_i, using Eq. (4.11) and the cumulative damage, D, in Eq. (4.12) for all fatigue tests under two-block loading conditions were calculated and listed in Tables 4.2-4.4 for test conditions I-III, respectively. The value of N_{f1} for the first block of loading was obtained from the best curve fit based on ΔW_{HL}^{T} life data for PEEK specimens under fully-reversed (R_ε = -1) constant amplitude loading [17]. The value of ΔW_{HL}^{T} value for the second loading block represents the total strain energy density at half-life cycle in the second loading block. This value was then used to obtain the corresponding fatigue life, N_{f2}, from the best fit to ΔW_{HL}^{T} life data in [18].

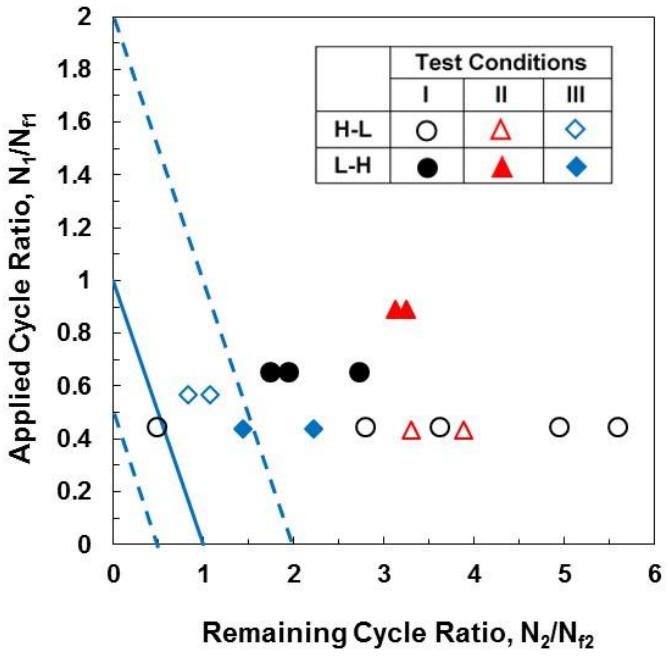

(a)

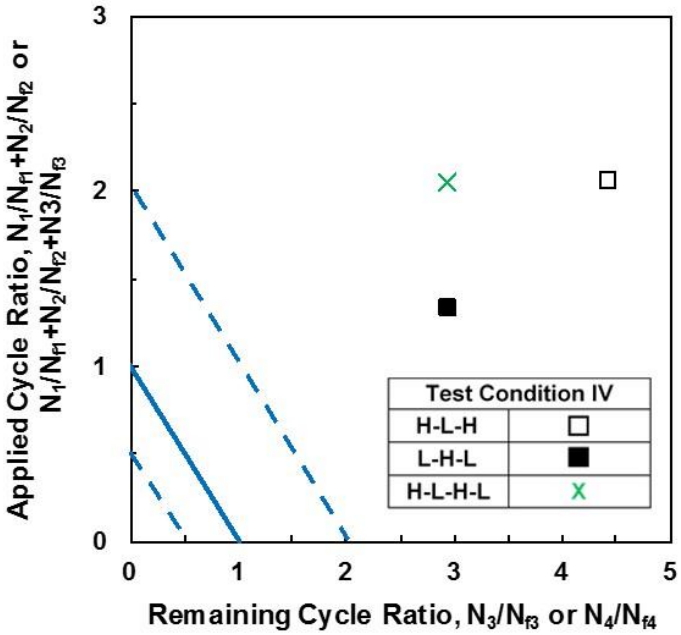

(b)

Figure 4.5 Cycle ratios in (a) two-block loading (test conditions I-III), and (b) three- and four-block loading (test condition IV) experiments obtained using the strain-based LDR for PEEK polymer.

The line in each figure represents predictions of the model.

Similar approach was also employed to determine the cumulative damage for PEEK specimens with three- and four-block cyclic loadings, as listed in Table 4.5. For these tests, N_{fi} values for the initial loading blocks (i.e. the first two loading blocks for three-block tests and the first three loading blocks for four-block tests) were obtained from the fatigue data under the same test conditions in [17]. For the last loading block, N_{fi} was determined by calculating the corresponding ΔW_{HL}^{T} value and using the curve fit of ΔW_{HL}^{T} life data [17] obtained from fully-reversed constant amplitude loading.

A similar plot as in Fig. 4.5 was generated for the cumulative damage obtained using the energy-based LDR as shown in Fig. 4.6. In this figure, it is evident that the LDR with ΔW_{HL}^{T} as damage parameter was not able to predict the cumulative fatigue damage for PEEK under multi-block loading conditions, except for test condition III whose lives were minimally influenced by the load sequence. Very conservative predictions, with cumulative damage ranging between 0.9 and 6, was also obtained using the LDR with ΔW_{HL}^{T} as tabulated in Tables 4.2-4.5. Therefore, the LDR with ΔW_{HL}^{T} is not a suitable approach for damage calculation of PEEK polymer under variable amplitude loading as the loading history and sequence greatly affect its fatigue behavior.

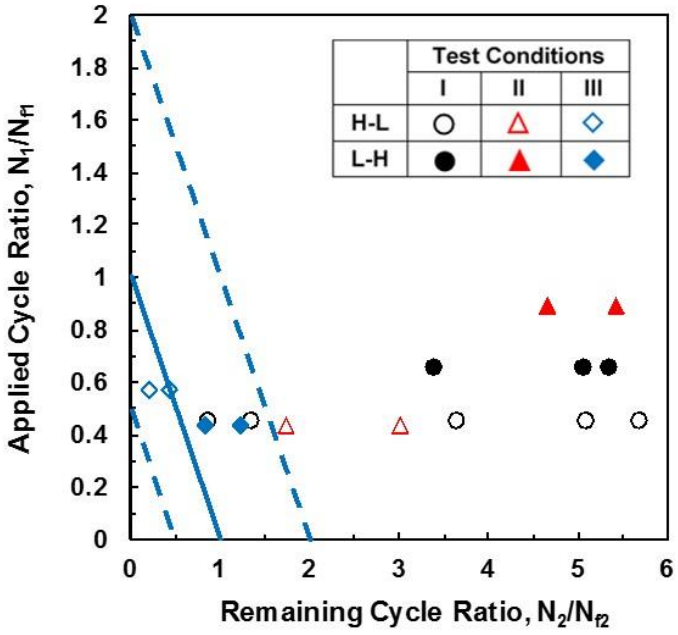

(a)

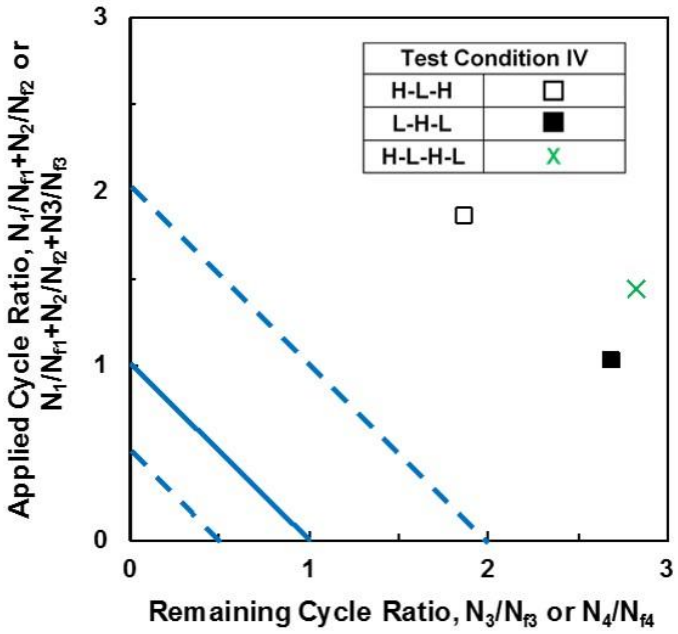

(b)

Figure 4.6 Cycle ratios in (a) two-block loading (test conditions I-III), and (b) three- and four-block loading (test condition IV) experiments obtained using the energy-based LDR for PEEK polymer.

The line in each figure represents predictions of the model.

4.4.2 The Direct Cumulative Damage (DCD) Method

Due to the shortcomings of the LDR in predicting the damage accumulation in PEEK polymer, the direct cumulative damage (DCD) method based on the strain energy density parameter is proposed in this study. To take the load history and sequence effect into consideration, $\sum W^T$ values from specimens under constant amplitude loading were plotted against fatigue lives to determine their linear relationship in a log-log scale, as shown in Fig. 4.4(a).

For the proposed DCD approach, the cumulative damage of a specimen under multi-block cyclic loading may be determined using the following simple relation:

$$\mathrm{D}= \frac{N_{f,e}}{N_{f,p}} = 1 \tag{4.13}$$

where the failure is deemed to occur when D equals to unity. In Eq. (4.13), $N_{f,e}$ is the overall fatigue life of a specimen (i.e. summation of number of cycles from all loading block). The predicted life, $N_{f,p}$, represents the number of cycle, which corresponds to the total summation of $\sum W^T$ from all loading blocks on the reference curve. For example, $\sum W^T$ for two-block loading was determined by combining $\sum W_1^T$ and $\sum W_2^T$, which represents the cumulative total strain energy density in the first and second loading blocks, respectively.

The cumulative damage obtained using the DCD method for specimens under loading conditions I-IV are listed in Tables 4.2-4.5, respectively. As seen in these tables, all cumulative damage values using the DCD method are within a factor of two from unity, ranging from 0.5 to 1.6. Furthermore, the cycle ratios N_1/N_f versus N_2/N_f were plotted for all data with two-block loading, as displayed in Fig. 4.7(a), and for fatigue

data with three- and four-block loading, as shown in Fig. 4.7(b). For test conditions I - III, the DCD method yields satisfactory predictions for the data with L-H loading, while it slightly overestimates the applied cycle ratios for the data with H-L loading, as seen in Fig. 4.7(a). Moreover, using the DCD method, the applied cycle ratios for the H-L loading appear to be significantly lower than the remaining cycle ratios, which is in contrast to that obtained using the LDR where the applied cycle ratios are approximately half of the total cumulative damage in the specimens. Nonetheless, excellent correlations can be noticed in Fig. 4.7(b) for test condition IV.

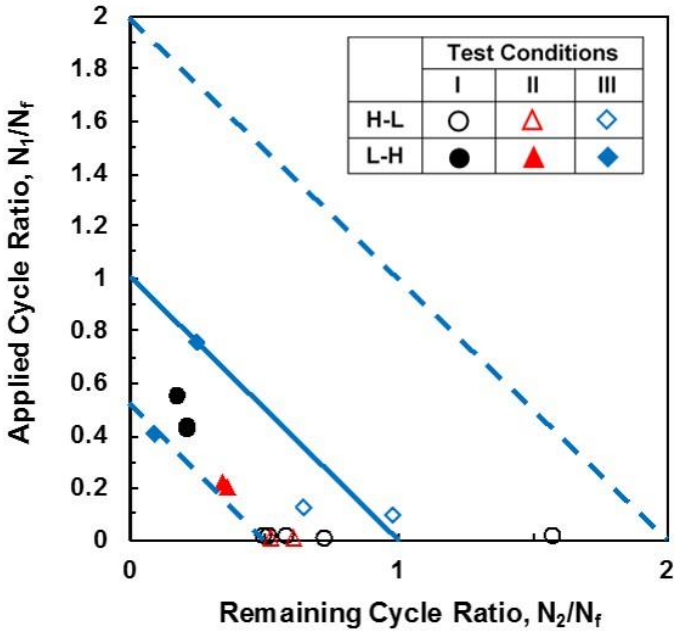

(a)

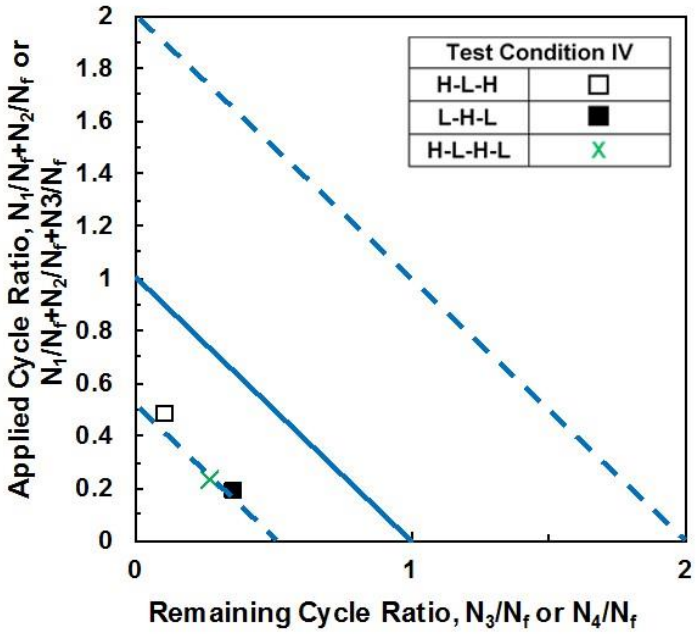

(b)

Figure 4.7 Cycle ratios in (a) two-block loading (test conditions I-III), and (b) three- and four-block loading (test condition IV) experiments obtained using the direct cumulative damage (DCD) method for PEEK polymer.

The solid and dash curves in each figure represent predictions of the DCD method and the LDR, respectively.

4.4.3 Comparison of Fatigue Cumulative Damage Predictions

The comparison of the cumulative damage obtained using the strain-based LDR, the energy-based LDR, and the DCD method with $\sum W^T$, are illustrated by the bar charts in Fig. 4.8. The damage predictions for PEEK specimens subjected to loading conditions I-IV are presented in Fig. 4.8(a)-(d), respectively. In general, the strain-based LDR appears to provide the most conservative damage predictions for PEEK polymer under test conditions I, II, and IV regardless of loading sequence. However, for test condition III where minimum load history and sequence effects on fatigue life of PEEK was noticed, the strain-based LDR was able to provide reasonably well cumulative damage predictions ($0.77 \leq D \leq 1.6$). On the other hand, better fatigue damage predictions were obtained using the energy-based LDR for test conditions I, II, and IV as compared to the LDR with strain amplitude. Nonetheless, as seen in Fig. 4.8, the energy-based LDR is not considered to be the appropriate damage model for PEEK polymer as the average of the damage predictions are not within a factor of three. The proposed DCD method, which considers the cumulative strain energy density to capture both load history and sequence effects, provides the best fatigue damage predictions for PEEK under various mean strains and frequencies when compared to both LDRs.

Furthermore, to illustrate the capability of using $\sum W^T$ as damage parameter for PEEK polymer under non-constant amplitude loading, $\sum W^T$ for all specimens in Table 4.2-4.5 were plotted against $2N_f$, as presented in Fig. 4.9(a). The $\sum W^T$ value for each specimen was determined by combining the cumulative total strain energy density from all loading blocks.

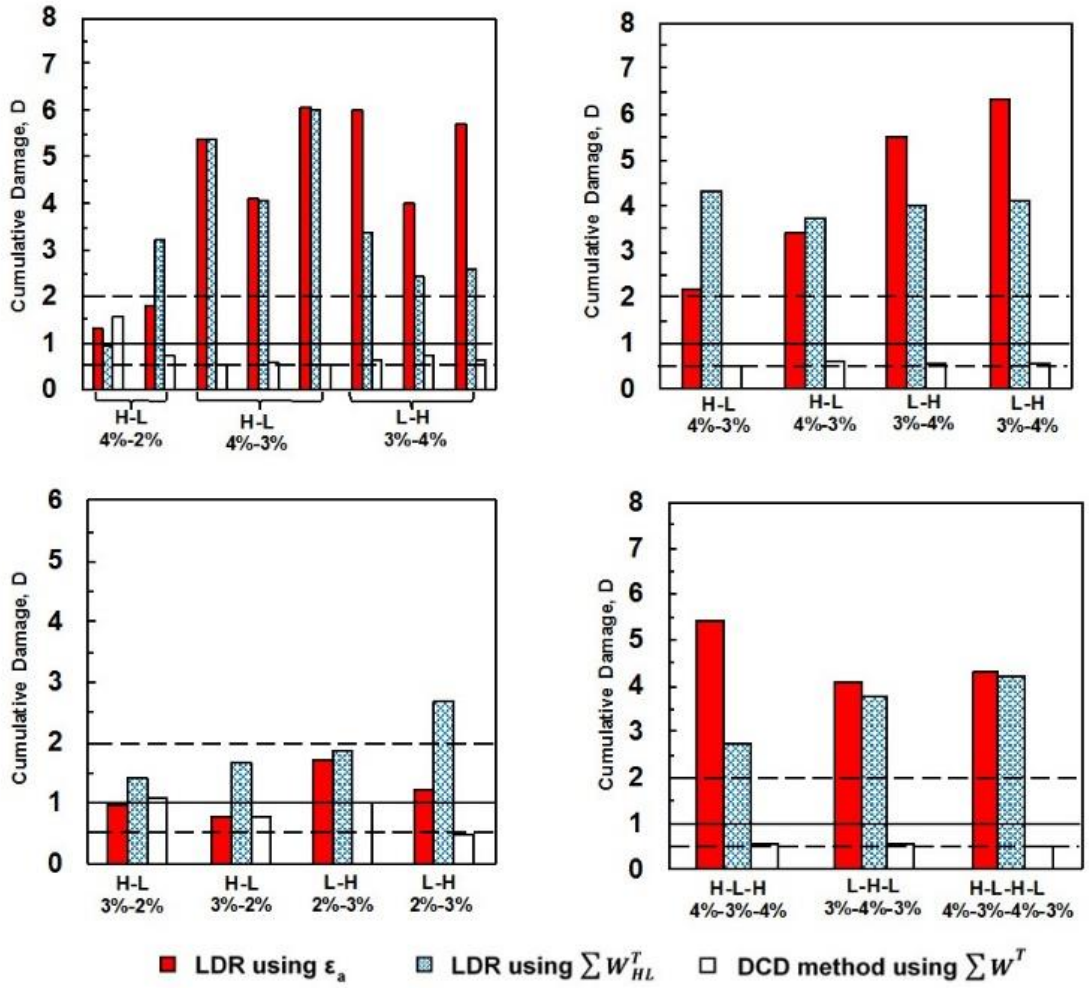

Figure 4.8 Bar charts showing the comparisons of the cumulative damage using the strain-based LDR, the energy-based LDR, and the DCD method for PEEK polymer under (a) two-block loading with zero mean strain and nominal temperature rise, (b) two-block loading with zero mean strain to study the frequency effect, (c) two-block pulsating tension loading with nominal temperature rise, and (d) three- and four- block loading with zero mean strain and nominal temperature rise.

In addition to the fatigue data under variable amplitude loading, the data for PEEK specimens subjected to constant amplitude cyclic loading were included in this figure, including

- constant amplitude fully-reversed (R_ε = -1) loading with nominal temperature rise [17],
- constant amplitude fully-reversed (R_ε = -1) loading with various frequencies to study the frequency effect [17], and
- constant amplitude loading with mean strains (R_ε = 0, 0.2, and 0.25) and nominal temperature rise (i.e. data in Table 4.1) [18].

As depicted in Fig. 4.9(a), an excellent correlation between $\sum W^T$ and fatigue lives for all loading conditions was obtained. Using the relationship established in Fig. 4.9(a), fatigue lives of PEEK were calculated and plotted against the experimentally observed lives, as shown in Fig. 4.9(b). The correlation between the predicted and experimentally observed PEEK fatigue lives are within scatter bands of two with R^2 = 0.92, which is an indicative that this simple yet effective approach may be utilized for life prediction for PEEK polymer under constant and non-constant amplitude loadings with various strain ratios and frequencies. Further investigation is required to obtain its applicability for fatigue life prediction for PEEK under other variable amplitude loading conditions.

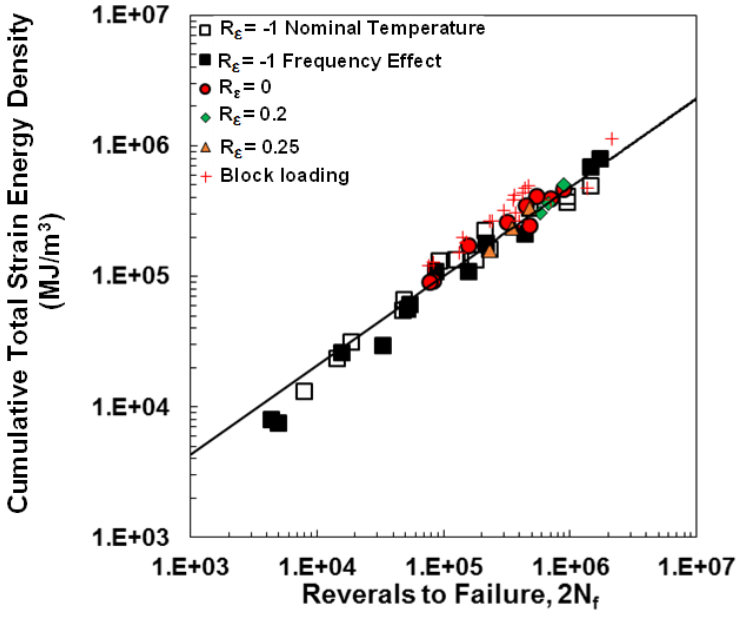

(a)

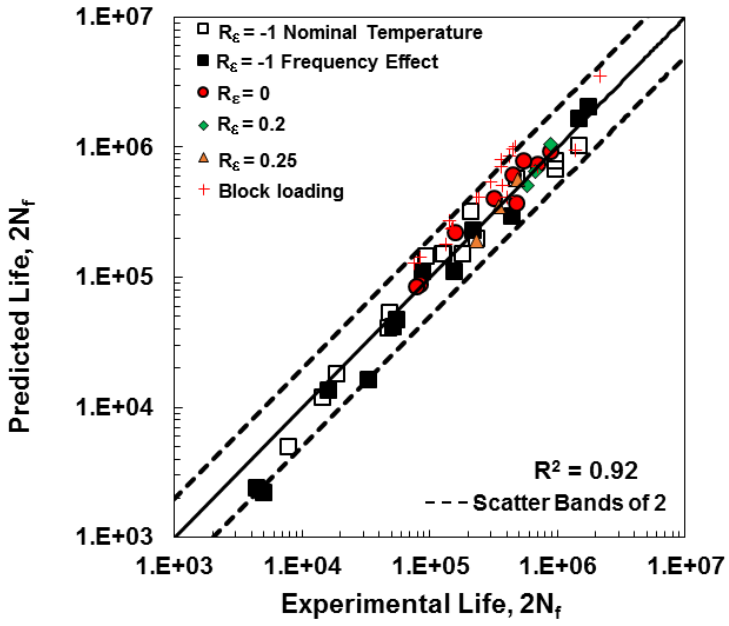

(b)

Figure 4.9 (a) Cumulative total strain energy density, $\sum W^T$, versus reversals to failure, $2N_f$, for PEEK under different test conditions, including constant amplitude loading and block-loading with various strain ratios and frequencies, and (b) predicted fatigue lives using energy-based approach with $\sum W^T$ versus experimentally observed fatigue lives.

4.5 Conclusions

In this study, the applicability of various fatigue models to account for the mean strain and load history/sequence effects for PEEK polymer was investigated. The analysis presented in this study is based on the experimental data from a series of uniaxial strain-controlled test under various constant and non-constant amplitude loading conditions [17, 18]. Three fatigue models; the strain-based model, the stress-strain-based model, and a model based on the strain energy density, were examined to correlate the constant amplitude fatigue life data with non-zero mean strain.

The cumulative damage in specimens under multi-block loading conditions were determined using the LDR in conjunction with either the strain amplitude or the total strain energy density at half-life, ΔW_{HL}^{T}. The DCD approach with the total cumulative strain energy density, $\sum W^{T}$, as the damage parameter was also proposed to correlate the fatigue damage for PEEK under various multi-block loading conditions. Based on the analysis presented in this study, the following conclusions can be drawn.

1. Since PEEK polymer exhibited mean stress relaxation behavior in a presence of mean strain, and minimal effect of mean strain on PEEK fatigue life was observed [18], the strain-based fatigue model was found to correlate mean strain data for PEEK polymer reasonably well.
2. Contrary to the expectation, the SWT model, which involved the fatigue parameter with both stress and strain terms, was not able to provide accurate life predictions for test data with mean strain. Such result may be attributed to the large scatter of the stress responses (i.e. stress amplitude) for specimens under non-zero mean strain conditions.

3. The energy based fatigue model using $\sum W^T$ provided a satisfactory correlation between the fatigue life data under constant amplitude loading with mean strains. This energy model was able to capture the change in shape and size of the hysteresis stress-strain loop throughout the cyclic process due to both cyclic softening and mean stress relaxation.
4. The LDR with either the strain amplitude or the total strain energy density at half-life, ΔW_{HL}^T, overestimated the cumulative damage in PEEK specimens subjected to fully-reversed cyclic loading. However, acceptable predictions were obtained for specimens subjected to pulsating tension two-block loading with nominal temperature rise (i.e. test condition III) using the strain-based LDR. Since the LDR is the cycle-by-cycle approach in which the overall damage is obtained by adding the damage induced in each loading block, the load interactions effect is not included in the LDR.
5. Regardless of loading conditions (zero or non-zero mean strain), the $\sum W^T$ life curve constructed using the constant amplitude fatigue data was able to capture the cumulative damage in PEEK specimens.
6. The DCD method proposed in this study was able to include the loading history/sequence effects and provide an acceptable predictive capability for PEEK fatigue life under different loading blocks, including two-, three-, and four-blocks of loadings with zero and non-zero mean strains at various frequencies. The method also accounts for the significantly longer fatigue lives of PEEK polymer when subjected to fully-reversed (R_ε = -1) pre-loading, irrespective of loading sequence.

7. It has been shown that the energy-based approach with $\sum W^T$ as a damage parameter was able to correlate PEEK fatigue lives under constant and non-constant amplitude loadings, with zero and non-zero mean strains at various frequencies. This approach is fairly straightforward and should be further investigated to obtain its applicability for fatigue life prediction of polymer or other materials under realistic service loading conditions.

4.6 References

[1] Kurtz SM, Devine JN. PEEK biomaterials in trauma, orthopedic, and spinal implants. Biomaterials 2007; 28:4845–69.

[2] Schwitalla, A., Müller, W. D. PEEK dental implants: a review of the literature. Journal of Oral Implantology 2013; 39(6):743-49.

[3] Cho D Y, Liau W R, Lee W Y, Liu JT, Chiu CL, Sheu PC. Preliminary experience using a polyetheretherketone (PEEK) cage in the treatment of cervical disc disease. Neurosurgery 2002; 51(6):1343-50.

[4] Jockisch KA., Brown SA, Bauer TW, Merritt K. Biological response to chopped-carbon-fiber-reinforced PEEK. Journal of biomedical materials research 1992; 26(2):133-46.

[5] Fatemi A, Yang L. Cumulative fatigue damage and life prediction theories: a survey of the state of the art for homogeneous materials. International Journal of Fatigue 1998; 20:9–34.

[6] Lin SH, Ma CCM, Tai NH. Mechanical properties and morphology of different carbon fiber lengths in reinforced polyetheretherketone (PEEK) composites. Journal of Advanced Material 1996; 28(2):56–62.

[7] Jones RM. Mechanics of composite materials. 2nd ed. Taylor & Francis; 1998.

[8] Hoppel CP, Pangborn RN, Thomson RW. Damage accumulation during multiple stress level fatigue of short-glass-fiber reinforced styrene-maleic anhydride. Journal of Thermoplastic Composite Materials 2001; 14:84–94.

[9] Noguchi H, Kim Y-H, Nisitani H. On the cumulative fatigue damage in short carbon fiber reinforced poly-ether-ether-ketone. Engineering Fracture Mechanics 1995; 51:457–68.

[10] Zago A, Springer GS. Constant amplitude fatigue of short glass and carbon fiber reinforced thermoplastics. Journal of Reinforced Plastics and Composites 2001; 20:564–95.

[11] Zago A, Springer GS, Quaresimin M. Cumulative damage of short glass fiber reinforced thermoplastics. Journal of Reinforced Plastics and Composites 2001; 20:596–605.

[12] Yao W, Himmel N. A new cumulative fatigue damage model for fibre-reinforced plastics. Composite Science and Technology 2000; 60:59–64.

[13] Broutman L, Sahu S. A new theory to predict cumulative fatigue damage in fiberglass reinforced plastics. Composite Materials Testing and Design 1972; 497:170–88.

[14] Harris B, Gathercole N, Reiter H, Adam T. Fatigue of carbon-fibre-reinforced plastics under block-loading conditions. Composites Part A: Applied Science and Manufacturing 1997; 28:327–37.

[15] Lee C, Jen M. Fatigue response and modelling of variable stress amplitude and frequency in AS-4/PEEK composite laminates, Part 1: Experiments. Journal of Composite Materials 2000; 34:906–29.

[16] Lee C, Jen M. Fatigue response and modelling of variable stress amplitude and frequency in AS-4/PEEK composite laminates, Part 2: Analysis and formulation. Journal of Composite Materials 2000; 34:930–53.

[17] Shrestha R, Simsiriwong J, Shamsaei N, Moser RD. Cyclic deformation and fatigue behavior of polyether ether ketone (PEEK). International Journal of Fatigue 2016; 82:411–27.

[18] Shrestha R, Simsiriwong J, Shamsaei N. Mean strain effects on cyclic deformation and fatigue behavior of polyether ether ketone. Polymer Testing 2016;55:69-77.

[19] Shrestha R, Simsiriwong J, Shamsaei N. Load history and sequence effects on fatigue behavior of a thermoplastic polymer. Polymer Testing 2016; DOI: 10.1016/j.polymertesting.2016.09.026.

[20] Stephens RI, Fatemi A, Fuchs HO, Stephens RR. Metal fatigue in Engineering. 2nd ed. New York: John Wiley & Sons; 2000.

[21] ASTM E739-10, Standard practice for statistical analysis of linear or linearized stress-life and strain-life fatigue data, ASTM International, West Conshohocken, PA, 2015.

[22] Smith K, Topper T, Watson P. A stress-strain function for the fatigue of metals (Stress-strain function for metal fatigue including mean stress effect). Journal of materials 1970; 5:767-778.

[23] Golos, K ,Ellyin F. Generalization of cumulative damage criterion to multilevel cyclic loading. Theoretical Applied Fracture Mechanics 1987; 7:169-176.

[24] Ellyin F. Fatigue damage, crack growth and life prediction. Springer Netherlands; 1996.

[25] Miner MA. Cumulative damage in fatigue. Journal of Applied Mechanics 1945; 12:159–64. Hidden test to allow template to find last page in document